Building Pathology and Rehabilitation

João M. P. Q. Delgado *Editor*

Masonry: Building Pathologies and Design

Springer

Building Pathology and Rehabilitation

Volume 22

This book series addresses the areas of building pathologies and rehabilitation of the constructed heritage, strategies, diagnostic and design methodologies, the appropriately of existing regulations for rehabilitation, energy efficiency, adaptive rehabilitation, rehabilitation technologies and analysis of case studies. The topics of Building Pathology and Rehabilitation include but are not limited to - hygrothermal behaviour - structural pathologies (e.g. stone, wood, mortar, concrete, etc…) - diagnostic techniques - costs of pathology - responsibilities, guarantees and insurance - analysis of case studies - construction code - rehabilitation technologies - architecture and rehabilitation project - materials and their suitability - building performance simulation and energy efficiency - durability and service life.

More information about this series at http://www.springer.com/series/10019

João M. P. Q. Delgado
Editor

Masonry: Building Pathologies and Design

Springer

Editor
João M. P. Q. Delgado
CONSTRUCT-LFC
Department of Civil Engineering
University of Porto
Porto, Portugal

ISSN 2194-9832 ISSN 2194-9840 (electronic)
Building Pathology and Rehabilitation
ISBN 978-3-030-80495-4 ISBN 978-3-030-80496-1 (eBook)
https://doi.org/10.1007/978-3-030-80496-1

This Springer imprint is published by the registered company Springer Nature Switzerland AG
The registered company address is: Gewerbestrasse 11, 6330 Cham, Switzerland

Preface

Masonry is used in flexural applications such as retaining walls, roof and floor beams, and lintels; however, its main application has been in load-bearing walls or columns primarily resistant to compression loads.

The building degradation can be interpreted as the continuous reduction in performance over time. If the performance decreases below the functionality limits, the functional service life limit is reached. So, the eventual identification of potential hidden defects is extremely useful, which can compromise the building's performance and, if identified late, can have very costly repairs or be out of warranty terms. In other words, building pathology provides a systematic scientific approach to analyse (experimentally and numerically) and propose new rehabilitation strategies in a failed building. The objectivity it brings to bear helps to make an investigation independent of prejudice and of matters of blame. The building pathologist is concerned with what has happened and how it came to happen, rather than with attributing blame.

The main purpose of this book, *Masonry: Building Pathologies and Design*, is to provide a collection of recent research works related to blast-resistant design, building pathologies, seismic coating, bottle-shaped concrete struts, delayed ettringite formation and waterproofing.

The book is divided into eight chapters that intend to be a resume of the current state of knowledge for benefit of professional colleagues, scientists, students, practitioners, lecturers and other interested parties to network. At the same time, these topics will be going to the encounter of a variety of scientific and engineering disciplines, such as civil, mechanical and materials engineering.

Porto, Portugal — João M. P. Q. Delgado

Contents

Application of Blast Resistant Design Model for Safer Cities

Prafulla Parlewar

Abstract Cities across world are affected continuously with terrorist attacks. These attacks happens particularly on Embassies, Parliaments, trade centres and others significant buildings. The nature of the blast intensity in case of terrorist attach depends upon the detonator used and its distance from the ground zero. The research here present a design of blast resistant building planned in Mumbai, India. The design showcase a model blast resistant method that can be applied for the design of similar buildings affected by terrorist attacks. Some of the key aspect of this model methods are blast intensity, blast load and retaining wall. Moreover, the chapter, illustrates how does the structural components of building reacts during the blast? How can we plan for safer cities? How the important institutional buildings can be protected in event of terrorist attach? What kind of urban planning is essential for blast resistant cities. Furthermore, a case illustrates the details design for blast resistant buildings.

Keywords Blast resistant design · Urban planning · Safer cities

1 Introduction

The blast resistant design for institutional, civilian, commercial and industrial buildings is required due to prediction of terrorist attacks. The chapter here illustrate a blast resistant design for operational purpose in a industrial plant. The blast resistant building is design as per the IS Code IS 4991 (1968). The proposed design is an industrial building of size located at 30 m from the ground zero. The research here illustrates model process of design which can be used for design of blast resistant buildings.

Many cities across globe are affected with terrorist attacks to institutional and commercial buildings. In year 2001, New York World Trade Center (WTC) was attached by terrorist by hitting the building with hijacked air strike. The building collapsed due to the heat and caused large number of civilian casualties. In many cities, numerous attacks happen in congested locations. Some of these attaches are

P. Parlewar (✉)
City Development Corporation (P) Ltd., Mumbai, India

J. M. P. Q. Delgado (ed.), *Masonry: Building Pathologies and Design*, Building Pathology and Rehabilitation 22, https://doi.org/10.1007/978-3-030-80496-1_1

either use of bombs in vehicles, grenades or various other types of blasts. Substantial number of civilian causalities happens in these types of attacks. Also, governmental buildings are some important targets for terrorist attack. Globally, various design criteria are developed to make safe cities from terrorist attacks.

The research here illustrated how to design a blast resistant building? How this model process can be applied for the design blast resistant institutional, commercial or industrial buildings? What are the affect of terrorist blast on the design of the building? What is difference between the terrorist and industrial blast criteria? How the same parameters are applied for design of the blast resistant buildings? How can we plan safer cities by designing blast resistant buildings? Some of these questions are investigated in this research.

Generally, the blast by terrorist attack are conducted by car bombs, TNT packages, suicidal human bombs or grenade attacks. However, in case of industrial establishment, the blast happens mainly due to the operational structures like hydrogen units or inflammable cylinders. As per the IS code 4991 (1968) similar design criteria is used for all types f buildings. Hence, in this research model process is illustrated through a project designed in industrial establishments.

2 Blast Resistant Design Criteria

The blast resistant criteria for the design of the building requires understanding of loading due to car bombs, TNT packages, grenade or suicidal human attack. Some of the affect of the blast are flying splinter and heat that affect buildings and human life. Also, the blast can affect the breaking the facade glazing, cause communication failure and cut off the power leading to panic during the blast. The criteria for the design of the blast resistant building can be structural and architectural design.

The structural design criteria includes the design of blast load of the building. The important structural components that require to design the blast load are the retaining wall, foundation, columns and slabs. In many cases the blast resistant building is considered as a box concrete shape to reduce the impact on the building. In India, the IS Code 4991 (1968) provides the design criteria for the buildings. The major criteria for the design includes the affect of the rapidly moving shock waves during the blast. This shock waves affect the building at the peak intensity. Significantly, this peak intensity last for short time and causes major damages to the structure. The exterior surfaces in direction of the blast faces the main load. This load is then transmitted in the beams, columns, and slabs. In case, load is not sustained by the members, then the failure of the structural members affect the human life. Human life is affected by the broken structural members fallen due to the peak period blast. As all this impact happens in a short time, it becomes difficult for humans to survive during the blast. So, to reduce this impact, building is design like a cohesive unit. Each structural components plays an important role in reducing damages to the human life. Peak overpressure and maximum impulses are mainly dependent on the distance to the explosion, the blast waves angle of incidence, and the flow resistance of the structural

shape. The urban form of the building and urban set up can highly reduce the effect of the blast on the building [1]. In many structure, the facade is treated with the blast wall. This blast wall reduces the impact on the other structural members. Moreover, the structural components are permitted for higher deflection within the plastic range of materials.

The architectural criteria for the design of the blast resistant building includes site planning, orientation of building, layout planning, facade design, ergonomics and building services. In cities, old buildings or new buildings buildings are affected by the terrorist blast. Some times many important institution use old buildings in down-town area. In such buildings, there is very less passage between the road and the building. However, the newly planned building, it become easy for undertaking site planning. So, in case of the old building, the parking is avoided in front of the building. However, it is advisable to keep the parking across the road. Buildings are also protected by using bollards, and pavement to avoid pedestrian movement. In a project of the Embassy building in Yangon, Myanmar, the pedestrian paving around the building was designed in Reckli formliner with spikes. So, the movement of the pedestrian can be avoided around the building. Also, the facade was treated with blast resistant doors and old glass windows were replaced with bast proof glass. The glass was also designed with one side opaqueness to avoid the visibility of the pedestrian inside the building. In case of the planning a new building, the facilities can be divided into the safety zones. Also, large open spaces can be planned in front of the buildings. Parking spaces are kept away so that the cars do not reach the buildings. This criteria reduces the source of the blast on the building. The building orientation during site planning include exposing the blast wall towards the source of blast. Layout of the building is not preferred as irregular shape. Because it causes more damages during the blast attack. A regular geometry permits load transfer through all the structural members of the building. Some of the challenges for the architects and engineers are the design of facade for the blast resistant design. Generally, the shock wave causes breakages to glass in building. So, to overcome this challenge, use of glass need to be avoided in the buildings exposed to the blast. A building façade is considered to be the first barrier of resistance against explosion waves, and therefore a building facade has an important role in reducing a building's vulnerability and human casualties. In case of a lack of enough resistance, explosion waves enter a building and bring about irreparable damage to the building [2]. In many structures, wall cladding are attached to the structural system, therefore the blast reaction from the edges are being transferred to the structural system [3]. This reaction is function of ductility and fundamental time period of wall cladding. Ergonomic plays an important role inside the building for the operation and human activities. It is particularity observed that the activities and furnitures shall be user friendly to reduce the panic after the event of the blast. Finally, it is indeed important to design the building services like water supply, electrification, drainage and sanitation to reduce the impact of the blast. Out of these services, electrification plays also an important role. Because during the blast, the cut off of electricity causes panic. So, concealed type of wiring in steel conduits are provided in the blast proof buildings.

3 Building Profile

The proposed blast resistant building is located at 30 m from the source of the blast. The building is 8.9 m long and 10.70 m wide (Figs. 1, 2, 3, 4 and 5). It is planned as single storey building in Reinforce Cement Concrete (R.C.C.). The bare charge of 100 kg was consider as per the IS code 4991 (1968). Building includes two rooms, pantry and toilet organised for the operations for controls of the industry. The structural elements are designed as follows: (a) wall thickness of 400 mm, (b) columns of size 400 mm x 500 mm, and (c) beams of size 400 mm x 600 mm. The building height is 4.0 m from the floor bottom to slab bottom. The entry is planned in a protected way. So the shock waves do not affect the entry and rooms inside the building. Internal wall are made of 9 in. thick brick masonry. The raft foundation of 1.0 m depth was proposed as per the design criteria of the blast resistant building.

The interior of the building is planned with concealed electrification. Use of false ceiling is avoided in the building. Ergonomics was proposed as per the safety of the blast proof building. No openings were provided in the building, however, Variable Refrigerant Volume (VRV) air conditioning system was provided for effective air circulation inside the building. All the VRV indoor units were planned to be floor mountable than ceiling mounted (Table 1).

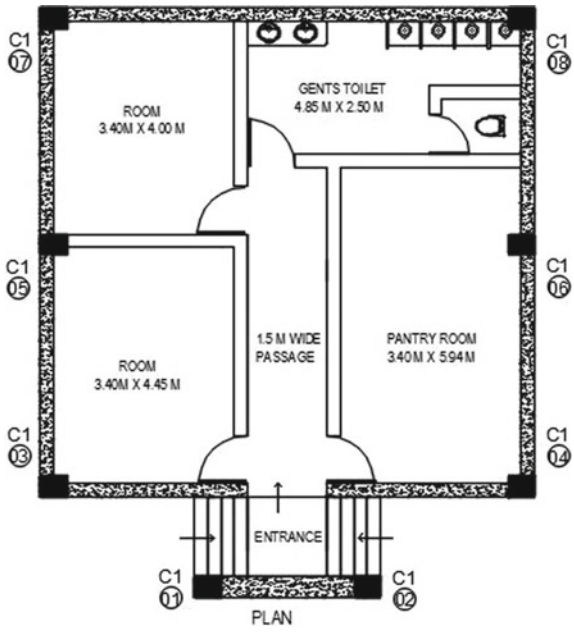

Fig. 1 Plan of blast resistant building

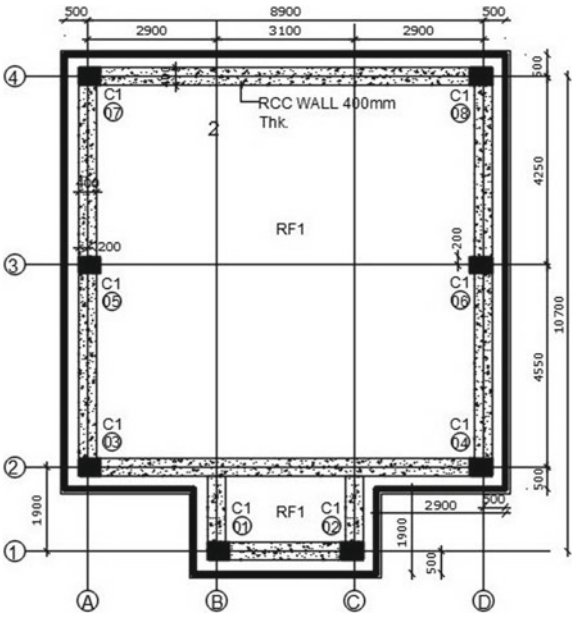

Fig. 2 Plan of plinth level blast resistant building

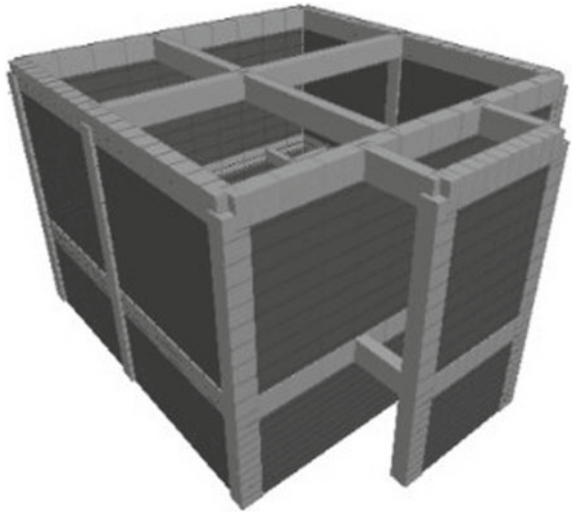

Fig. 3 3D model of blast resistant building

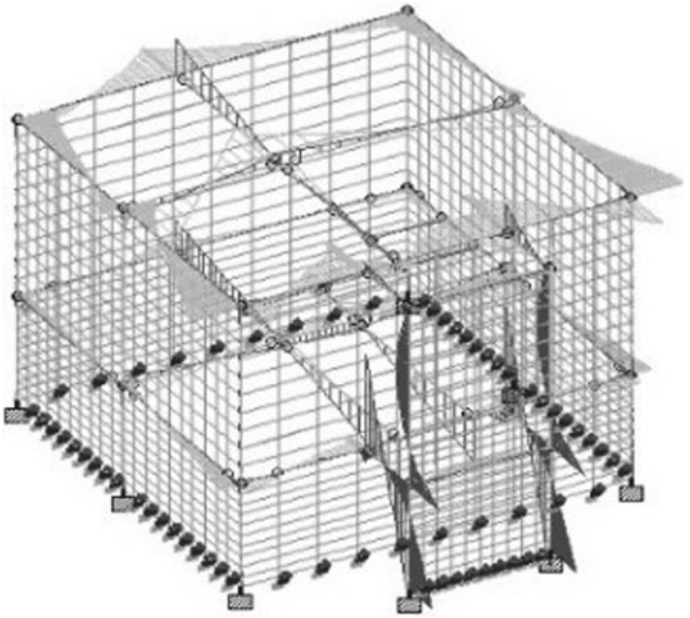

Fig. 4 Image showing load 8 bending at Z axis

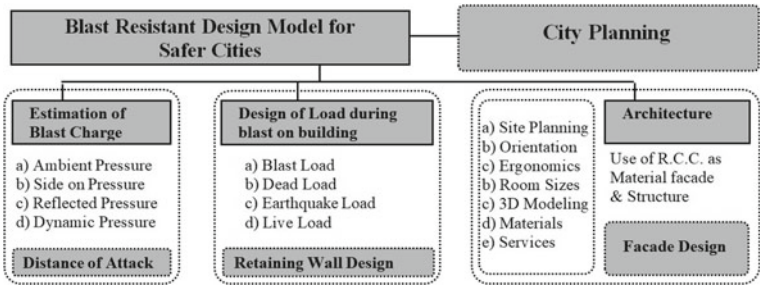

Fig. 5 Model of blast resistant design

Table 1 Minimum wall thickness in cm

S/N	Material of Wall	Charge of 50 kg	Charge of 100 kg
1	R.C.C.	30	38
2	P.C.C.	34	45

4 Load and Blast Pressure—The Model

The proposed building model for the blast resistant design could be illustrated as: (a) estimation of charge on the building, (b) design for load during the blast, and (c) architectural design (Fig. 6). The estimation of the charge depends on the distance of the blast. As the distance increases, the blast waves on the building reduces. Also, the the transfer of the blast waves inside the building reduces. So for 0.1 Tonne explosion and a building of 4 m height, estimation of charge of blast is Distance $x = 20/(0.1)^{1/3}$. The proposed model building is located at a distance of 30 m. However, in case of the terror attack the distance may reduce for the building. In case the buildings are away from the road, the distance increase. Similarly, the blast can also happen inside the building. The ambient pressure (Pa) is assumed as 1.00 kg/cm^2. The interpolation is between 42 and 45 m. Some other important considerations are: (1) peak side on pressure (Pso), (2) Peak reflected over pressure (Pro), and (c) Peak dynamic pressure (qo). The time for positive phase of grade on pressure is represented by To. Td is duration of equivalent irregular pulse. The value of To and Td are multiplied by $(0.1)^{1/3}$ to get the values of respective quantities for actual explosion at 0.1 Tonne charge. After, this mach number of incident shock front is determined by formula $M = \sqrt{1 + \frac{B}{7} - \frac{Pso}{Pro}}$. If U is shock from the velocity and a is velocity of sound in air, then U = M x a. U gives the pressure on the building. The Tc represent the clearance

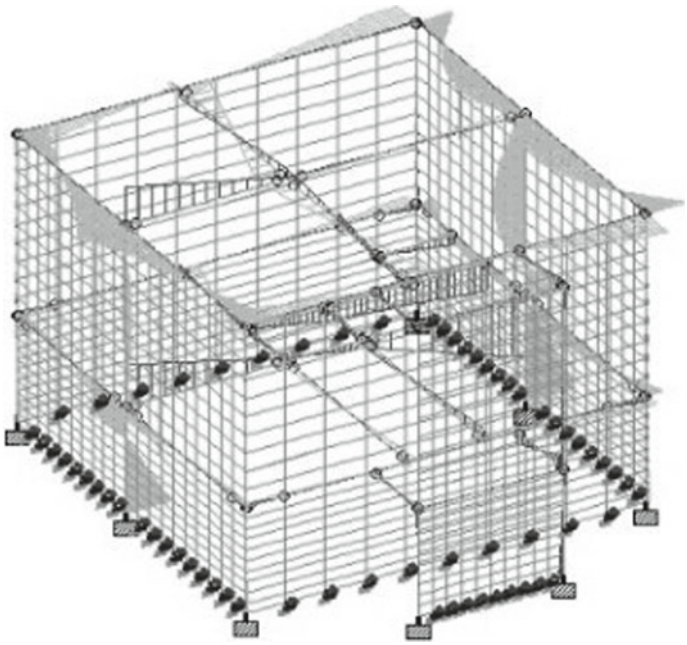

Fig. 6 Image showing load 10 bending at Z axis

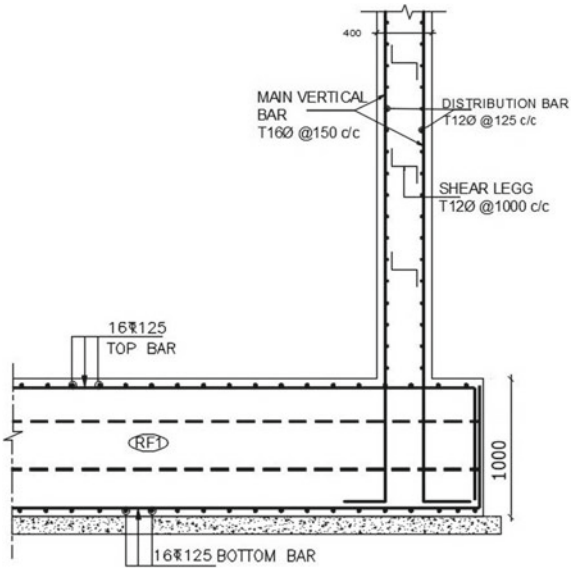

Fig. 7 Plan showing design of retaining wall and foundation

time, Tt represent the transit time, and Tr represent the pressure rise time on the back face. Hence based on this, the intensity of the blast is estimate. This similar model can be used to determine the charge of the blast due to terrorist attack. The distance can vary as per the situation of the blast. Along with the estimation of the charge on the building the wind load, earthquake load, live load and blast pressure in considered for design (Fig. 7).

For 0.1 Tonne Explosion

H = 4 m,

Building at 30 m from ground zero

Estimation for charge of blast

Distance $x = 30/(0.1)^{1/3}$

$= 64.65$ m

Assuming ambient pressure

$Pa = 1.00\ kg/cm^2$

Interpolation between 42 & 45 m

For scaled distance

$P_{so} = ?$

$$P_{ro} = ?$$

$$q_o = ?$$

(1) P_{so} = Peak side on pressure

$$= 0.76 + (0.68 - 0.76)/(45\text{-}42) \times (64.65 - 42)$$

$$P_{so} = 0.35 \text{ kg/cm}^2$$

(2) P_{ro} = Peak reflected overpressure

$$P_{ro} = 0.81 \text{ kg/cm}^2$$

(3) q_o = Peak dynamic pressure

$$q_o = 0.042 \text{ kg/cm}^2$$

The scaled time 'T_o' (Time for positive phase of grade on pressure)

$$T_o = P$$

$$T_o = 37.71 \text{ ms}$$

T_d = Duration of equivalent irregular pulse

$$T_d = 28.32 \text{ ms}$$

Values obtained $T_o$and T_d are multiplied by $(0.1)^{1/3}$ to get the values of respective quantities for actual explosion at 0.1 Tonne charge

$$T_o = 37.71 \times (0.1)^{1/3}$$

$$T_o = 17.50 \text{ ms}$$

$$T_d = 28.32 \text{ x } (0.1)^{1/3}$$

$$T_d = 13.15 \text{ ms}$$

M = Mach number of incident shock front

$$M = \sqrt{1 + \frac{B}{7} - \frac{Pso}{Pro}}$$

$$M = 1.14$$

$$a = 344 \text{ m/s}$$

a = Velocity of sound in air

U = Shock from velocity

$$= M \text{ x } a$$

$$= 392.00 \text{ m/s}$$

$$= 0.392 \text{ m/ms}$$

Pressure on Building

$$H = 4.0 \; B = 9.2, \; L = 29.80$$

$$S = \frac{1}{2} \text{ B or H whichever is less}$$

$$S = \frac{1}{2} \times 9.2 = 4.6 \text{ or } S = 4$$

Hence, $S = 4.0$

T_c = Clearance time

T_t = Transit time

T_r = Pressure rise time on back face

$$T_c = \frac{35}{U} = \frac{3 \times 4.0}{0.392} = 30.61 \text{ ms} > T_d$$

$$T_t = \frac{L}{U} = \frac{29.80}{0.392} = 23.72 \text{ ms} > T_d$$

$$T_r = \frac{45}{U} = \frac{4 \times 4.0}{0.392} = 40.81 \text{ ms} > T_d$$

For roof and side $C_d = 0.4$

$$C_d = 0.4$$

$$P_{so} + C_d \text{ x } q_o = 0.35 + (0.4 \times 0.042)$$

$$= 0.3332 \, \text{kg/cm}^2$$

5 Cities and Terrorist Attacks

Many cities across globe are affected by the terror attacks. In history, the attach of terror has been on many important cities. In year 2008, Mumbai, India underwent series of terror attack by shooting and bombing important places. These places were Taj Mahal Hotel, Oberoi Tirdent Hoel, Leopord Cafe and other places. In these blast, hand grenades were used and it effected the interior parts of the buildings. The quantity of illegal arms and explosives seized from the different centres and groups indicate that terrorists are sufficiently equipped to strike terror in big cities. The targets have also been expanded to important strategic locations [4]. Usually Terrorists choose their targets to maximise the impact of their attack, or rather its consequences, and minimize the efforts [5].

The terror attach also affect the urban economics and urban renewal. If the price of space after the destruction is not high enough to cover the costs of new construction, then the direct impact of bombing will be permanent [6]. In cities, the distance of the blast from the building play an important role in the destruction and loss of human

life. In Murrah Building in Oklahama, detonation was equivalent of 4000 pounds of TNT at a stand-off distance of approximately 15 ft and in many urban locations, it would be possible for smaller vehicles to park even closer to a building than the distance in the 1995 bombing [7]. In the cities, the landuse and zoning regulation is important to reduce the affect of terrorist attack. The protection of buildings or quarters is still possible if there is a clear use with access controls. It becomes difficult when there are mixed uses [1]. These can be achieved with planning a special zones with separate regulation in planning process. City builders—including architects, urban planners and designers—are increasingly expected to consume and, through practice, to re articulate the risk-and-threat discourse in concrete forms [8]. Thus, the R.C.C. structure are most safe and ductile for the erection of blast resistant building in urban areas. Some other planning consideration involved in cities are landuse patterns. Public lands should be combined with dwellings and greenery, but an overload in the shape of different land uses, especially in city centres and local city centres, should be avoided [9].

6 Conclusions

Thus blast resistant building illustrated in this research indicate a model method of: (a) estimation of intensity of blast, (b) design of retaining wall, and (c) architectural design. The estimation of intensity of blast depends on the distance and intensity of blast. Some of the important criteria while estimation are the mach speed and ambient pressure. The design of wall thickness is the most important criteria. Also, it is important to look into the external cladding, interior and ergonomic for the design.

The cities across the world are continuously affected by the blast. Some significant building are the public administration buildings, luxury hotels, Embassy building and world trade centres. In making safer cities, it is indeed important to look for blast resistant building design that avoid damages due to blast attack. The proposed model building indicates the various parameters for design of the blast resistant building. Such, model method can be applied on design of the blast resistant buildings to make safer cities.

References

1. Gebbeken N, Doge T (2010) Explosion protection architectural design, urban planning and landscape planning. Int J Protect Struct:1–22
2. Hasheminasab H, Zolfani SH, Bitarafan M, Chatterjee P, Ezabadi AA (2019) The role of Façade materials in blast-resistant buildings: an evaluation based on fuzzy Delphi and fuzzy EDAS. Algorithms 12:119
3. Singh J, Roy A (2015) Thickness of concrete and steel front wall claddings for various blast pressure in blast resistant buildings

4. Khurshchev Singh T (2006) Terror trends: mega cities, maximum impact. Strategic Anal 30(3):655–661
5. Matijosaitiene I, Petriashvili A (2017) Urban planning and design for terrorism resilient cities. J Sustain Archit Civ Eng:27–38
6. Glaeser EL, Shapiro JM (2002) Cities and warfare: the impact of terrorism on urban form. J Urban Econ 51(2):205–224
7. Federal Emergency Management Agency (FEMA) (2013) Blast-resistance benefits of seismic design—phase 2 study: performance analysis of structural steel strengthening systems. CreateSpace Publishing
8. Coaffee J, O'Hare P, Hawkesworth M (2009) The visibility of (in)security: the aesthetics of planning urban defences against terrorism. Secur Dial:489–511
9. Stankevice I, Sinkiene J, Zaleckis K, Matijosaitiene I, Navickaite K (2013) What does a city master plan tell about our safety? Comparative Analysis of Vilnius, Kaunas, and Klaipeda, Social Sciences

Design of Facade for Blast Resistant Buildings

Prafulla Parlewar

Abstract The facade of blast resistant buildings are important for safety during the event of blast in cities and industrial complexes. The design of these buildings includes design of blast wall and estimation of intensity of blast. Blast wall plays significant role in reducing the blast waves on the building. Generally, this blast wall faces towards the source of blast. Significantly, these are main facades of the building viewable by visitors. So, it is indeed important to design these wall to make aesthetically appealing for visitors. Many of these building are located at important locations in cities and industrial complexes. So, making a landmark design is required for these types of the buildings. The research here illustrate a design of facade for the blast resistant building with use of innovative material made from concrete by use of polyurethane formliner. Moreover, it looks into the questions like how the blast wave affect the exterior of building? How to rehabilitate the old building facade? How concrete can be used as a material for making aesthetic in blast resistant building? Furthermore, it also illustrate the design criteria for the blast resistant buildings with emphasise on the architectural design.

Keywords Blast resistant design · Blast design code · Blast facade design

1 Introduction

The facade is the most important part of the blast resistant building. Because during the impact of blast the facade resist the pressure, heat and fire. In building, facade are treated with concrete, glass, metal and many more types of materials. But, most of these materials are fragile to the intensity of the blast. Fragile materials causes the human casualties and damages to the various parts of building during the blast. In such events, what can be most appropriate material for design of facade of blast resistant buildings? What are the methods to rehabilitate the existing facade of blast resistant buildings? How can blast wall of facade behave during the blast? How can we design a landmark building for resisting the blast? What are the important

P. Parlewar (✉)
City Development Corporation (P) Ltd., Mumbai, India

J. M. P. Q. Delgado (ed.), *Masonry: Building Pathologies and Design*, Building Pathology and Rehabilitation 22, https://doi.org/10.1007/978-3-030-80496-1_2

criteria for the aesthetic improvements of blast resistant buildings? Some of these questions are investigate in this chapter. Furthermore, a project in industrial complex is illustrated for its design for rehabilitation of facade. The blast proof building was designed as per the IS code 4991 (1968) with blast wall of 380 mm thick. The building is a significant building in the campus of petrochemical complex. So, building was designed as a visual landmark with visibility in day and night (Figs. 5 and 12).

In industrial complexes, blast resistant building generally looks like plain concrete boxes. Many industrial complexes maintain the architectural design of the buildings to improve the aesthetic of overall complex. However, design of blast resistant facade remains challenging to many designers in these industrial complexes. Also, during the terror attack, the facade remains an important element affected during the blast. So, the building suspected for the terrorist attack in cities requires special design consideration for facade. If innovative materials are not used in facade, then the aesthetic and structural criteria can not be designed in the blast resistant buildings. So, how to design the facade of blast resistant buildings? What are the innovative materials for the design of the facade to resist terror attack? Concrete by use of polyurethane formliner is one such material which provides strength and aesthetic for the blast resistant buildings. This material is supplied by many companies. Once such company is know as Reckli located in Germany. Often precast concrete components are more aesthetically pleasing than cast-in-place components. Additionally, precast concrete can be more economical than cast in-place concrete. Since precast components can be made with the same formwork repeatedly, the cost for constructing the component drops [1].

The literature on facade design of blast resistant building worldwide indicates that designers emphasise on making explosion proof glazing systems. However, in this research a practical approach is suggested for making the blast resistant design in concrete. Some authors have indicated that glass is in general also the most fragile part of a structure and its failure results in splinters that could seriously injure persons inside the building [2]. When air blast pressure fracture window glass, flying and falling glass shards pose a major hazard to anyone in the proximity [3]. It is indeed important that the design of exterior window systems and cladding need to provide higher or equal resistance to lateral-load than the transparency or panel for the framing, connections and supporting structure [4]. If building facades disintegrate, the direct blast pressure entering the building can cause injuries to occupants and even structural collapse. Blast-resistant glazing should therefore be used in buildings to minimize, if not eliminate, the hazard from potential terrorist attacks [5].

A building facade is considered to be the first barrier of resistance against explosion waves, and therefore a building facade has an important role in reducing a building's vulnerability and human casualties. In case of a lack of enough resistance, explosion waves enter a building and bring about irreparable damage to the building [6]. Moreover, some author has also explained that progressive collapse is the most serious consequence of blast loading [7]. Threats to building occupants due to blast loads generally result from a combination of blast overpressure injuries due to a breach of the facade system and glass fragmentation injuries. In petrochemical facilities, the effect is very large and not limited to only one structure and the

complete facility is at the stake if a control building collapses in case of blast [8]. In general the facade can be seen as a system capable of transforming the blast input duration and peak pressure over a different combination of the two parameters, but for the majority of cases without significant changes to their product (impulse) [9]. Aluminium foam retrofitting is a methods tried in old building. But the construction method of the reinforced wall significantly enhanced its performance sustaining blast loads, even without protection by the aluminium foam [10]. The literature indicate that the facade is the most important part of building to stop the spread of effect of blast waves inside the building. Furthermore, it can be stated that brittle materials like glass can not be accepted in the blast resistant buildings.

2 Building Profile

The rehabilitation of building in industrial complex included a main control room used for the production of lubes. It was designed as the blast resistant building. The main purpose of the building is to sustain the operations during the event of the blast. So, building was designed as per the IS Code 4991 (1968). The ground zero was located at 20 m from the building. Hence the building was designed with 380 mm thick blast wall.

The rehabilitation master plan included following components: (1) complete rehabilitation of exterior facade as an landmark in the industrial campus, (2) revitalization of the internal offices, pantry, toilets, and store rooms, and (3) rehabilitation of main control room and server room. The external facade rehabilitation was main goal of the master plan for redevelopment of the building. The length of the facade is 40 M $\times$ 22 M. The building at the time of rehabilitation was more than 35 year old. Due to rain and weather conditions, it is expected that the R.C.C. blast wall must have undergone substantial corrosion. Also, strength of the concrete is reduced than the original strength. The compressive strength on the blast walls was found to be 22.56 Mpa during the rebound hammer test. However, strength in the roof was in range between 50.01 and 77.47 Mpa. Ironically, this observation shows that the strength of the concrete is reduced in wall and columns due to the weather conditions. But the strength in the slab had remained unchanged due to the water proofing on the slab. This indicated the necessity to rehabilitation of the facade.

The concept of the rehabilitation was to make aesthetically appealing exterior and add strength to the blast wall. Hence the rehabilitation was proposed in concrete designed from polyurethane formliner. The proposed concept included in situ and off site concrete to give additional strength to the walls. The second part of the rehabilitation of the project involved revitalization of office, pantry, toilets and store rooms. This area were designed by making two zones: (1) zone for offices and stores, and (2) zone for pantry and toilets. The offices were planned with open working environment. A conference hall was placed in center of the office space. The third part of rehabilitation involved control room and server room. The design of these

rooms were undertaken by using metal wall panelling and ceiling system to avoid damages to operation during the impact of blast.

The facade of the original building was plain R.C.C. wall without any facade treatment. In case of blast resistant facade in R.C.C., the surface are exposed to direct weather conditions. Generally, concrete is highly permeable for rainwater. So, rain water percolates inside the R.C.C. walls. This causes damages to concrete and reinforcement. In these conditions reinforcement become brittle and major strength is reduced of the concrete. Also, the composition of concrete changes with percolation of waster in R.C.C. walls. Thus, it is important to treat the R.C.C. blast wall with concrete to add strength.

2.1 Rebound Hammer Test

The rebound hammer test indicate the compressive strength of the concrete. The test was conducted on the slab and wall of the building to understand the present scenario. The test was conducted at the equal intervals and average of the rebound was studied for compressive strength of the building. The five point on the wall were taken for studies. The test indicated that the rebound reading was 22.56, 28.44, 32.36, 24.52 and 28.44 Mpa on the wall. Thus, the average strength was 27.26 Mpa. Whereas, reading on the slab were 59.82, 63.74, 63.74, 50.01, 55.90, 63.74, 63.74, 50.01, 55.90, 63.74, 77.47, 61.78, 61.78, and 67.78 Mpa on slab. So, the average strength was found to be 60.93 Mpa. As compared to the strength of the slab, the strength of the wall is found to be less. Hence, the compressive strength is reduced of the blast wall.

3 Facade Blast Pressure

The important criteria to understand the blast resistant building facade is the pressure during the impact. In the analysis of facade of the blast resistant building the yield of the explosion from the ground zero play an important part of the design requirements. Also, the distance from the ground zero reduces the pressure on the facade. The peak initial pressure is indicated as P_{so} act mainly during the blast. On the facade of the blast proof building, the pressure rises instantaneously. So, the peak dynamic pressure q_o also rises instantly and affect the facade surface. During the blast, the shock wave moves outward in all directions in high speed and then a negative phase is followed creating a suction effect. At the time of blast effect, the waves create an impulse which spreads spherically and negatively affects some of the beams and slabs above at counter-gravity direction (+Y). It means, negative bending moment occurs at the midspan of the beam, and positive bending moment occurs at the beam-column connection parts. This kind of load is the most critical situation for reinforced concrete [11]. Blast load design is complex problem and cannot be made separately

for each building element [12]. In order to mitigate the effects of explosions, the facades are first to be designed against conventional loads and then to be verified against explosive loads [13].

4 Facade Design

The facade design of blast resistant building can be understood in architectural and structural components. As the blast waves first reaches the facade, it is important to estimate the impact of blast on the facade of the building. Similarly, to resist this blast wave, materials with stable strength are required for the blast resistant buildings. R.C.C. is one such material which can be used for facade treatment in the blast resistant buildings.

The concept of facade design included making an landmark building with aesthetic appeal during day and night time. It is an important building in the industrial camplex. So, it needed a new facade makeover to show its significance in the industrial complex. Significantly, this building include offices and control room of the lube production in side the complex. The concept of architecture design was to exhibit the various lube products in the exterior in an abstract text art (Figs. 1, 2, 3, 4, 5, 6, 7 and 8). This concept is developed by using in situ concrete in polyurethane formliner.

These formliners gives exposed concrete facade a unique visuals. The in situ and off site precast techniques consist of use of poly urethane elastomer material. It has high flexibility and elasticity. This allow a clear release of the pattern on the concrete. It can make an exact reproduction of patterns as designed by the architect. The poly urethane formliner is cut to fit the formwork frame. Important care is taken to keep away the air cushion in the formliner while casting the concrete. Reinforcement is placed and ready mix concrete is mechanically placed inside formwork work. Sufficient vibration has to be undertaken by vibrator to reduce the air cushion. However, the frequency of the vibrator has to be low to avoid damage to the formliner.

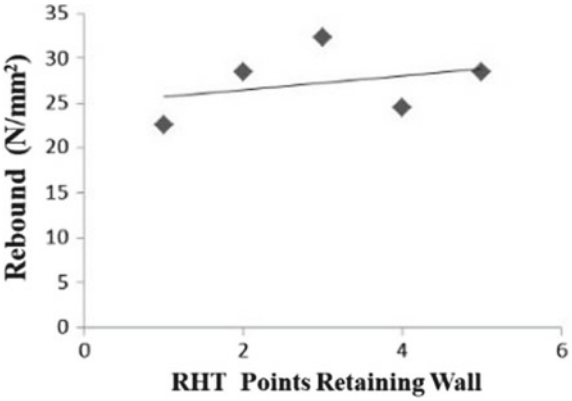

Fig. 1 RHT of blast wall

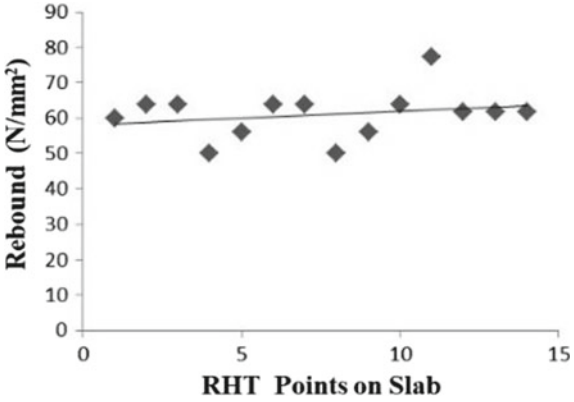

Fig. 2 RHT of slab

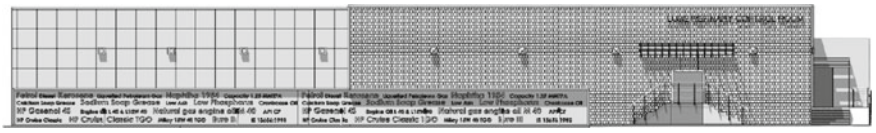

Fig. 3 Front elevation of building

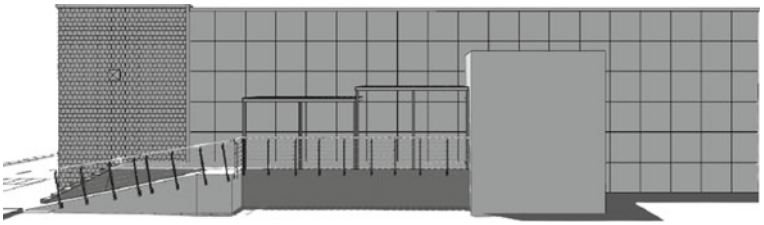

Fig. 4 Side elevation of building

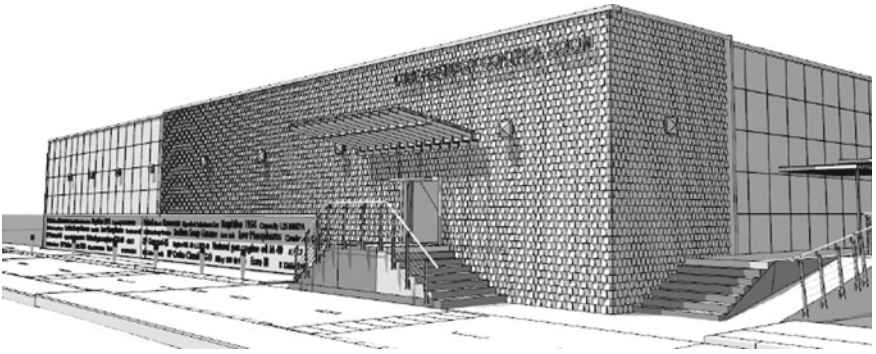

Fig. 5 View of building

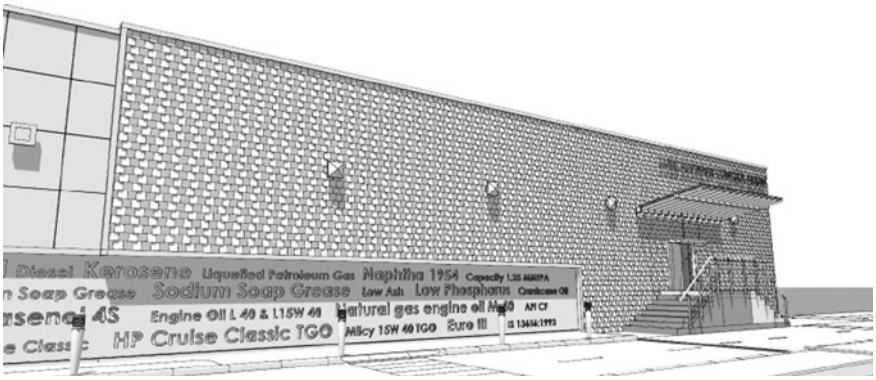

Fig. 6 View of front facade of building

Fig. 7 View of in situ text art in front facade of building

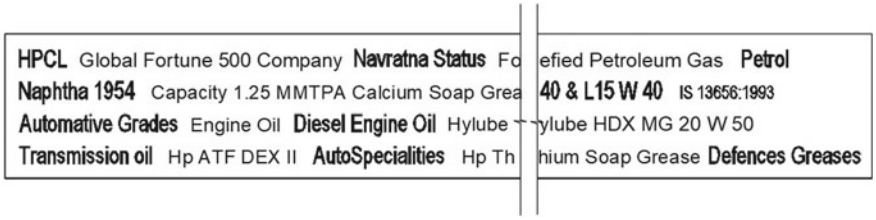

Fig. 8 Elevation of in situ text art

The facade have three types of concrete elements by using polyurethane formliner: a) in situ casting of concrete and b) offsite casting of concrete. The in situ casting of the concrete include the casting of text art in the facade. The text art is created on the surface of the blast wall of the building. The formliner for the text art is supplied by the Reckli. After, reaching at the accurate drawings, the formliners are manufactured in the factory and supplied at site. The polyurethane formliner are light weight and easy to install. The total size of the text pattern proposed was 28.8 M x 2.0 M. The casting was proposed one signal formliner. So, a formliner of size 29.00 M $\times$ 2.2 M was proposed for in situ casting. Generally, formliner are pasted with adhesive on the form work . So, after placing the form work, concrete is poured and compacted. Once the formwork is removed from the wall, the text art pattern appears on the blast wall. After removal of the formwork the finishing and curing is undertaken for the text pattern. The in situ concrete became a cohesive mass with the old blast walls. Thus, improving the strength of the blast wall. After the concrete reaches its strength, it is expected that the impact of the blast will be resisted by the cohesive mass. Significantly, provision of such facade treatment have advantage of providing additional strength to the blast wall. Age of the building is about 35 years. It is expected that the strength of the wall may have been reduced due to weather conditions. It was evident in the rebound hammer test that the strength of the concrete is reduced from original. Some of the important effect on the R.C.C. wall and slabs are the corrosion of reinforcement due to the weather conditions. This corrosion in concrete is not visible and sometime cannot be estimated easily. So, it it important to add the strength to the concrete by undertaking such in situ treatments. Hence, such concrete design provides aesthetic and structural strength to the facade of blast resistant building.

The second element of the design of the facade of the blast resistant building is use of off site cast tiles (Figs. 9 and 10). The predetermined patterns are easily available from Reckli. So, numerous patterns can be used in the exterior of the building. As an addition on the surface of the building, various patterns can be used on the main facade of the building. These are off site cast tiles prepared in high grade concrete. This act as an additional surface barrier during the impact of the blast. The off site casting of Reckli is relatively easy. The tiles in the project were casted in 1.0 M $\times$ 1.0 M size with 10 cm thickness. The process of the casting of the tiles include preparation of formwork. The polyurethane formliner is pasted with adhesive on the surface of the form work. The 1.0 m x 1.0 m frame reinforcement is placed as per the design criteria. The concrete is mechanically placed and careful compaction is done to avoid damages to the formliner. Once the formliner is removed, the pattern get imprinted on the concrete tiles. The concrete tiles are cured for more than fifteen days. This formliner is used for multiple repetitions. Hence, multiple casting of the tile can be undertaken.

These tiles are erected on the facade by use of M. S. tube framing. Frame of 1.0 square metre was used on the blast resistant wall. During the casting of the tiles, the fasteners are pre-inserted for joining the tiles on the framing system. The pipe size used in the framing was 110 mm $\times$ 110 mm. The tiles were placed in layers starting

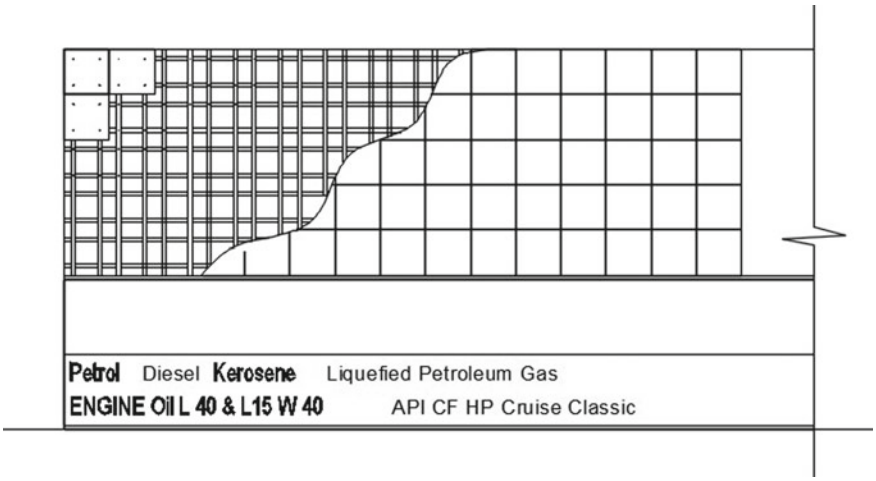

Fig. 9 Detail of facade of Building

Fig. 10 Detail section of front wall (**a** 380 mm thick blast wall, **b** off site cast tiles, **c** in situ text art, and **d** slab)

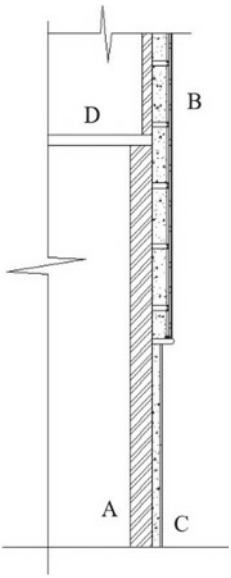

from the bottom till the end of top. Finally, the tiles are finished at joineries to finish the surfaces.

The aesthetic assembly of the facade was organised with plain tiles, irregular tiles and text art. This assembly encourage aesthetic contrast of the shapes i.e. plain and irregular. So, this aesthetic contrast make the facade appealing to the viewer. The facade was also having text pattern as a focus or focal point. This focus is eye catching for any visitor and it make the reader involved to read the various products

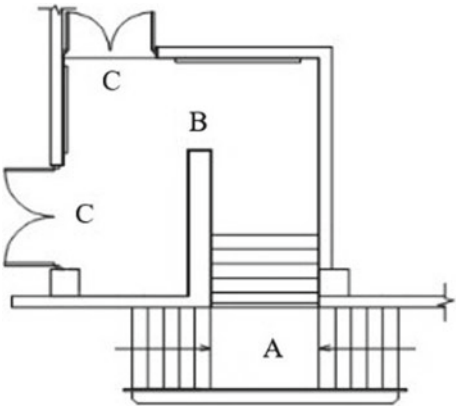

Fig. 11 Plan of Entrance Lobby (**a** Steps, **b** blast wall, **c** entry, and **d** entry

and important in the text art of facade. These type of text art makes the facade interactive with human psychology. Finally, the entrance to the building is designed as a second focus and attraction to make visitor perceive the aesthetic easily.

The entrance lobby in the facade is designed such that it reduces the impact of the blast inside the building (Fig. 11). This is done by making a barrier wall partition in R.C.C. in the lobby. So, a person need to take a turn while entering inside the building. Significantly, this reduces the impact of blast wave at the main operation of the building. Koccaz had indicated that the foyer areas should be protected with reinforced concrete walls; double-dooring should be used and the doors should be arranged eccentrically within a corridor to prevent the blast pressure entering the internals of the building [14].

5 Conclusions

The facade is the most important part of the blast resistant building. Because it is the first part of building which resist the pressure and impluse to reach the other parts of the building. In many old and new blast resistant building, innovative material are required in facade for resisting the blast wave. In urban areas, glass is predominantly used as a facade material. Also, in many buildings steel is used toward the blast wave. Glass can not be fully treated to resist the blast source. Moreover, use of steel is also acceptable due to the extensive heat generated during the impact. Because the steel members during the extensive heat condition can lead to failure of the building. During the blast, for very short time extreme intensity heat is exposed to the bast surface. So, steel and glass both can be potentially hazardous materials as it causes human causalities. Some of the advantages of the design of facade by using the concrete in polyurethane formliner are summarised as follows:

Fig. 12 View of building during night

(a) The design of facade in polyurethane formline provide multi options of design for old and new facade of the blast resistant buildings. The old facades can be aesthetically integrated to make an landmark building in cities and industrial complexes.
(b) The design of facade can be undertaken with in situ and off site casting of the concrete. Both have its own advantages. The in situ casting provide direct connectivity with the blast facade. Moreover, it directly add to the thickness, strength and resistant of the wall. Whereas, the off site concrete cast is more flexible to make tile of required sizes and install on site.
(c) The most important advantage of this type of technique is strength of structure for mitigation of pressure and impulse during the event of the blast.
(d) In overall, it can be summarized that the aesthetic consideration are one of the important part of the design of the facade of the blast resistant building. So, integrating it with the aesthetic and structural requirement make the building landmark in cities and industrial complexes.

Hence, innovative material like concrete casting from polyurethane formliner can provide better solution for facade of blast resistant buildings. Indeed, in situ casting of concrete in polyurethane formliner provides additional thickness and strength to the blast wall.

References

1. Giovino G, Olmati P, Garbati S, Bontempi F (2014) Blast resistance assessment of concrete wall panels: experimental and numerical investigations. Int J Protect Struct 5:348–366. https://doi.org/10.1260/2041-4196.5.3.349
2. Martin L, Michel A, Chiara B, Doormaal J, Christof H, Husken G, Millon O, Saarenheimo A, Solomos G, Thamie L, Valsamos G, Williams A et al (2016) Design of blast-loaded glazing windows and facades: a review of essential requirements towards standardization. Adv Civ Eng 2604232:14. https://doi.org/10.1155/2016/2604232
3. Norville H, Conrath E (2001) Considerations for blast-resistant glazing design. J Archit Eng 7(3)
4. Okeke F, Chendo T, Sam Amobi C (2019) Resilient architecture a design approach to counter terrorism in building for safety of occupants. IOP Conf Ser Mater Sci Eng 640:012003
5. Hasitha D, Thambiratnam D, Perera N (2015) Design guidance for blast-resistant glazing. J Archit Eng 21(3)
6. Hasheminasab H, Hashemkhani Z, Bitarafan M, Chatterjee P, Abhaji Ezabadi A (2019) The role of facade materials in blast-resistant buildings: an evaluation based on fuzzy Delphi and fuzzy EDAS. Algorithms 12(6):119. https://doi.org/10.3390/a12060119
7. Mohamad N, Musa M, Ismail N, Yusof M, Husen H (2010) Damage evaluation procedure for building subjected to blast impact 39:326–335
8. Singh J, Roy A (2015) Thickness of Concrete and steel front wall claddings for various blast pressure in blast resistant. Buildings. https://doi.org/10.2118/175325-MS
9. Zobec M, Lori G, Lumantarna R, Ngo T, Nguyen C (2014) Innovative design tool for the optimization of blast-enhanced facade systems. J Facade Des Eng 2(3–4):183–200
10. Alsubaei FCF (2015) Performance of protective perimeter walls subjected to explosions in reducing the blast resultants on buildings. In: Electronic thesis and dissertation repository, 2976. https://ir.lib.uwo.ca/etd/2976
11. Sevim B, Toy A (2020) Blasting response of a two-storey rc building under different charge weight of TNT explosives. Iranian J Sci Technol Trans Civ Eng 44:568–577
12. Bedon C, Figuli L (2017) An overview on current methods and trends for enhancing the blast resistance and protection of existing windows. In: Proceedings of 21st international conference. Transport means
13. Keat A, Das A (2014) Blast-resistant design of facades. The Magazine of The Institution of Engineers, Singapore, pp 14–15
14. Koccaz Z, Sutcu F, Torunbalci N (2008) Architectural and structural design for blast resistant buildings

Application of Geometric Patterns in Architectural Design Process

Prafulla Parlewar

Abstract Geometric patterns in interior and exterior of building provides an appealing aesthetic. The chapter here illustrates a project for rehabilitation of the cafeteria in an administrative building. In this project the rehabilitation of old interior was undertaken through use of innovative aesthetic consideration of design. Geometric patterns are parts of design combinations used by many designers in exterior and interiors. The research here investigates how geometric patterns can be applied in the architectural design process? What is the process of rehabilitation in small spaces in buildings? How materials are designed in rehabilitation of interior spaces? What are the architectural considerations for design of interiors? How structural criteria are assessed before rehabilitation of old interiors? Indeed, it is important to combine aesthetic and structural knowledge in rehabilitation. So, the research here illustrates an application of hexagonal patterns in the architectural design process for rehabilitation of old interiors.

Keywords Building pathology · Architectural design process · Rehabilitation

1 Introduction

The rehabilitation of old building interiors requires innovative methods and architectural design which provide elegant ambience for visitors. In this rehabilitation process, it is important to analyse the building pathologies and develop architectural design for better aesthetic. The architectural design process for designing requires use of elegant materials. Once, such a project was designed by rehabilitation of an old cafeteria in Mumbai, India. This project included rehabilitation into a cafeteria for the Global Fortune 500 Company. The research here investigates the question on how to rehabilitate old buildings? What is a design process for redesign small spaces inside the buildings? How to apply the geometric patterns in the architectural design process? How do quality materials give good ambience in the interior spaces? The

P. Parlewar (✉)
City Development Corporation (P) Ltd., Mumbai, India

J. M. P. Q. Delgado (ed.), *Masonry: Building Pathologies and Design*, Building Pathology and Rehabilitation 22, https://doi.org/10.1007/978-3-030-80496-1_3

research thus illustrates a complete sequence of rehabilitation of a cafeteria used in a main administrative building.

The various literatures on the application of geometric patterns in the architectural design process have indicated the importance of aesthetics in the design process. Importantly, the earliest theories of Christopher Alexander have indicated the problem solving approach in the architectural design process. Alexander in his books "The timeless way of building" and "A pattern language" has introduced a theory and practical approach to architectural and urban design [1, 2]. Leopold [3] also investigated fundamentals for design processes, in order to escape from an arbitrary design and finding a rational basis for design processes. When we look back in the history of architecture, we can find the background of geometric structures as important fundamentals for designing, for example in symmetry concepts or using transformations. In Islamic architecture, patterns are extensively used as a part of interior design. The objective judgement of beauty can be used to explain the aesthetics of Islamic patterns; helping to understand the shape grammar and formal mathematical rules that generate these patterns beauty and strength. In addition, the subjective judgement of beauty can be applied to understand the aesthetic spirituality of users according to their personal experiences and imagination [4]. One of the main reasons that made geometric patterns widely spread in the Egyptian artistic and architectural domain is its major usage in most Egyptian traditional crafts, gifts, pottery, textiles, copper works, handmade jewellery, wood works and ceramics [5]. Attempting to humanize space should be the first priority for everyone and more so for the architect. In a civilization which is more or less urban, responsible for giving order to the living space. Accordingly city planners, policy makers, contractors, green-spaces specialists and artists are in harmony with architects, more or less responsible for creating consistency between man and his environment [6]. Jia [7] had identified how to apply CAD based patterns of traditional Chinese interiors in the redesign of the interior spaces. Some of the major observations found by them are the requirement of knowledge of the generation, inherent application scenario, material and processing methods and implicit cultural significance of traditional patterns used in the interior space based on their different features, analyzed there fixed and variable elements, for application for indoor environment. In the history of architecture geometric rules based on the ideas of proportions and symmetries formed fixed tools for architectural design. Proportions were analyzed in nature and found as general aesthetic categories across nature and art. Therefore proportions such as the golden section were seen as the power to create harmony in architecture as well as in art and music [8]. Leopold [9] also studies the use of geometry in art by Gerard Caris. He uses the geometric order structures for experiencing them in aesthetic compositional processes. In this way he explores many geometric relationships in an aesthetic expression.

Liotta [10] had worked extensively on use of patterns in Japanese architecture. He explains that the most mysterious forces in the universe manifest themselves via patterns, as they are a collector able to receive cosmic energy, metabolize and filter it, and finally release it in ordered shape back to life. Patterns can be seen as latent forms potentially ready to incarnate into tangible and intangible elements where there is no apparent structure, and also as connecting agents, able to articulate

space and to produce diversity and beauty. Liotta [11] has also undertaken studies on the work of famous Japanese architect Tadao Ando. He explains that that Tadao Ando thinks space by geometry aimed at evoking light and conceived to go beyond eternity; an impossible challenge, and for that very reason, one worth pursuing. Graphical analysis of the system indicates the presence of elements of the Fibonacci sequence, as the segments of the base, the facade construction, as well as the complete composition. The combination of continuous separation of the adoption of the form of pure geometric square, circle, rectangle in the definition of the elements of the composition produced are aesthetically valuable and monumental circuits which have become more representative models of contemporary modern architecture [12].

The design process for the rehabilitation of old interiors requires investigation on building pathologies, problem of spatial organization, study of building services and allied parts of the building. The design process of this rehabilitation includes a systematic architectural design process to identify the problems and building interiors. Such, investigation is conducted by study of old spatial configuration, materials and building services. Moreover, a design process is needed to achieve an accurate design. How is this design process developed to rehabilitate buildings? What is the role of using geometry to develop the architectural design of these buildings? Geometric pattern plays an important role in creating aesthetics in the design. From historic times architects and engineers have identified the various uses of geometry in the design of the buildings. The early human settlements in the prehistoric times use circular geometry to shape houses. As human civilization progressed, the architects and engineer developed theories to use geometry in the design of the buildings. During the Bauhaus school of thought in Dessau, Germany, geometric shapes played a significant role in the design of the building. In the post-modern architecture many architects used geometry as an important element for the buildings. Hence, design of the building interiors can be developed with an innovative process by developing geometry as a tool for the design. Our research is based on an executed project of design of cafeteria illustrating implementation and demonstration in practice. Generally, architectural design requires a problem solving approach in which design can be created for the best fit. This problem solving approach for rehabilitation of interior includes developing various design elements that can be used in geometry for the developing elegant interiors. Such a design process can be adapted in the rehabilitation of the interior of various buildings. So, the research argument simplifies a design process that can give a problem solving approach for practitioners for rehabilitation of old building spaces.

2 Project Profile

The project is a redesign of an old cafeteria in an industrial complex in Mumbai, India. The project component included study of the pathology of the build, its structural strength and quality of old materials. The total area of the project is 125 m^2. It includes a dining area, pantry and rest rooms. The project is located in the administrative

building in the industrial complex. It is also accessible easily on the ground floor by visitors. The key part of the project included entrance lobby, main dining space, pantry and restrooms. The ergonomic studies were undertaken in the dining and pantry for understanding the problems of the old design. Some of the critical points found were the inability of the pantry for processing and storing the food for customers. Also, there were inadequacies of the spaces for keeping the various materials during the functioning of the pantry. The old pantry shape, size and height were also not sufficient to undertake the ergonomic operation for keeping the flood materials in the pantry platform. Hence, complex arrangement of storages, refrigeration and services were important in this pantry area. The height of the old pantry was not ergonomically adequate. The project had following components: (a) stability analysis of the building for renovation, (b) redesign of ambience of interior and (c) providing state of art services inside the cafeteria. The design was developed with options of interior seating arrangements. In these options, the group of seating can be changed as per the suitability of the requirements for the dining (Figs. 1 and 2). This flexible seating plan provided a system to change the interior as per the requirement for the activities inside the cafeteria. Moreover, options of seating were also developed due to the requirement of wall mounted seating. In this design of the cafeteria, seating arrangement flexibility gives a multi number of options for changing the internal seating for any event. Thus, this design makes the entire space more functional and flexible. The project vision was to make a modern design to impress visitors to the Global Fortune 500 Company. Thus, the project involved use of State of the Art materials and services.

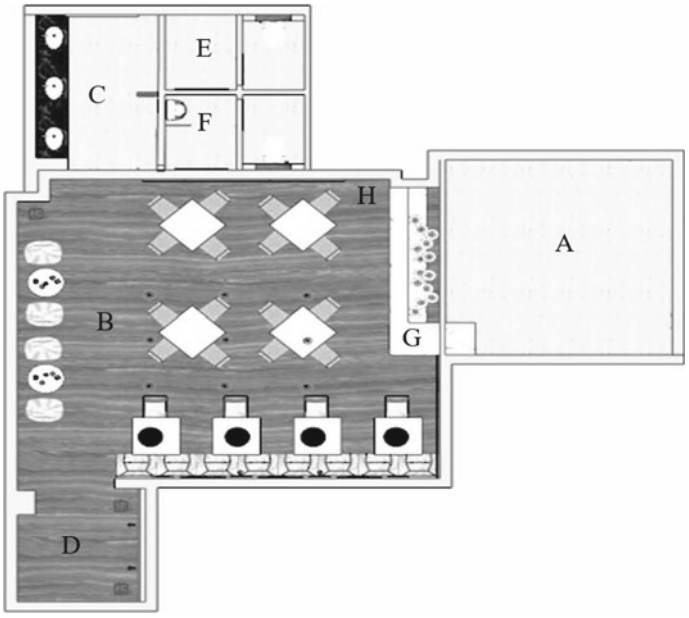

Fig. 1 Plan of Cafeteria (A-Kitchen, B-Dining Hall, C-Hand Wash, D-Entrance Lobby, E-Female Toilet, F-Male Toilet, G-Pantry Counter, and H-Art Work)

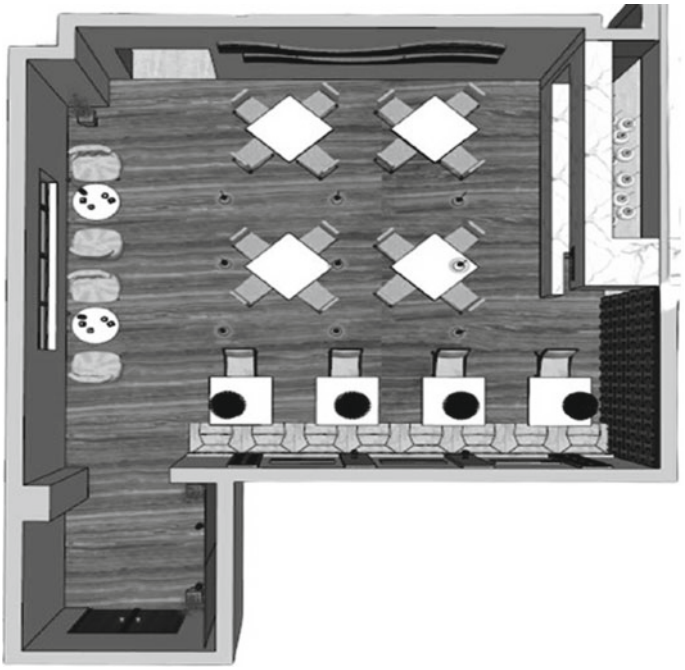

Fig. 2 Dining Area Plan

2.1 Rebound Hammer Test

The rebound hammer tests identify the compressive strength of concrete. So, before the start of the project rebound hammer test was undertaken to understand the compressive strength of columns and beams. This indicated that the structure is safe to undertake any type of renovation work. It is important to take such tests, because of provision of extra load from wall panelling, air conditioning, sprinklers, ducting, false ceiling, lighting etc. (Tables 1 and 2).

3 Architectural design process

The general question of research is what is the architectural design process? And how geometric patterns can be applied in the design process to rehabilitate buildings? The architectural design process can be understood in following parts: (a) study and investigation by applying the geometric patterns and (b) final design output (Fig. 3). The design investigation in the project involves investigation of existing material, ergonomics and services. The important steps for design of the building are how can aesthetic developed for good ambience? What are the methods to be followed for

Table 1 Rebound Hammer test on columns

S. No.	Column No.	Compressive strength (Mpa)	Remark
1	C1	24.52	Good
2	C2	26.48	Good
3	C3	30.40	Good
4	C4	32.36	Good
5	C5	26.48	Good
6	C6	32.36	Good
7	C7	28.44	Good
8	C8	22.56	Average

Table 2 Rebound Hammer test on beams

S. No.	Beam No.	Compressive strength (Mpa)	Remark
1	B1	44.13	Good
2	B2	30.40	Good
3	B3	28.44	Good
4	B4	28.44	Good

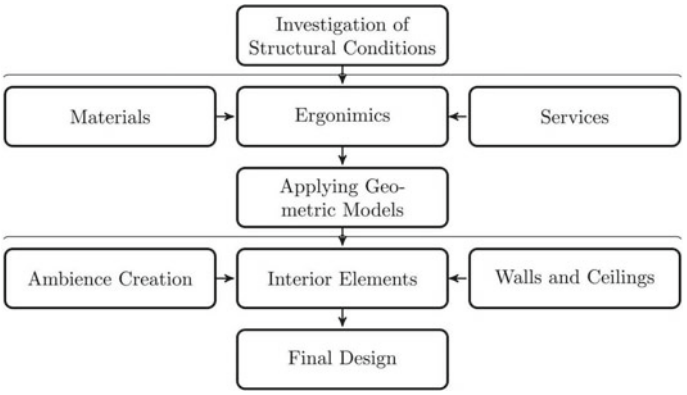

Fig. 3 Architectural design process

development of good ambience? The geometric applications are one of the answers to such methods. In the project, a hexagon is taken as an element of design. This element is applied in vertical and horizontal directions to create an interesting combination for the interior. This concept is implemented in wall panels with irregular shapes, Then this pattern is continued in the ceiling. These two combinations provide interesting ambience. Thus, the application of geometric design can be used to redesign the interiors.

4 Application of Geometric Patterns

The application of the hexagonal pattern in the interior of the cafeteria is illustrated in the following components: (1) ceiling, (2) lighting, (3) wall panelling, (4) Art Work, (5) Entry, (6) Pantry and (7) Other areas. The hexagonal geometry was taken as a basis for development of the interior ambience. Hexagon can be broken or connected to make more patterns. So, on this basis wall panels were developed inside the interiors. Later, hexagonal patterns are combined in vertical surfaces. With this combination the interior was enhanced by use of different materials like marble. The interior material like marble used in the rehabilitation was as follows: (a) flooring, (b) walls, (c) counter, and (d) wall panelling. Furthermore, the aesthetic is maintained by designing quality furniture, art work and lighting (Figs. 4 and 5).

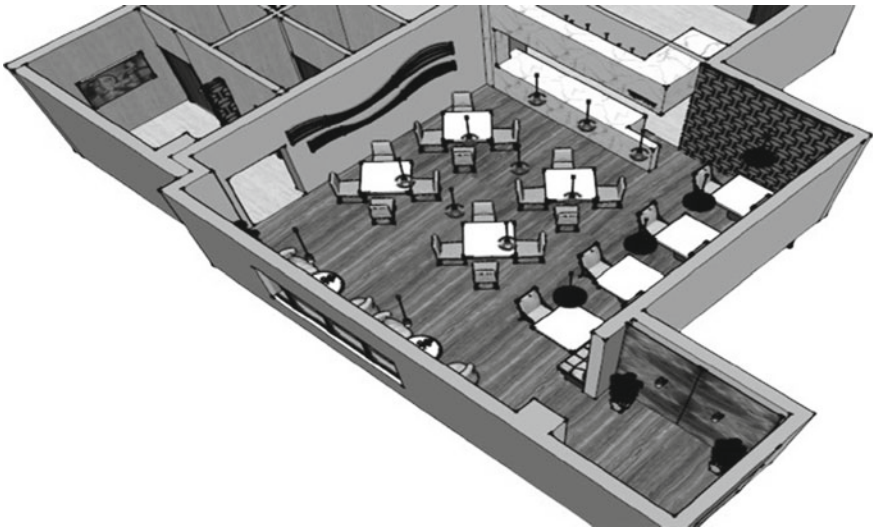

Fig. 4 View of Cafeteria

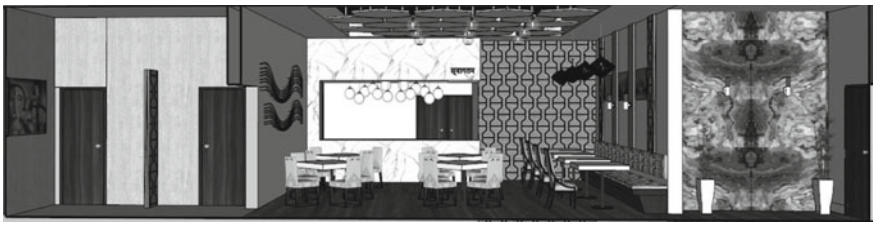

Fig. 5 Section of Cafeteria

4.1 Ceiling Design

The application of the geometric pattern of interior requires organised design. The pattern was applied on the wall panels and to maintain the harmony of the structure, the pattern was also applied in the ceiling design. The combination of the wall and ceiling provided a visual impact on the visitors. The ceiling design is based on the idea of the hexagonal clouds. Generally, these types of design of ceiling provide multiple solutions for building services. So, the building services like electrical, sprinklers, smoke detectors, heat detectors, and lightings can be undertaken easily in this ceiling. The ceiling is fixed in combination with three types of ceilings. In the beginning, the gypsum ceiling is prepared in the periphery of the room ceiling. Then, 2 ft x 2 ft panels ceiling is provided in dark black colors. Finally, the hexagonal clouds are fixed in the ceiling. These hexagonal clouds are supported with the galvanised iron (GI) suspenders. These GI suspenders provide flexibility to remove the clouds for the maintenance of services inside the ceiling (Fig. 6).

4.2 Lighting Design

The lighting design plays an important role in the design of interior to attract the visitor attention in the overall ambience of the interior spaces. The geometric patterns applied in the ceiling design are further enhanced by providing glass suspended lights that reflect in the ceiling as well as the floor. The reflectivity on the ceiling gives an interesting feature to the geometric patterns applied on the ceiling. The lighting designs are developed in combination of aesthetic and functionality of the interior. The color of lighting has also proven to have an effect on human impression. In a real interior space, different types of artificial lighting have various color temperatures Gemelli et al. [13]. A warm color light is provided in the ceiling. Multiple types of lights are used in the interior which are as follows: (a) suspended ceiling glass lights,

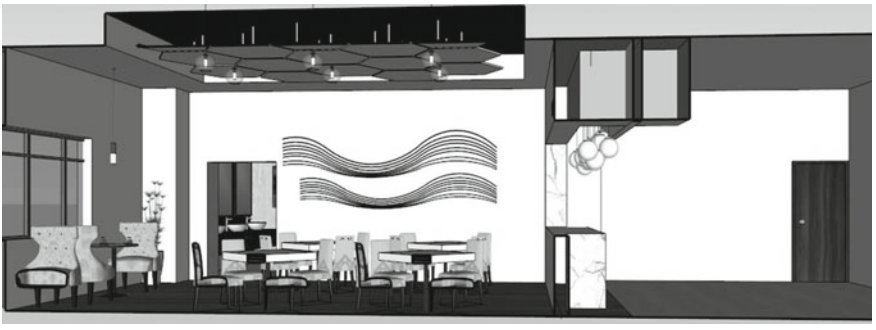

Fig. 6 Section of Cafeteria

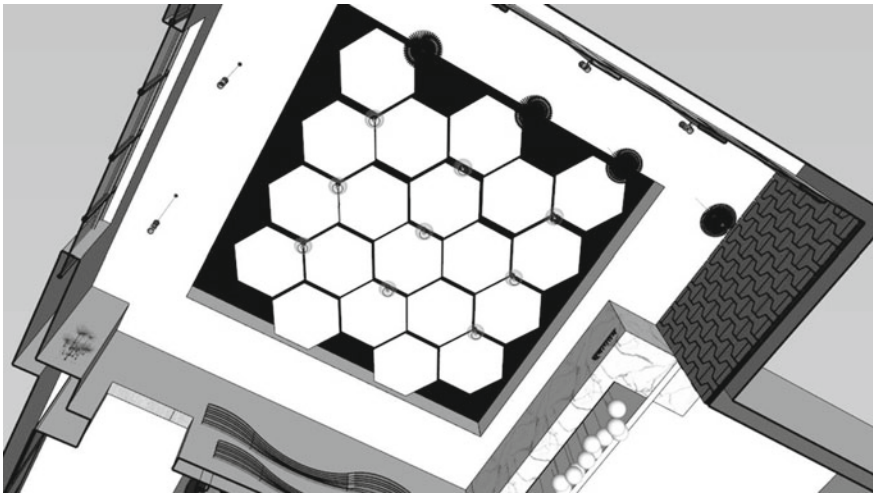

Fig. 7 Design of ceiling

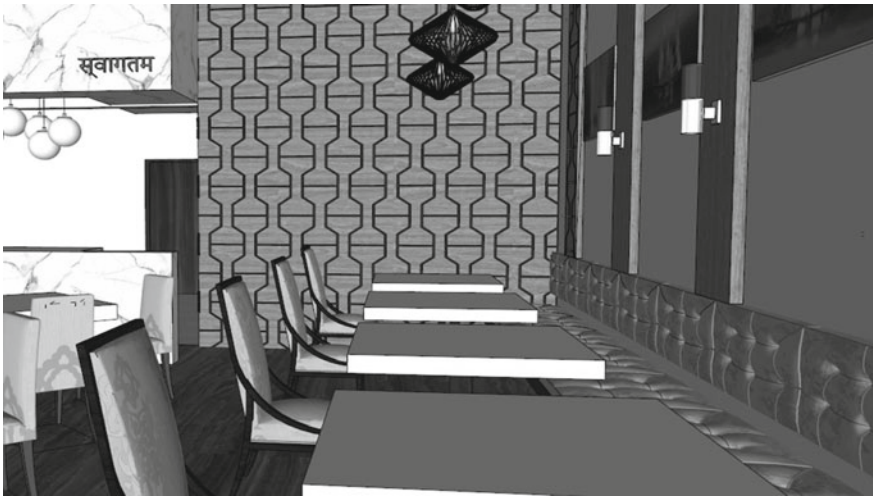

Fig. 8 Design of wall

(b) round suspended lights, (c) wall surface lights, (d) art work with spot lights. Lee et al. [14] had explained that the combination of the lighting system enhances the overall ambience of the interior. When the lighting fixtures varied, the ceiling shape was perceived as a significant factor in providing differences in perceptions of amenity (Figs. 7, 8, 9 and 10).

Fig. 9 Sectional view

Fig. 10 Sectional view

4.3 Wall Panelling

The application of hexagonal pattern in the wall panel is developed by using the hexagonal shapes. These wall panels are divided in two parts: (a) full wall panelling near the pantry and (b) vertical bands behind fixed seating. These panels are made in marine ply with laminate. Grooves are made in the profile of the hexagon. These grooves are having LED lights to give visibility of the hexagonal patterns.

4.4 Art Work

To further enhance the aesthetic, interior is provided with the art work. The art work is developed by use of brass plates in curved shapes. The shapes of the bass plates are kept in an abstract pattern for good visual appearance. Spot lights are further used to enhance the aesthetic of the brass art.

4.5 Entry Design

The entry to the cafeteria was a beginning point of the project. So, an important material idea was needed at the entry. The marble slab in mirror paging is one such idea which gives a sudden impression on the visitor. This is a high finish Italian marble that provides aesthetic in the entry. The marble finish gives a clear and elegant appearance. Further, to impress visitor, the aesthetic of this marble wall lighting was used vertically. The area is further enhanced with use of decorative artificial landscape. The lobby was designed to showcase the achievement of the various medals received by the employees of the company. So, a small showcase was designed in the lobby area. Thus, the combination of marble aesthetic makes the lobby an interesting entry place for visitors.

4.6 Pantry Design

The important component of the design is the counter top of the pantry. The counter top of the pantry is designed with Statuario marble. The Statuario marble is the most premium type of marble. If the marble has fewer grains, then it becomes the most premium quality material for interior spaces. The aesthetic and functionality of the pantry counter was further enhanced by using suspended circular light.

4.7 Other Areas

The old building was not having sufficient space for hand wash and restroom. So, the building spaces were rehabilitated for making the accurate design of the hand wash and restrooms. The planning was done such that the separate rest rooms were organised at the end of the cafeteria. Once a person enters the cafeteria an abstract photo is visible for the visitor. This is like a visual focus for the visitor from the entry. A modern and elegant design of the hand wash keeps the visitor engaged psychologically in the visual aesthetic of the project, a yellow color marble is used in the flooring and wall to make the aesthetic of the hand wash and the restrooms.

Fig. 11 Completed view of Cafeteria

Fig. 12 Hexagonal patterns construction

This marble with the porous veins gives an impressive finish in the interior. Further the hand wash is placed in on the black marble top. The hand wash area is further enhanced by use of large mirror and golden finish taps and accessories (Figs. 11 and 12).

5 Conclusions

Thus, the architectural design process includes a system of integrating aesthetic, planning, material and building services. One of the methods developed in aesthetics is through applying the geometric patterns in the architectural design process. The hexagonal patterns used in the design process, develops wall panelling and ceiling system. This type of design is one of the approaches for developing architectural design. There is a possibility to develop multiple types of combination by applying geometric patterns in the rehabilitation of interiors. Some other ways can be using circular, rectangular or other types of the patterns. These patterns can be developed in flooring walls, ceiling, panelling or furniture design. The next step in the process is to use innovative materials as per the suitability of the project requirements. Finally, building services are designed to complete the overall design. Hence application of geometric patterns in the architectural design process can provide an approach for making better designs for rehabilitation of buildings.

References

1. Alexander C (1977) A pattern language. Oxford University Press, New York, NY, USA
2. Alexander C (1979) The timeless way of building. Oxford University Press, New York, NY, USA
3. Leopold C (2015) Structural and geometric concepts for architectural design processes. Boletim da APROGED 32:3–13
4. Fatihaddin Eves B, Gashoot M (2018) Implementing Islamic patterns in interior design to enhance the spiritual aesthetic. WIT Trans Built Environ 177:137–147
5. Mahmoud H (2017) Geometric patterns in Egyptian architecture & interior design. Acad Res Commun Publ 1:11. https://doi.org/10.21625/archive.v1i1.140
6. Tabaeian T, Einifar A (2011) A study of the perspectives of architectural and environmental psychology (theoreticians and psychologists). Int J Arch Urban Dev 1(1)
7. Jia H, Kuai S, Dong J (2021) Application of CAD-based traditional patterns in interior design. E3S Web Conf 236: 05069. https://doi.org/10.1051/e3sconf/202123605069
8. Leopold C (2006) Geometry concepts in architectural design. In: 12th international conference on geometry and graphics, Salvador, Brazil, pp 6–10
9. Leopold C (2016) Geometry and aesthetics of pentagonal structures in the art of Gerard Caris. In: Bridges Finland conference proceedings, pp 187–194
10. Liotta SJ, Belfiore M (2012) Patterns and layering: Japanese spatial culture, nature and architecture. A journey in the activities of Kengo Kuma Lab at the University of Tokyo, Publisher Gestalten
11. Liotta S-J (2019) Tadao Ando's places and encounters—emotional geography, Domus, December

12. Atanasijevic J (2017) Fibonaccis aesthetics in the works of Aldo Rossi. In: XII international scientific conference Serbian language, literature, art, Kragujevac, Serbia, pp 297–308
13. Gemelli A, Shiratuddin MF, Kemp D (2013) The impact of lighting on impressions of interior space. Int J Design Objects 6. https://doi.org/10.18848/2325-1379/CGP/v06i02/38653
14. Lee S, Alzoubi HH, Kim S (2017) The effect of interior design elements and lighting layouts on prospective occupants' perceptions of amenity and efficiency in living rooms. Sustainability 9(7):1119. https://doi.org/10.3390/su9071119

A Novel Seismic Outer Coating for Rehabilitation of Existing Masonry Buildings

A. Formisano, G. Vaiano, and A. Roffo

Abstract In this work a novel seismic outer coating applied to masonry structures are studied in order to investigate obtained benefits both from seismic and energetic points of view. The innovative seismic coat consists of a frame made up of Cold-Formed Steel (CFS) members, within which a thermo-acoustic alveolar insulation is inserted. OSB (Oriented Strand Board) panels are bolted to the frame on the outside. The system is completed with an ultra-thin heat reflective insulation, a ventilated wall and a brick finishing. In this way, the CFS frame acts as system withstanding vertical loads, OSB panels provide the seismic action dissipation and the remaining elements are responsible for energy efficiency. The system is connected by bolts on the perimeter walls of masonry buildings and covers the entire facades starting from the foundations. The aim of this research is to find a solution to combine the increase both in term of seismic safety and energy efficiency with a light, flexible and economical system which can replace the traditional thermal coat thanks to both the higher energy performance and an additional seismic resistance, which is not provided by the traditional envelope systems. Firstly, an experimental test on a masonry wall has been simulated by ABAQUS code and, afterwards, the seismic benefits deriving from using the novel coat have been shown in the implemented FEM model through a parametric analysis. Finally, the coat system has been applied to a case study building hosting the high school "Leccisotti", in the district of Foggia, Italy, with the aim to evaluate the increase of seismic safety and energy behaviour deriving from its use.

Keywords Seismic coating · CFS frame · OSB panels · Retrofit · Masonry building

A. Formisano (✉) · G. Vaiano · A. Roffo
Department of Structure for Engineering and Architecture, School of Polytechnic and Basic Sciences, University of Naples "Federico II", P.Le V. Tecchio, 80125 Naples, Italy
e-mail: antoform@unina.it

G. Vaiano
e-mail: generoso.vaiano@inwind.it

J. M. P. Q. Delgado (ed.), *Masonry: Building Pathologies and Design*, Building Pathology and Rehabilitation 22, https://doi.org/10.1007/978-3-030-80496-1_4

1 Introduction

Italian civil buildings are characterized by very disparate construction types and, according to the last census, about 60% of the existing structures are made of masonry. Most of these buildings are old and characterised by low-quality masonry, since the materials choice always was influenced by the availability on site and, therefore, by the simplicity of transportation.

From a structural point of view, masonry can be defined as a material with a much greater compressive strength than tensile one. From a mechanical point of view, masonry is an inhomogeneous, anisotropic and elastic material. The most important factor to investigate is that these structures are very seismically vulnerable [9, 12, 18]. In fact, seismic vulnerability is increased by the poor mechanical properties of the masonry material, so that buildings can suffer important damages, until collapse, even for low seismic excitations [2, 4, 19]. In addition, during seismic events masonry building can show a repetition of different local mechanisms. One of the most dangerous mechanisms is the façade global overturning, where masonry perimeter walls detach from the building outside [5, 6, 11].

A centuries-old building heritage, the absence of seismic criteria in the design as not required at the time, the architectural modification interventions without adequate structural checks are some of the factors which conferred to Italian buildings a greater seismic risk. In order to reduce the seismic vulnerability, different retrofitting techniques, both traditional methodology [7, 15, 16] and innovative ones [8, 13, 17], are available.

In this paper a proposal for seismic retrofitting of masonry structures is provided. In particular, a novel seismic outer coating, characterized by a CFS frame with external OSB panels fixed on the building perimeter walls, is proposed.

The novel seismic coating has required a FE study, where various steps are dealt: the first has been the calibration of an experimental test on a simple masonry wall, the second has been the application of the retrofitting system on the mentioned wall, considering different connection systems and distances among CFS profiles and, finally, the application of this system to a case study building has been sone in order to evaluate the improvement in terms of seismic safety and energy efficiency. The aim of this research was to find a solution to combine the increase both in term of seismic safety and energy efficiency with a light, flexible and economical system applied from building outside.

The reference experimental test, carried out by Augenti et al [1], consisted of a quasi-static test on a tuff masonry wall having a central opening. The test foresaw of the application of both vertical forces and a horizontal force in displacement control on the masonry walls. The coating system was then applied to a school building case study through a numerical analysis developed by the FE software SAP2000. The case study was the high school “Leccisotti” located in the district of Foggia in Italy. The building was included in the UEFA-ELENA project “Integrated interventions on public buildings” coordinated by Prof. S. Pampanin from Sapienza University of Rome.

Finally, the results deriving from application of the proposed novel seismic coating can be of interest within of the initiative promoted by the Italian Government dealing with 110% Superbonus tax detraction. In this framework, the 110% Superbonus represents a facilitation provided for by Relaunch Decree (law of 19 May 2020, n. 34) in order to recover the building heritage mainly used for residential purposes. In particular, this government tax measure allows to deduce from fiscal point of view the expenses incurred from 1 July 2020 to 30 June 2022 for specific seismic-energetic requalification interventions of residential buildings.

2 Experimental Test

The reference experimental test consists of a quasi-static monotonic push test on a tuff masonry wall with a single central opening. The masonry wall geometry is shown in Fig. 1 [1]. Figure 2 shows the experimental apparatus used for the quasi-static test, which is carried out in two phases: at first, vertical forces of 200 kN are applied on the wall top by hydraulic jacks; after, the wall is subjected to a horizontal force through the actuator. The test is conducted in displacement control in order to record the resistance degradation in the post-peak phase. The horizontal force is applied in order to obtain increasing displacements at a constant speed of 10 μm/s until to a displacement of 28 mm, which corresponds to a total drift of 1%.

At the end of test a damage to the spandrel without involving the adjacent node panels is observed. Figure 3 shows the crack pattern observed after the monotonic test. After the formation of vertical flexural cracks and diagonal shear ones at the ends of the spandrel, macroscopic cracks at the piers base are observed.

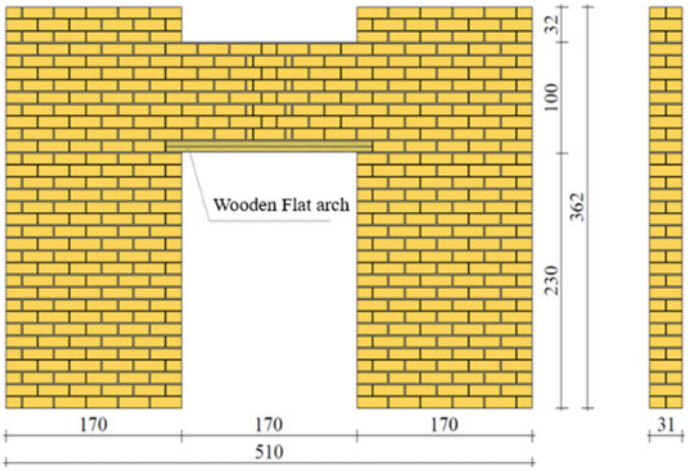

Fig. 1 Experimental test: wall geometry

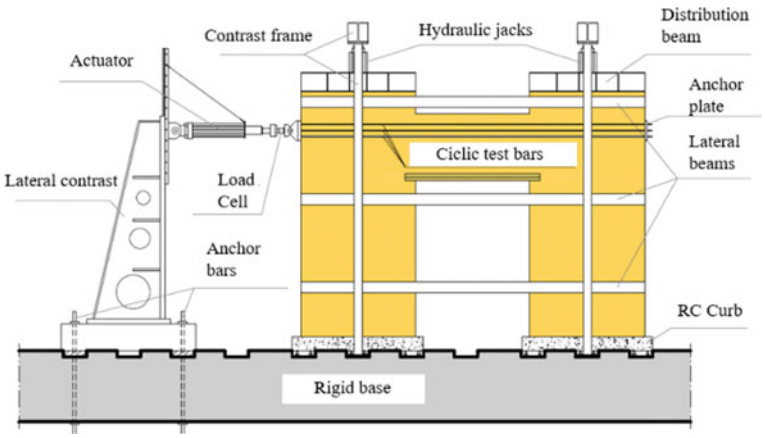

Fig. 2 Experimental test: loading apparatus

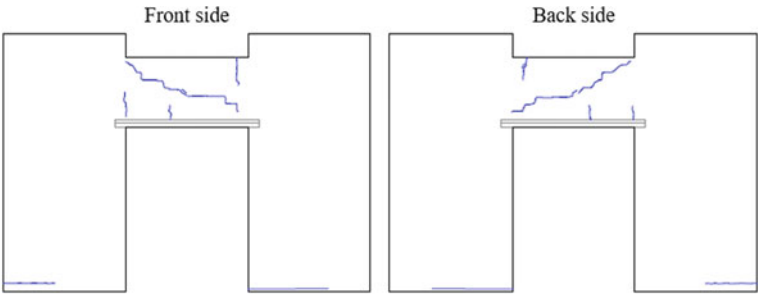

Fig. 3 Crack pattern at the end of the monotonic test

The wooden flat arch, although having a limited anchorage length, played an important role in supporting the weight of the overlying masonry, forcing the upper part to transmit the horizontal force to piers.

Figure 4 shows the experimental force–displacement curve relative to the monotonic push test.

3 Numerical Simulation

The experimental test just described is replicated by a non-linear finite element analysis using ABAQUS software (Fig. 5a). Mechanical and physical characteristics both for masonry (Density $\rho = 1600$ kg/m^3, Elastic modulus E = 1300 MPa, Poisson ratio $\nu = 0.207$) and wood ($\rho = 570$ kg/m^3, E = 9500 MPa, $\nu = 0.40$) derived from experimental tests on material samples.

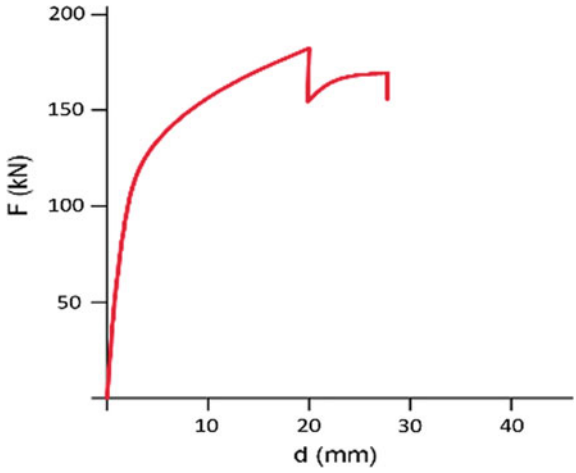

Fig. 4 Experimental test: force–displacement curve

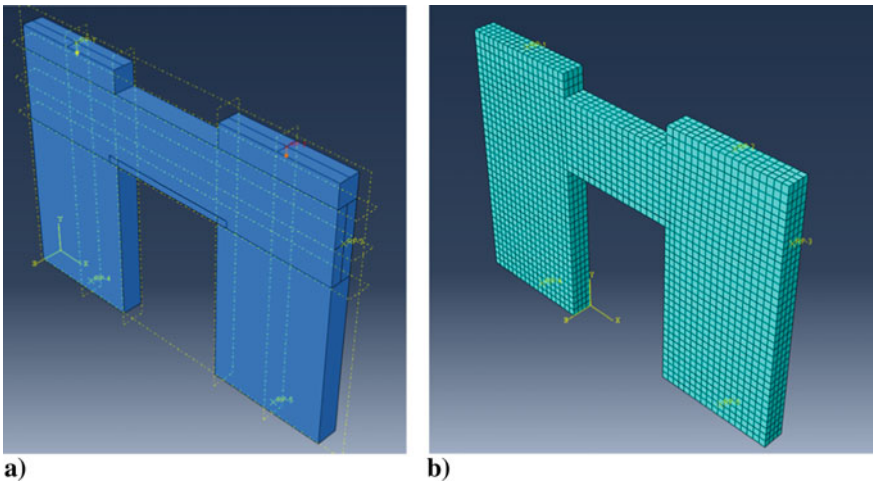

Fig. 5 Numerical model: geometry (**a**); mesh (**b**)

For masonry, concrete damage plasticity is used to simulate the compression and tensile behaviours. In particular, under compression loads, an elastic–plastic behaviour with hardening is assumed. The concrete damage plasticity is a constitutive behaviour implemented for RC structures, but it can be extended to masonry ones without errors. The basic assumptions are:

- to consider different yield stresses in tensile and compression phases;
- to distinguish the different behaviour of the material in tensile and compression: softening in tension, hardening followed by softening to failure in compression;
- to evaluate a different degradation of elastic stiffness in tension and compression.

Boundary condition and loads application are the same as those described in experimental test. In particular, piers are fixed to the ground and the system is laterally loaded in the same point where the actuator is applied (Fig. 2). Finally, with regard to the mesh definition, in order to both optimize the analysis times and obtain accurate results, a structured mesh of 100 mm size is used (Fig. 5b).

Figure 6 shows the comparison in term of force–displacement curve between the experimental test and the numerical one. By the comparison is clear that numerical calibration has been done very accurately. Figure 7 shows, instead, the comparison

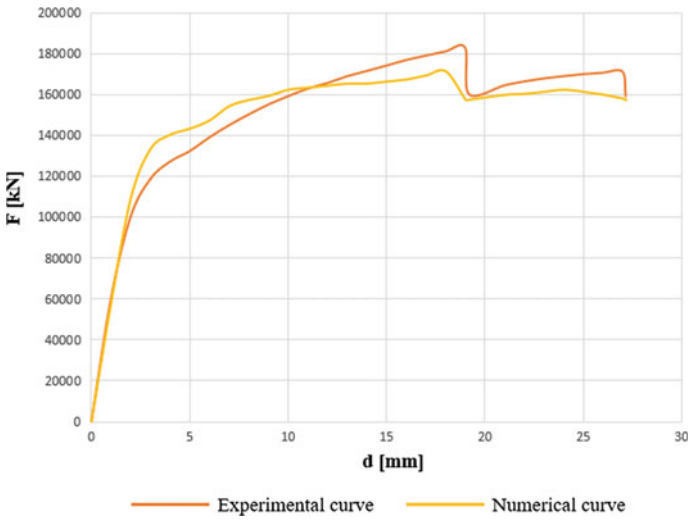

Fig. 6 Comparison between experimental and numerical curves

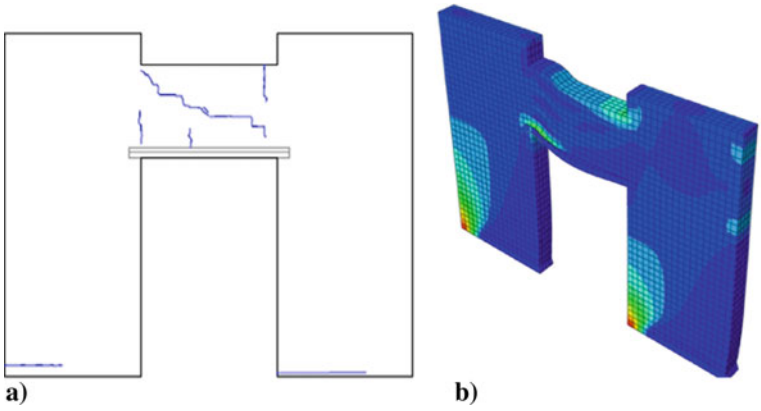

Fig. 7 Comparison between experimental (**a**) and numerical (**b**) damages of the wall at the test end

of the wall final configuration at the test end. Also in this case the numerical results are very faithful to the experimental ones.

4 A Seismic Upgrading Technique: A Novel Seismic Outer Coating

Following the numerical calibration, a novel seismic coating is proposed to upgrade the seismic and energy behaviour of existing masonry buildings. The system is composed of a Cold-Formed Steel (CSF) frame covered by Orientated Strand Board (OSB) panels connected by self-perforating screws to the frame members. The CFS frame-OSB panel composite system, representing the seismic-resistant part of the coating system, is connected by mechanical anchors to the masonry walls. In the spaces within horizontal and vertical frame members, a thermal insulation layer is placed. On the OSB panel, a further insulation layer is attached and, finally, a secondary framed structure is positioned as supporting system of the cladding panels, so to define a ventilated wall. A picture of the implemented seismic coating, together with the used CFS member, is shown in Fig. 8.

Numerical analyses are carried out using the FE software ABAQUS. The steel class is S355 and mechanical properties of OBS panels are those contemplated in the UNI EN 300-2006 standard. Three different CFS frame configurations are considered: transom have always a distance of 110 cm, while mullions are arranged with a pitch of 275, 425 or 551 mm (Fig. 9).

A preliminary modelling phase is done with the purpose to evaluate the maximum contribution provided by the seismic coating if connections are effective up to the wall failure. Therefore, tie constraints are used for the mullion-transom, for the CFS frame-wall (Fig. 10) and for the CFS frame-OSB panel connections (Fig. 11). In particular, the contact between the CFS frame and the OSB panels is done in the zones corresponding to the location of holes, while the tie constraint simulates the

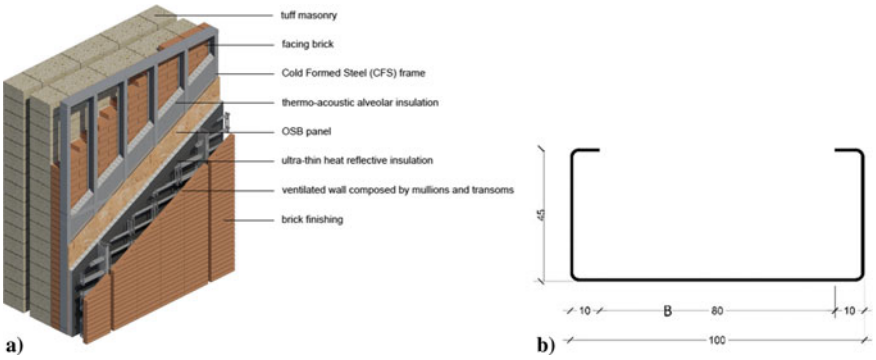

Fig. 8 The proposed seismic coating (**a**) and the CFS cross-section (**b**)

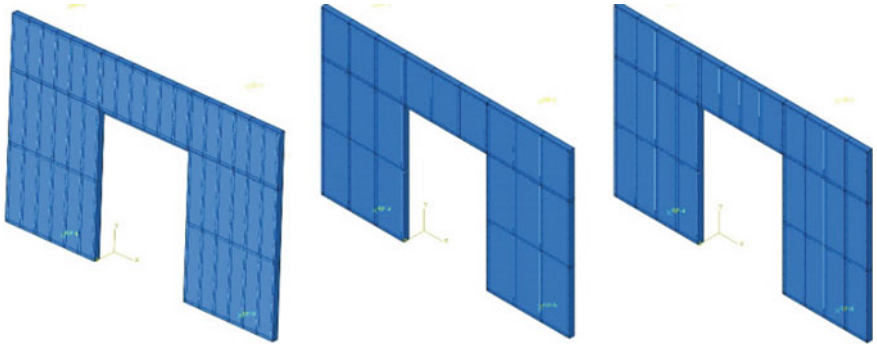

Fig. 9 CFS frame arrangements: mullion pitch of 275, 425 and 551 mm

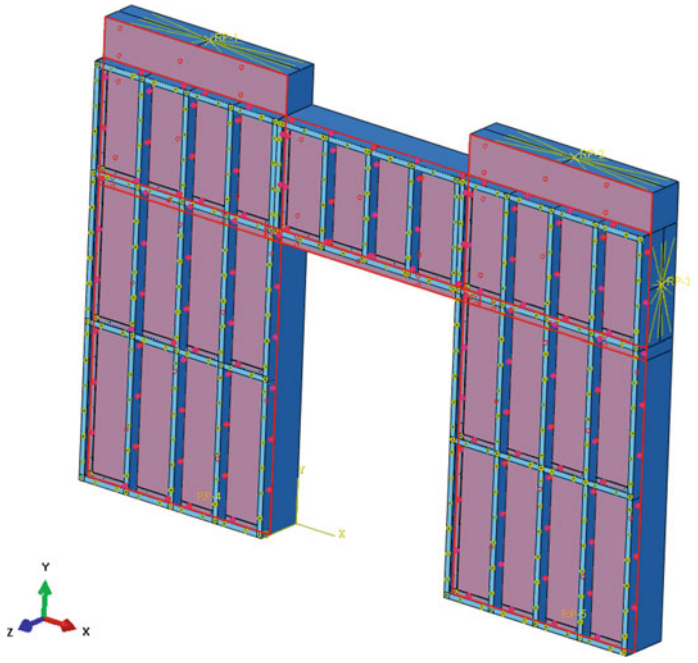

Fig. 10 Tie constraint between CFS frame and existing masonry wall

connectors behaviour. In the same way, the contact between the CFS frame and the masonry wall is assumed as perfect, so to simulate the ideal behaviour of connections to resist without failure to the maximum lateral force sustained by the wall. In the numerical model, three different hole pitches, namely 200, 400 and 600 mm, are considered. The performed non-linear analyses are interrupted when a stress level similar to that recorded in the un-reinforced masonry wall is reached.

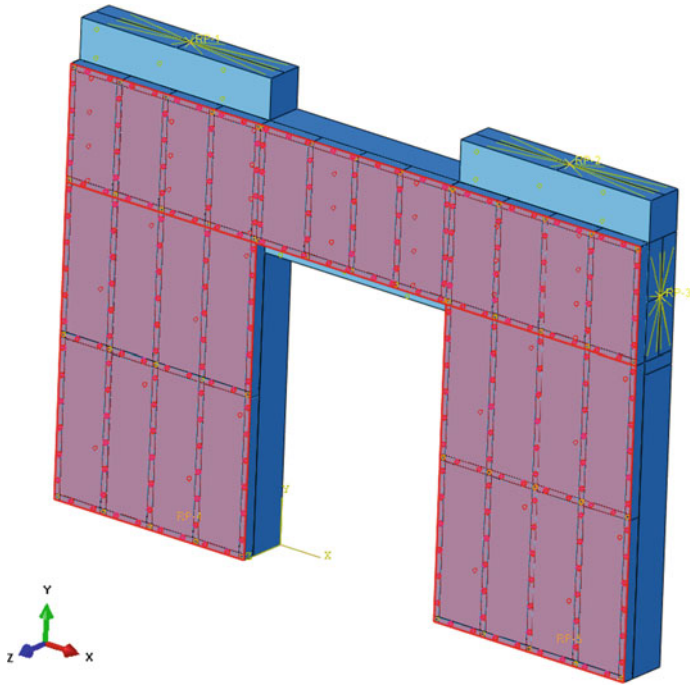

Fig. 11 Tie constraint between CFS frame and OSB panel

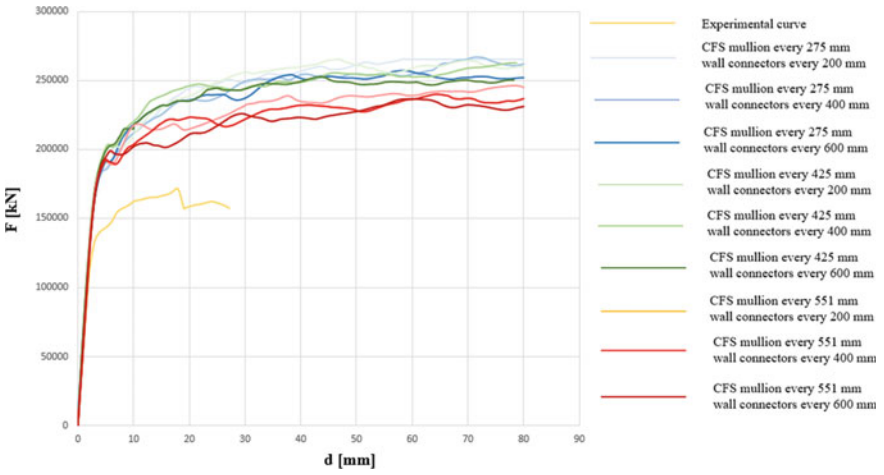

Fig. 12 Numerical results in term of force-displacement curves

Table 1 Seismic upgrading numerical results achieved from seismic coating systems

Pitch [mm]		Increase [%]	
CFS mullions	Wall connectors	Resistance	Ductility
275	200	47	190
275	400	45	190
275	600	39	190
425	200	44	190
425	400	46	190
425	600	39	190
551	200	36	190
551	400	31	190
551	600	28	190

Figure 12 shows results of the numerical simulation in terms of force-displacement curves.

The masonry wall seismic upgrading using this seismic coating system brings numerous advantages from a structural point of view, giving a satisfactory increase in term of both resistance and ductility with respect to the bare wall. In particular, the system resistance increases with the decrease of both the mullions pitch and the CFS frame-wall connector ones. The resistance contribution is mainly given by the OSB panels, which play a fundamental role in absorbing part of the seismic action. Table 1 shows the increases in term of resistance and ductility of the examined configurations of seismic coating systems.

5 The Seismic Coating Application to a Case Study

The case study is the high school 'I.S.I.S.S. Leccisotti' located in the Italian city of Foggia. This school is included in the UEFA-ELENA project "Integrated interventions on public buildings", coordinated by Prof. S. Pampanin from Sapienza University of Rome.

The building has a L-shape plan and develops on two storeys (Figs. 13, 14, 15 and 16). Walls are made of masonry tuff stones; perimeter walls are composed by two layers of tuff stones separated by an air chamber and are covered from outside by a brick cladding as surface finishing.

The 'I.S.I.S.S. Leccisotti' high school was built in absence of seismic regulations, so to be conceived to resist only vertical loads.

The aim of this study is to verify through non-linear analyses the benefits in terms of both seismic and energetic viewpoints due to the application of the seismic coating. At first, the school in the actual state is studied. Numerical model and non-linear analyses are implemented using the FE software SAP2000.

Fig. 13 Aerial photogrammetry of the case study school building

Fig. 14 Street view of the case study school building

The equivalent frame model is used to model masonry walls (Fig. 17), where piers and spandrels are schematized through one-dimensional element which are deformable towards axial and shear actions (Fig. 18). These elements are connected to each other by rigid links. Masonry walls are connected all together through a diaphragm constraint.

Each pier is composed by three parts: one deformable in the middle having a certain strength value and the other two placed at the ends having infinite strength and stiffness. The length of rigid parts depends on the size of the nodes.

The effective length of deformable part (H_{eff}) can be defined according to [3]:

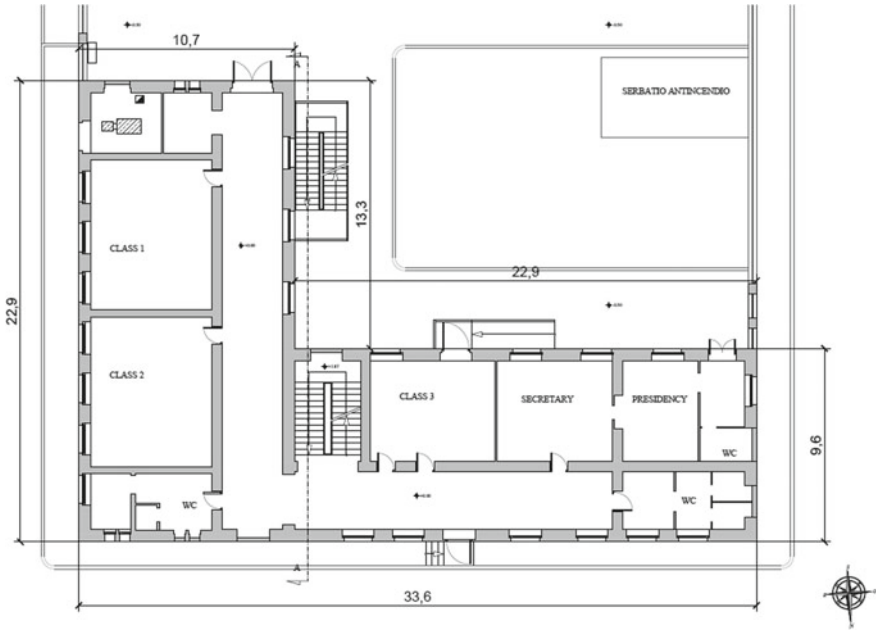

Fig. 15 First floor plan of the 'I.S.I.S.S. Leccisotti' high school

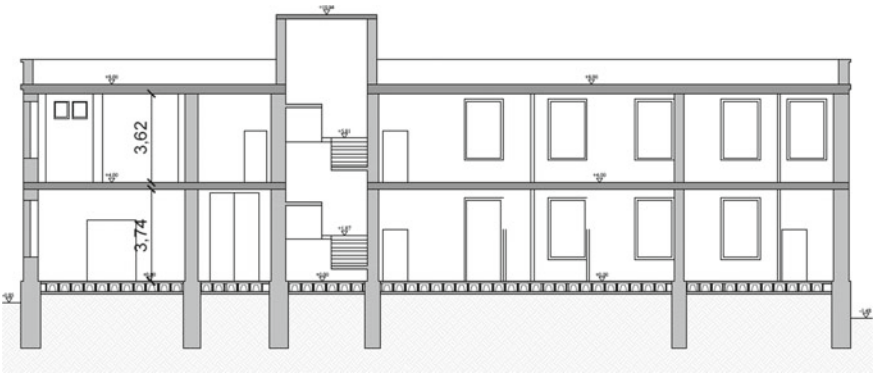

Fig. 16 Section of the 'I.S.I.S.S. Leccisotti' high school

$$H_{eff} = h' + \frac{1}{3} D \frac{(H - h')}{h'}$$

where:

H_{eff} is the deformable height of masonry piers;
H is the inter-storey height;

Fig. 17 Equivalent frame schematization of the east wall of the building

Fig. 18 Nodes, spandrels and piers of the east wall of the building

D is the width of masonry piers;
h'' is the height of masonry piers.

It is assumed that the piers have an elastic–plastic behavior. Failure mechanisms are achieved in the following ways:

- Compression-bending moment, which caused rocking following the achievement of the ultimate moment;
- Shear, with diagonal cracking following the achievement of the ultimate shear.

Spandrels are represented with horizontal axis frame elements. It is assumed that the deformable part corresponds to the length of openings and the remaining part is modeled with infinitely rigid elements.

In the absence of tensile-resistant elements, such as concrete curbs or metallic tie rods, the resistance towards horizontal stresses is neglected. In such conditions, the masonry piers have a cantilever behavior. Figure 19 shows the numerical model implemented in the case study inspected.

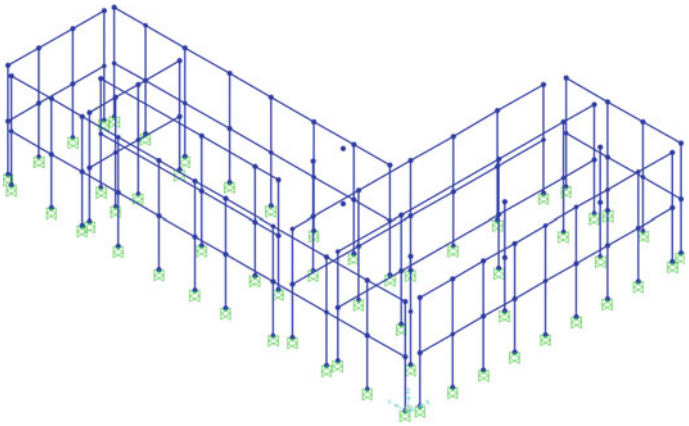

Fig. 19 Equivalent frame of the masonry school developed with the FE software SAP2000

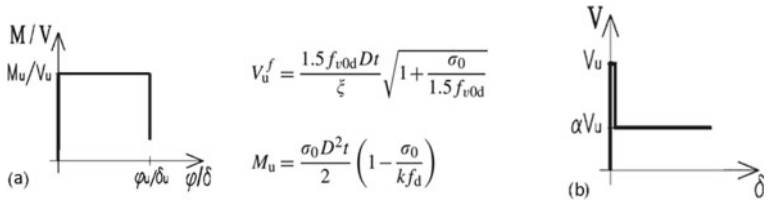

Fig. 20 Behaviour of plastic hinges for piers (**a**) and spandrels (**b**)

Plastic shear and moment hinges are considered for piers and shear plastic hinges are taken into account for beams. Figure 20 shows the behaviour of plastic hinges used for piers and spandrels [14], where ultimate rotation and deformation under flexural and shear stresses correspond to 0.08% and 0.04% of the effective height, respectively.

The FE model is fixed at the base and two rigid diaphragms are arranged in correspondence of the two floors. The pushover analysis is performed in both x and y directions and force–displacement curves are shown in Fig. 21a, b.

A reinforcement system consisting in the application of the mentioned novel seismic coating is used to retrofit the examined school. In particular, a Cold Formed Steel (CFS) frame covered by 15 mm thick Oriented Strand Board (OSB) panels is applied over the equivalent frame to represent the retrofit system.

The OSB panel is schematized by two diagonals, whose force-displacement behaviour is calibrated in the SAP2000 environment starting from the experimental test on a single wall with dimensions of 3.00 × 2.40 m investigated in [10]. Figure 22 shows the SAP2000 model of a single module constituted by the CFS frame and the overlapped OSB panels.

The external CFS frame is modelled according to the equivalent frame theory; the reinforcement system is connected to the point of intersection between piers and

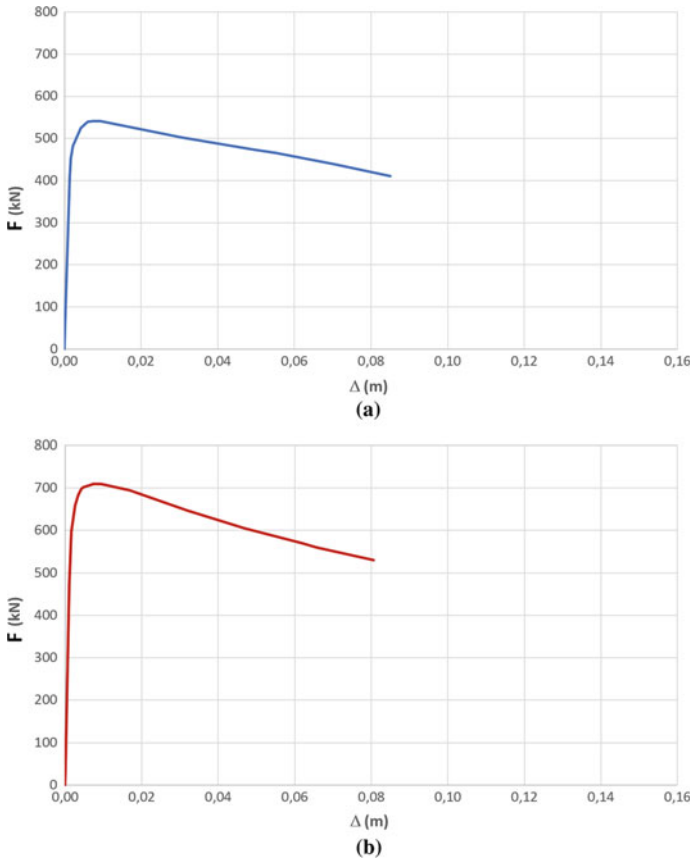

Fig. 21 Nonlinear static analysis: x-direction (**a**) and y-direction (**b**)

spandrels through a body constraint (Figs. 23 and 24). The CFS elements has released their ends towards bending moments to have hinged connections.

Seismic coating is applied on all the perimeter walls, as depicted in Fig. 25, and pushover analyses are carried out. Figure 26a, b show the comparison between the unreinforced building (UB) and the seismically improved one (IB) in term of force–displacement curve. Obtained results demonstrate that the seismic coating improves significantly resistance and ductility of the existing building. In 'x' direction an increase of 31% and 45% in term of strength and ductility, respectively, is reached. Instead, in 'y' direction the strength and ductility increases are of 18% and 47%, respectively.

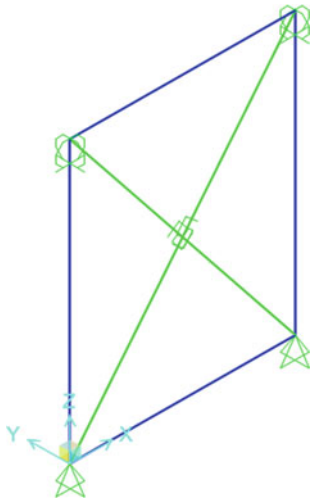

Fig. 22 Numerical model setup by SAP2000 software of a single module constituted by the CFS frame and OSB panel

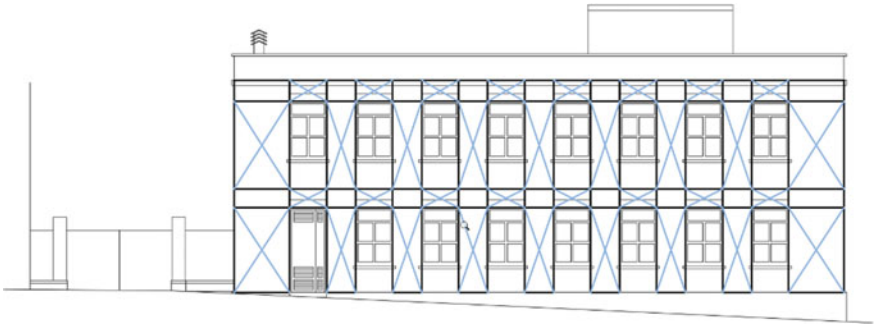

Fig. 23 Scheme of the seismic coating system applied to the masonry wall

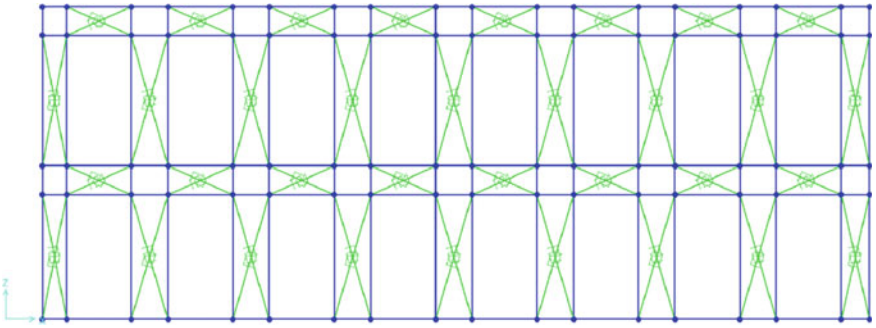

Fig. 24 Reinforcement system FE model of the masonry wall developed by the SAP2000 software

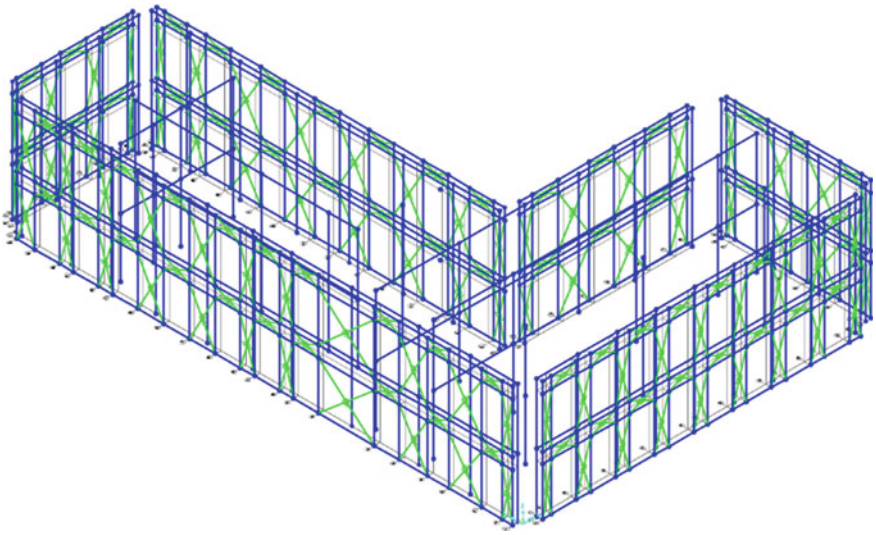

Fig. 25 3D Numerical model of the reinforced school building

6 Italian Government Tax Deduction: 110% Superbonus

In order to recover the built heritage mainly used for residential purposes, the Italian Government has approved the 110% Superbonus, which is a facilitation provided by Relaunch Decree (Law of 19 May 2020, n. 34), allowing for the 110% expenses deduction rate incurred from 1 July 2020 to 30 June 2022 for specific interventions in the field of anti-seismic and energy efficiency interventions.

With regard to the seismic upgrading, the 110% Superbonus tool allows to receive a tax detraction up to 96.000,00 Euros if seismic reinforcement interventions are carried out. It is possible to attain seismic upgrading or retrofitting of the existing building is one or two seismic classes are exceeded, respectively, after interventions are carried out. Therefore, the seismic classification of the building before and after the interventions is needed and the main parameters to be evaluated are the average annual loss (PAM) and the seismic safety index (IS-V). The PAM classes are identified in Table 2. IS-V life safety index is the ratio between the PGA referred to the ULS and the PGA demand. The seven IS-V classes are listed in Table 3. The structure risk class is the worst between the PAM class and the IS-V one.

For the examined case study, the used seismic coating allows to overcome one risk class, so to attain the building upgrading. It can be evaluated as the area subtended by the curve representing the direct economic losses as a function of the average annual frequency of exceedance of events causing attainment of the limit states considered in the standard codes (Fig. 27).

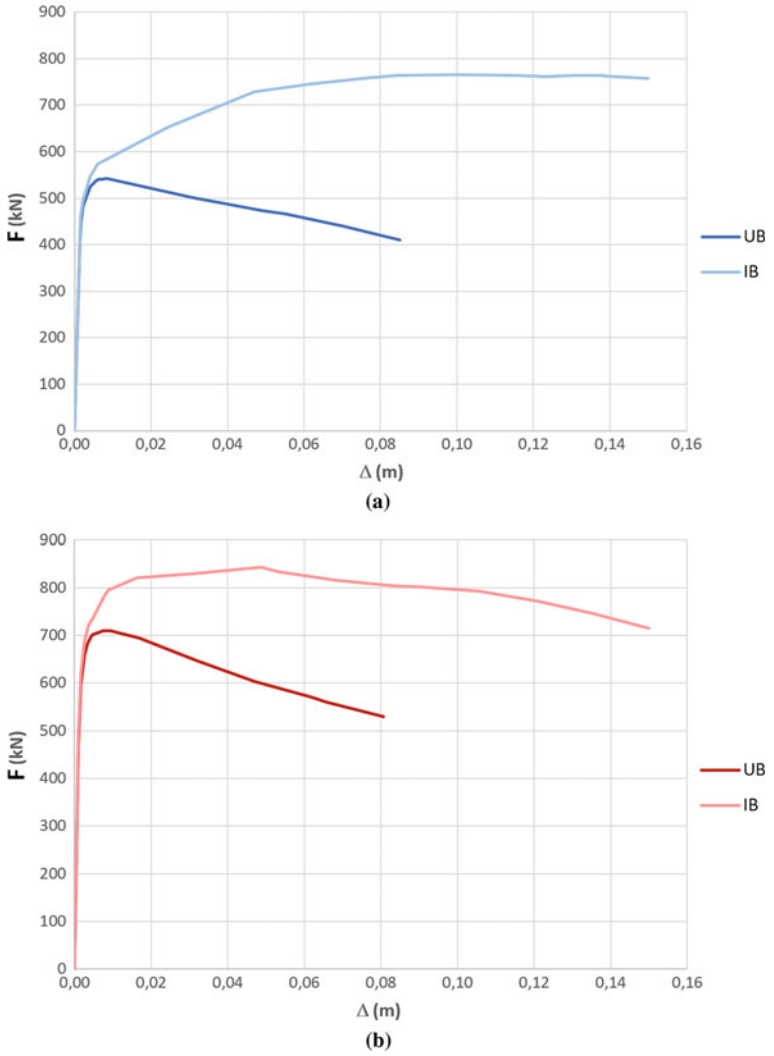

Fig. 26 Comparison between the unreinforced building (UB) and seismically improved one (IB) in the non-linear field: analysis in x-direction (**a**) and y-direction (**b**)

Finally, the energy upgrading interventions on the building enclosure allows to receive a tax detraction up to 50.000,00 Euros if a reduction of two energy classes is achieved.

According to the Italian standard, the energy classes range from 'G' (the worst) to 'A' (the best), the latter being divided into A1, A2, A3 and A4 (the most efficient) classes. In the case under study, the energy efficiency interventions foresee the installation of the thermal coating and the replacement of old windows with new ones made of double glasses with internal air chamber. Focusing on the performance

Table 2 PAM classes

Annual Loss (PAM)	Class
PAM $\leq$ 0.50%	A+
0.50% < PAM $\leq$ 1%	A
1% < PAM $\leq$ 1.5%	B
1.5% < PAM $\leq$ 2.5%	C
2.5% < PAM $\leq$ 3.5%	D
3.5% < PAM $\leq$ 4.5%	E
4.5% < PAM $\leq$ 7.5%	F
7.5% < PAM	G

Table 3 IS-V classes

Life safety index (IS-V)	Class
100% < IS-V	A+
80% < IS-V $\leq$ 100%	A
60% < IS-V $\leq$ 80%	B
45% < IS-V $\leq$ 60%	C
30% < IS-V $\leq$ 45%	D
15% < IS-V $\leq$ 30%	E
IS-V $\leq$ 15%	F

of the thermal coating, it is noticed that the transmittance of the wall improves from 0.7721 W/m^{2}K (unreinforced building) to 0.1903 W/m^{2}K (reinforced building). This intervention, together with the new windows, allow to overcome 4 energy classes, from D to A2.

7 Conclusions

In this work the use of an innovative low-cost sustainable and reversible seismic coating as energetic and seismic upgrading system of existing masonry buildings is proposed. The system potentiality has been demonstrated initially through FEM simulations carried out in the ABAQUS FE software. Parametric analyses on different configurations of CFS frame varying mullions and connectors pitches has been done aiming at understanding the advantages in terms of strength and ductility provided by the proposed system. The increase in terms of resistance is between 28 and 47%, while in terms of ductility is 190%.

To confirm the performance increases obtained from the refined FE analyses, the seismic coating has been applied to a case study represented by an Italian high school masonry building. In this case SAP2000 software is used to perform pushover analyses on the case study. Also in this case, the improvement of seismic performances

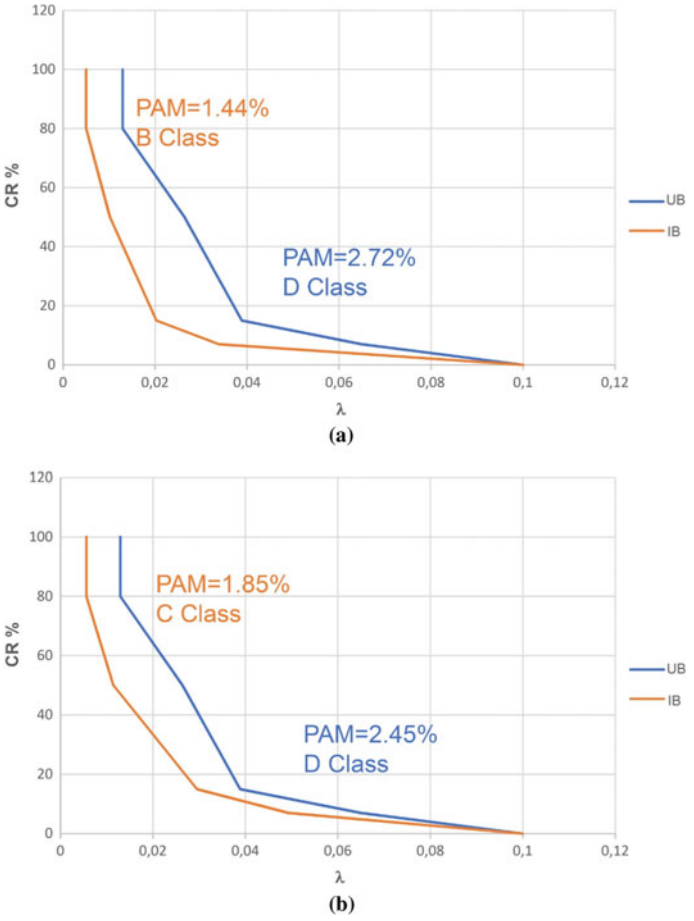

Fig. 27 PAM of the school building in 'x'-direction (**a**) and 'y'-direction (**b**)

in term of strength and ductility has been significantly large. In particular, in 'x' direction an increase of 31% and 45% in term of strength and ductility, respectively, is reached. Instead, in 'y' direction the strength and ductility increases are of 18% and 47%, respectively.

Finally, the 110% Superbonus tool promoted by the Italian government, introduced with the Relaunch Decree (Law of 19 May 2020, n. 34), is taken into consideration. The installation of the seismic coating allows to overcome one seismic risk class and four energy classes, making the system suitable for receiving the maximum of the economic incentives provided by the Italian standard.

The achieved outcomes allow to conclude that the proposed system can effectively replace the traditional thermal coating thanks to both the higher energy performance and an additional seismic resistance, which is not provided by the traditional envelope systems.

Acknowledgements The Authors would like to acknowledge Prof. S. Pampanin, from Sapienza University of Rome, and Dr. Lorenzo Diana, from University of Naples "Federico II", for providing information on the case study school building. Also, the contribution of the technical staff (Arch. Giuseppe Maisto, Eng. Feliciano Ricciardelli and Eng. Daniele Spiniello) of the Irondom s.r.l. company, which is the manufacturer of the seismic coating system, is gratefully acknowledged.

References

1. Augenti N, Parisi F, Prota A, Manfredi G (2011) Quasi-static tests on a full-scale perforated masonry wall with and without inorganic matrix composite materials (in Italian). In: Proceedings: ANIDIS 2011 14th Italian national conference on earthquake engineering, University of Bari (Italy)
2. Clementi F, Gazzani V, Poiani M, Mezzapelle PA, Lenci S (2017) Seismic assessment of a monumental building through nonlinear analyses of a 3D solid model. J Earthquake Eng. https://doi.org/10.1080/13632469.2017.1297268
3. Dolce M (1989) Schematization and modeling for actions in plan of the walls (in Italian). In: Course on the consolidation of masonry buildings in seismic zone, Order of Engineers, Potenza (Italy)
4. Fonti R, Borri A, Barthel R, Candela M, Formisano A (2017) Rubble masonry response under cyclic actions: experimental tests and theoretical models. Int J Masonry Res Innov 2:30
5. Formisano A, Chieffo N, Milo B, Fabbrocino F (2016) The influence of local mechanisms on large scale seismic vulnerability estimation of masonry building aggregates. AIP Conf Proc 1790. Article ID:130010. https://doi.org/10.1063/1.4968728
6. Formisano A, Vaiano G, Fabbrocino F, Milani G (2018) Seismic vulnerability of Italian masonry churches: the case of the nativity of blessed virgin Mary in Stellata of Bondeno. J Build Eng 20:179–200
7. Formisano A, Vaiano G, Fabbrocino F (2019) Seismicand energetic interventions on a typical South Italy residential building: cost analysis and tax detraction. Front Built Environ 5:12. https://doi.org/10.3389/fbuil.2019.00012
8. La Manna AG, Brigante D, Mauro A, Formisano A (2017) Concept, prototyping and application of a tensioning system for FRP ties into masonry structures. Key Eng Mater 747:298–304
9. Lagomarsino S (2015) Seismic assessment of rocking masonry structures. Bull Earthq Eng 13:97–128
10. Liu X, Wu H, Sang L, Sui L, Xu C (2019) Estimation of inelastic interstorey drift for OSB/gypsum sheathed cold-formed steel structures under collapse level earthquakes, Hindawi Adv Mater Sci Eng 2019. Article ID: 2896938. https://doi.org/10.1155/2019/2896938
11. Livesley RK (1978) Limit analysis of structures formed from rigid blocks. Int J Numer Meth Eng 12:1853–1871
12. Lourenço PB, Mendes N, Ramos LF, Oliveira DV (2011) Analysis of masonry structures without box behavior. Int J Archit Herit 5:369–382
13. Milani G, Shehu R, Valente M (2017) Possibilities and limitations of innovative retro-fitting for masonry churches: advanced computations on three case studies. Constr Build Mater 147:239–263
14. Pasticier L, Amadio C, Fragiacomo M (2007) Non-linear seismic analysis and vulnerability evaluation of a masonry building by means of the SAP2000 V.10. Earthq Eng Struct Dyn 37:467–485. https://doi.org/10.1002/eqe.770
15. Pierdicca A, Clementi F, Isidori D, Concettoni E, Cristalli C, Lenci S (2016) Numerical model upgrading of a historical masonry palace monitored with a wireless sensors network. Int J Masonry Res Innov 1:74–99

16. Quagliarini E, Maracchini F, Clementi F (2017) Uses and limits of the equivalent frame model on existing unreinforced masonry buildings for assessing their seismic risk: a review. J Build Eng 10:166–182. https://doi.org/10.1016/j.jobe.2017.03.004
17. Ramaglia G, Lignola GP, Fabbrocino F, Prota A (2018) Numerical investigation of masonry strengthened with composites. Polymers 10:334
18. Sorrentino L, Cattari S, Da Porto F, Magenes G, Penna A (2018) Seismic behaviour of ordinary masonry buildings during the 2016 central Italy earthquakes. Bull Earthq Eng 17:1–25
19. Valente M, Milani G (2017) Effects of geometrical features on the seismic response of historical masonry towers. J Earthq Eng 22:p1-33

Numerical Analysis of Bottle-Shaped Isolated Struts Concrete Deteriorated by Delayed Ettringite Formation

I. S. Lira, F. A. N. Silva, A. C. Azevedo, and João M. P. Q. Delgado

Abstract The paper discusses the structural behaviour of concrete struts deteriorated by internal swelling reactions due to delayed ettringite formation (DEF). To assess this behaviour, non-linear finite elements analyses were performed using CDP model of ABAQUS, which was calibrated and validated. The effects of the internal swelling reactions were simulated numerically using a strategy of decreasing mechanical properties of concrete. MATLAB scripts were developed to automate the process of determining the CDP model parameters, especially those related to the damage in tension and compression with few input data. Decreases in the first crack and failure loads of 78 and 56% were observed which means that DEF expansions are an important issue in the load capacity of concrete structures. Besides, it was also observed a significant increase in cracks openings width, even for low expansion level, with values of 3.65 mm, and for high level of expansion with values of 4.51 mm. This is a relevant aspect for the durability of concrete structures that is severely affected by DEF expansions.

Keywords Numerical modelling · Nonlinear analysis · Bottle-Shaped concrete struts · Internal swelling reactions · Plasticity damage models

1 Introduction

In recent years, researches works have reported with relative frequency the occurrence of DEF expansions in the most varied concrete constructions, such as: bridges

I. S. Lira · F. A. N. Silva
Department of Civil Engineering, Universidade Católica de Pernambuco, Recife, Brazil
e-mail: fernando.nogueira@unicap.br

A. C. Azevedo · J. M. P. Q. Delgado (✉)
CONSTRUCT-LFC, Departamento de Engenharia Civil, Universidade do Porto, Rua Dr. Roberto Frias, s/n, 4200-465 Porto, Portugal
e-mail: jdelgado@fe.up.pt

A. C. Azevedo
e-mail: antonio.costaazevedo@fe.up.pt

J. M. P. Q. Delgado (ed.), *Masonry: Building Pathologies and Design*, Building Pathology and Rehabilitation 22, https://doi.org/10.1007/978-3-030-80496-1_5

[1–3], dams [4–8], railroads and motorways [9, 10], beams and columns [5, 11], spread footing and deep foundations [12, 13]. Most of this research state that the effects of internal expansion reactions in concrete elements might be associated to a significant change in strength and deformation properties of the material. Indeed, Sanchez et al. [14] state that part of the challenge for civil engineers, in addition to knowing the level of expansion to which the structures are exposed, is to understand how concrete mechanical properties are affected by these expansions and, also, how these expansions influence the durability of the structures of concrete. The existence of internal sulfate sources is linked to the DEF expansions [9, 15–18]. Escadeillas et al. [19] reported that only internal attacks of sulfates are related to DEF, while Collepardi [20] considers, in addition to internal attacks, external attacks caused by sources of sulfates. Collepardi [20], additionally, reported that the presence of water is a necessary condition for the migration of sulfate ions into the concrete. The author also reported that the deposition of ettringite occurs inside the microcracks and its propagation is due to the expansion of crystals of ettringite. Collepardi et al. [21] studied three parameters related to internal attacks by sulfates: (a) the sulfate content in the clinker or cement phase, (b) the curing temperature, and (c) the presence of preliminary cracks in concrete samples. The authors concluded that at curing temperatures below 80 °C there is no risk of DEF formation. Yan et al. [22] stated that the structure of the mortar, the morphology of the ettringite and the curing humidity are relevant issues to the formation of the reaction, which was observed at curing temperatures above 70 °C. Several researchers reported that high temperatures during large concrete volume casting above 70 °C are potential causes of concrete expansion due to DEF [4, 17, 18]. Mielich et al. [23] studied the influence of the NaCl solution as an external source of alkali on the creep behaviour of concrete. The authors reported an expansion greater than 0.5 mm/m after six cycles. The modulus of elasticity after 252 days showed a decrease of 17%. Reinhardt et al. [24] reported that internal expansions in concrete are dependent on the type of coarse aggregate used. Regarding tensile strength, it was observed a decrease close to 75%. Sobrinho [13] performed lab tests in concrete cores collected from pile caps affected by internal expansion reactions and reported a maximum decrease of 34.7% in the split tensile strength and 23% in the elastic modulus of concrete. Sanchez et al. [14, 25] discussed the evolution of damage caused by internal expansion reactions using multilevel approach. The authors used aggregates of different origins to produce concrete mixes, which were designed for the characteristic strength of 35 MPa. In the damage caused by DEF expansions, the authors observed maximum decrease in values of the modulus of elasticity of 86% and in the compressive strength of 50%. DEF chemical modelling for assessment of affected concrete structures was investigated by Sellier and Multon [12]. The model was fitted with different materials, heating cycles and storage conditions. The results obtained describe well the swelling potential obtained in several lab tests. The authors also showed that the output of the chemical model can be used in the poromechanical model through the concept of pressure induced by DEF in concrete. Giannini et al. [26, 27] reported the relevance of the stiffness damage test (SDT) to provide a wide range of deterioration levels in concretes elements affected by DEF expansion. The authors concluded that the

stiffness damage index (SDI) and the plastic deformation index (PDI) proposed by Sanchez et al. [25, 28, 29] can be satisfactorily used to characterize the DEF. Results of decreases in mechanical properties of concrete of 75% for its young's modulus and of 41% for its compressive strength were also reported by Giannini et al. [27].

To perform the numerical analyses in the research, it was adopted the strategy to take into account the effects of DEF expansions in concrete through the decrease of mechanical properties of strength and deformation of the material. This approach is consistent with several studies of the literature that observed this fact in numerical modelling and laboratory tests [8, 11, 12, 14, 25, 27, 30, 31].

In resume, this work presents a numerical analysis of the structural performance of isolated concrete bottle-shaped struts deteriorate by internal expansion due to delayed ettringite formation using the finite element method. A better comprehension of the effects of DEF expansions is an important issue for engineers because they can damage concrete structures severely. By the other hand, since experimental tests are generally costly and require a long period to obtain results, the use of computer simulations may be a viable strategy if one has a reliable modelling strategy. Concrete Damaged Plasticity (CDP) model was used to perform non-linear finite elements analyses. CDP is a continuum model, plasticity-based, damage model for concrete that assumes that the main two failure mechanisms are tensile cracking and compressive crushing of the concrete material. Among the various possibilities of a phenomenological approach of DEF expansions concrete, it was adopted the strategy of taking into account the effect that those expansions generate on the mechanical properties of concrete. This modelling strategy is convergent with several studies that have already confirmed the effect of reducing the mechanical properties of concrete, in an important way, when the material is affected by internal expansion reactions due to DEF [11, 14, 27].

2 Materials and Methods

2.1 Materials

Sankovich's works [32, 33] were used as experimental benchmark tests to evaluate and validate the finite element simulation of isolated bottle-shaped concrete struts deteriorated by internal swelling reactions due to DEF. Both linear and non-linear finite element analyses were performed using the Concrete Damage Plasticity Model (CDP) of ABAQUS [34], which is a continuum, plasticity-based, damage model for concrete. The model assumes that the main two failure mechanisms are tensile cracking and compressive crushing of the concrete material. The evolution of the yield (or failure) surface is controlled by two hardening variables that are linked to failure mechanisms under tension and compression loading, respectively.

Partially loaded unreinforced concrete panels with dimensions of 914.4 × 914.4 × 152.5 mm^3 were modelled, as well as the 304.8 × 152.5 × 50.8 mm^3 steel plates

at its top and base as it is shown in Fig. 1. Details of the two panels modelled are summarized in Table 1 [33].

MATLAB [35] scripts, based on Alfarah's work [36], were developed to automate the process of determining the CDP model parameters, especially those related to the damage in tension and compression with few input data. Table 2 shows one example of MATLAB script output to be used as inputs for the CDP model.

Expansions due DEF often affect concrete mechanical parameters that, in turn, modify inelastic strains and damage properties in tension and compression. By this reason, other MATLAB scrip was developed to calculate CDP model inputs information according to the level of expansion imposed to the concrete elements under investigation. Table 3 summarizes data obtained from Sanchez's and Giannini works that were used in the numerical simulations [14, 27].

Once the CDP model has been calibrated taking into account the level of expansions from DEF, two scenarios were created to discuss the results. In the first scenario it was considered that all the regions of the panel were affected by DEF expansions

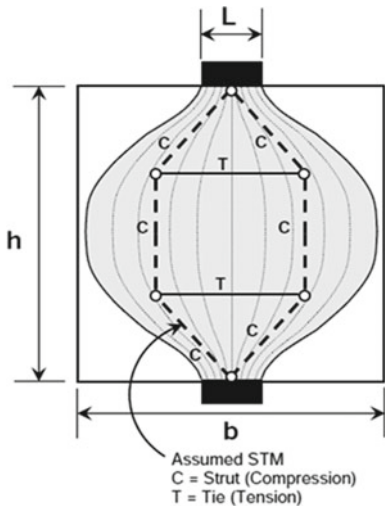

Fig. 1 Bottle-shaped struts and associated strut and tie model

Table 1 Panel results (S1-2 and S3-1)

Panel	Panel dimensions (mm)	Load plate dimensions (mm)	f_c (MPa)	1st cracking load (kN)	Failure load (kN)	Principal tensile strain (%)
S1-2	914.4 × 914.4 × 101.6	304.8 × 50.8 × 101.6	26.41	524.0	706.8	0.0022
S3-1	914.4 × 914.4 × 152.4	304.8 × 50.8 × 152.4	28.96	608.5	873.2	0.0014

Table 2 Input concrete properties for CDPM in ABAQUS (S1-2)

Elasticity		Plasticity	
Compressive strength, f_c (MPa)	26.41	Dilation angle (°)	5
		Eccentricity (−)	0.1
Elasticity model (MPa)	28,564.32	fb0/fc0 (−)	1.16
		K (−)	2/3
Poisson's ratio (−)	0.2	Viscosity	0.0029
Damage			
Compressive behavior		Compressive damage	
Yield stress (MPa)	Inelastic strain (−)	Damage parameter (−)	Inelastic Strain (−)
34.41	0	0	0
32.72	0.003	0.57	0.003
28.50	0.005	0.71	0.005
23.47	0.007	0.81	0.007
3.53	0.025	0.99	0.025
Tensile behavior		Tensile damage	
Yield stress (MPa)	Cracking Strain (−)	Damage Parameter (−)	Cracking Strain (−)
2.67	0	0	0
2.02	0.0002	0.63	0.0002
1.76	0.0004	0.74	0.0004
1.54	0.0005	0.81	0.0005
0.36	0.0025	0.99	0.0025

(fully affected panel). In the second one, it was took into account that the expansions were located only in the bottle-shaped strut region (partially affected panel), calculated using linear elastic analysis of the panel (see Fig. 2). The existence of bottle-shaped struts within the two ending cross-sections of partial loaded unreinforced concrete panels was already highlighted by theoretical studies and lab tests of other researchers [32, 37–40].

The justification for creating the second scenario was the need to analyse the effects of deterioration only on the part of the panel responsible for the load-bearing mechanism of the studied elements on its overall behaviour—its bottle-shape strut.

2.2 Computational Model

C3D8R finite elements were used to model the panel using a structured mesh with cubic elements with a side of 50.8 mm. This approach is consistent with previous

Table 3 Decrease rates in mechanical properties according to the level of expansion

Distress mechanism	Reference expansion level (%)	Damage results	
		Stiffness loss (%)	Compressive strength loss (%)
DEF 01 [14]	0.11 ± 1	56	34
	0.30 ± 1	62	43
	0.50 ± 1	77	47
	1.00 ± 1	86	50
DEF 02 [27]	0.10	13	0
	0.21	36	0
	0.34	65	28
	0.42	68	32
	0.51	71	33
	1.01	75	41
DEF 03 [27]	0.08	15	0
	0.18	24	2
	0.27	31	11
	0.33	21	0
	0.45	59	24

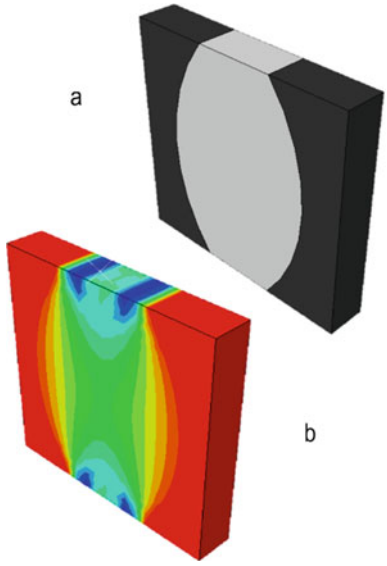

Fig. 2 S1-2 with the strut from linear elastic analysis of the panel

researches that used finite element model (FEM) for the analysis of concrete structures deteriorated by internal expansions [8, 41]. Discrete rigid family elements—R3D4—were used to model steel and top plates. This decision was taken after the study of several other modelling possibilities and it was the one that presented a better computational effort/work ratio of analysis and interpretation of results.

The resulting finite element mesh for panel S1-2 is presented in Fig. 3. The mesh of the plates is exhibited in Fig. 4. For the modelling of this panel with the upper and lower steel plates, 716 elements and 1211 nodes were used, totalling 3633 degrees of freedom. A coefficient of friction of 0.3 was used to simulate the contact interaction between the steel plates and the panel surface.

The applied load was a uniformly distributed compression stress on the contact surface of the steel plate-concrete panel, corresponding to the value of the rupture load of the lab tests [33]. The boundary conditions of the top plate were set so that only vertical displacements were enabled. This boundary condition allows the rigid body displacement of the plate in the direction of loading. The same procedures used to impose the boundary conditions on the upper plate were used on the lower plate with all three-translation degrees of freedom were restrained, in this case.

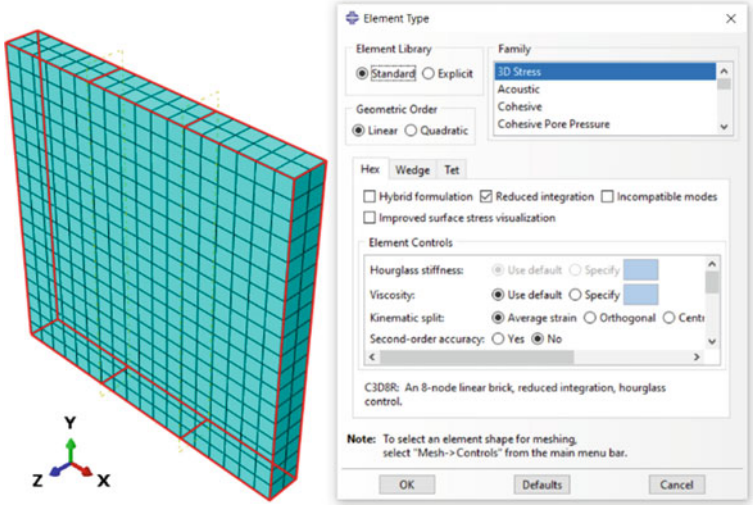

Fig. 3 Finite element mesh of S1-2 panel

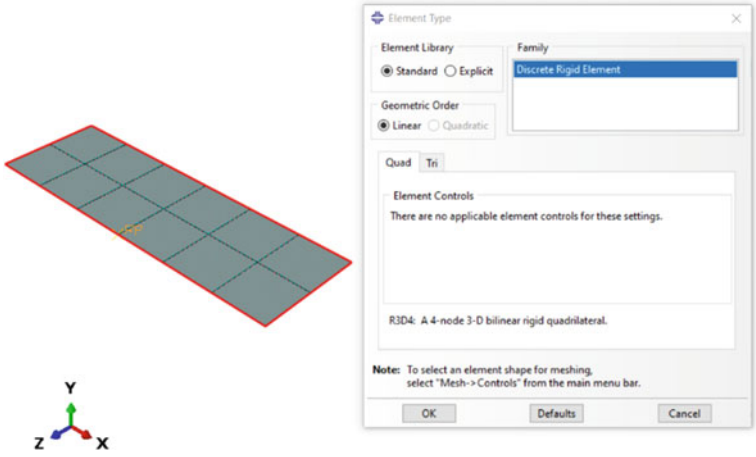

Fig. 4 Finite element mesh of the loading plates

3 Results and Discussion

3.1 Validation of the FEM

A plastic tensile strain of the model of S1-2 panel output is presented in Fig. 5 close to the failure view of the panel observed in lab tests. In this Figure, it is possible to observe a good correlation between the profiles of plastic tensile strains with those observed in the lab tests. This fact highlights that the numerical model developed was able to adequately describe the mechanisms involved in the rupture of the panel

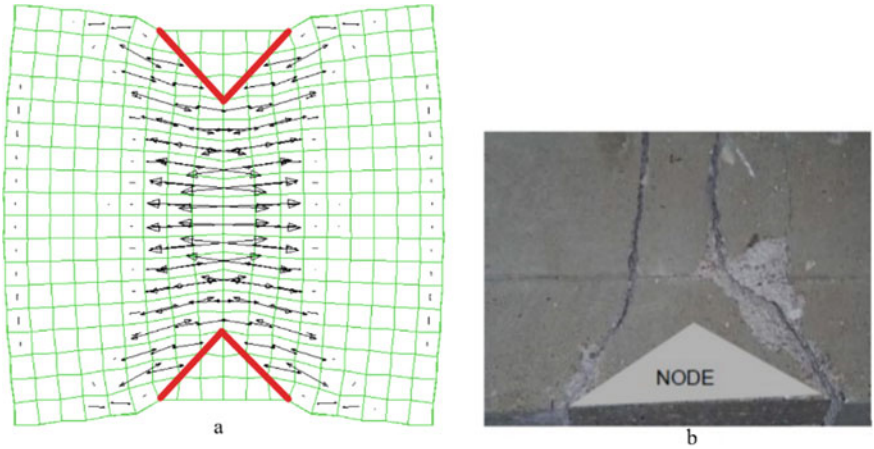

Fig. 5 Panel S1-2 **a** numerical plastic tensile strains profile, **b** lab failure

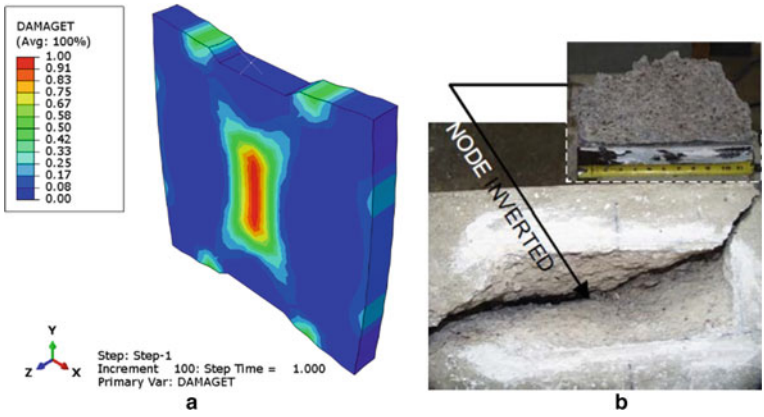

Fig. 6 Tensile damage of the S1-2 panel **a** numerical model and **b** lab test

understudy—formation of the compression cone at the top and base of the panel and changing the orientation of the plastic tensile strains in the vicinity of the compression cone.

The nodal region, both in the numerical and lab test models, presents the shape similar to that of an isosceles triangle with its base being two times its height. In this region, the stresses are mostly compression and, in its vicinity, can be observed the crushing of concrete (see Fig. 5b).

The tensile damage profile of the numerical model is displayed in Fig. 6 close to the S1-2 panel view at failure. In this Figure, it is possible to observe that the numerical model was able to describe the damage that occurred on the lateral faces of the panel. Sankovich [32, 33] reported the existence of damage in regions close to the compression edges at the top and base of the panel, a situation also described by the numerical model developed—damage of approximately 40%. Maximum tensile damage has reached to 100% in the central region of the panel, at failure.

The compression damage in the numerical models was less pronounced than the tensile damage, an aspect also verified in the lab tests. The magnitude of the damage in compression of the numerical model was approximately 71%. Despite this fact, the profile of compression damage is relevant to validate the location of the compression crushing of the concrete in the numerical models. Figure 7 shows the profile of compression damage, where the concentration of damage can be observed in the vicinity of the nodal region, consistently with crash regions of concrete observed in lab tests. It was possible to capture a strut narrowing with the increase of vertical load, during the loading process. Figure 8 exhibits this behaviour highlighting the tension and compression fields in the numerical model of S1-2 panel, which is quite similar to those observed in lab test.

The numerical model also captured the occurrence of vertical tensile stresses that are responsible for the narrowing of the strut observed in the lab tests. This fact

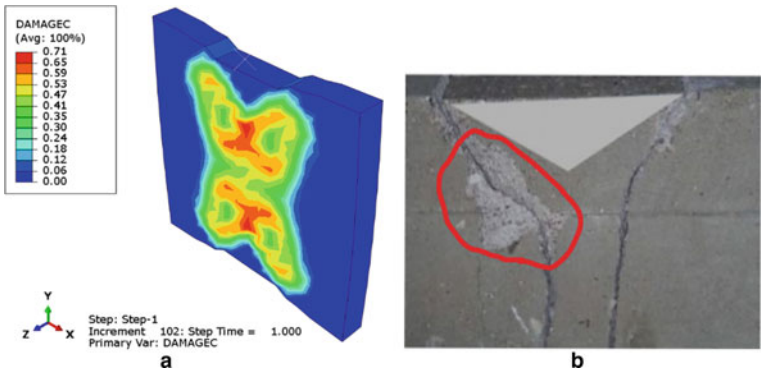

Fig. 7 Compressive damage in S1-2 panel: **a** numerical model and **b** lab tests

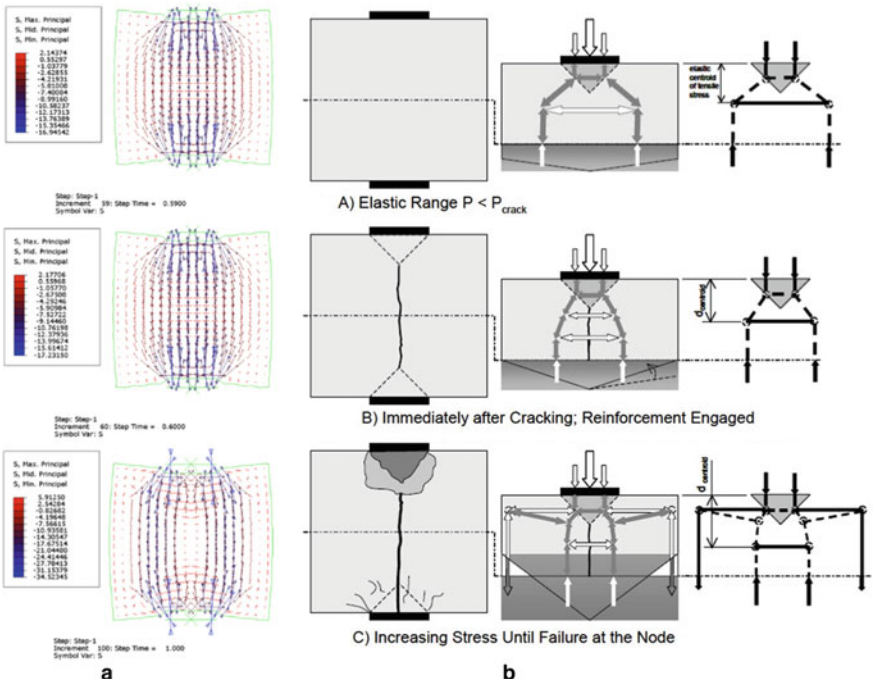

Fig. 8 Evolution of STM for different loading levels **a** numerical model and **b** lab tests

demonstrates that the numerical model was efficient in capturing the phenomenon discussed.

Table 4 summarizes the lab tests and numerical results for the panels investigated. In this Figure, the first cracking load and the maximum horizontal tensile strains are presented for the numerical model and lab tests. As it can be observed, the numerical

Table 4 Comparison of numerical and lab tests results

Panel	First cracking load (kN)		Error (%)	Maximum tensile strain (‰)		Error (%)
	Num.	Exp.		Num.	Exp.	
S1-2	424.1	524.0	− 19.1	0.0025	0.0022	− 13.64
S3-1	681.1	608.5	11.93	0.0012	0.0014	− 14.3

model was able to predict the first cracking load of the investigated panels with acceptable precision, considering the complexity of the studied phenomenon. The maximum error in the first cracking load and the maximum tensile strain was − 19.1% and -14.30%, respectively.

Two verifications were performed regarding vertical deformations: one comparing the results of the S3-1 panel at the first cracking formation and the other at failure with data of the S3-10 panel. This option is justified by the similarity in the instrumentation of these two panels. Figure 9 presents this comparison. The behaviour of the numerical model for the first cracking and failure loads was similar to those observed in lab tests—maximum vertical strains in the center of the panel decreasing to the edges of the panel.

Figure 10 shows the envelope of vertical strains measured at half the height of the panels along their length. This Figure also shows the strains obtained in the lab tests. The results showed in this figure highlights that the responses of the numerical panels investigated were located inside the experimental envelope.

Given the results presented in this section, one can conclude that the numerical models developed were able to efficiently describe the experimental behaviour of the panels investigated, an aspect that validates the numerical models.

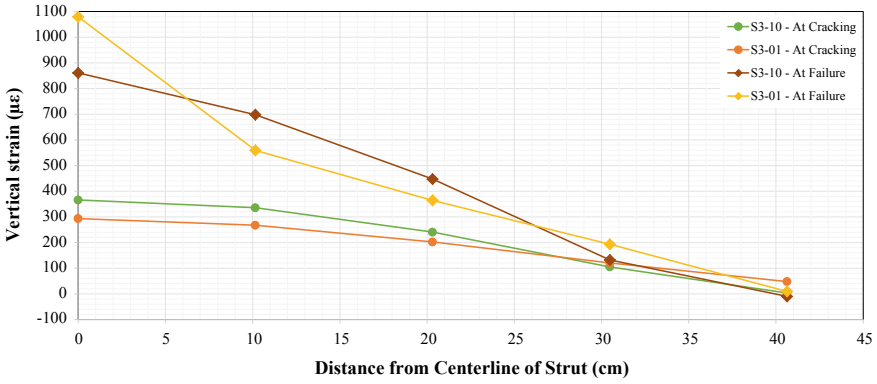

Fig. 9 Comparison between vertical strains at first cracking and failure of S3-10 and S3-1 Panels

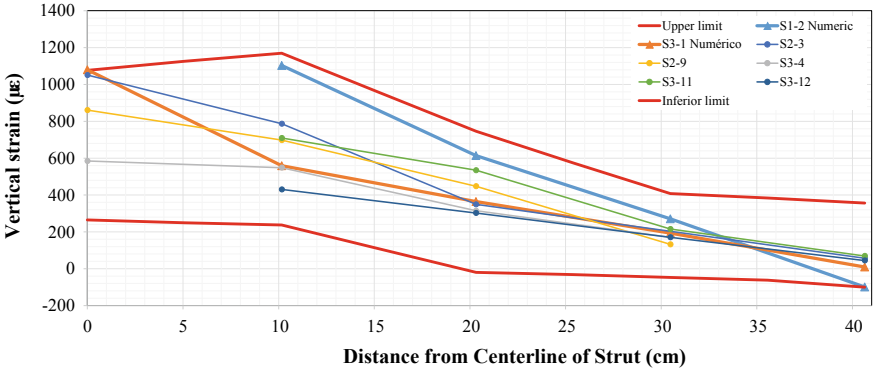

Fig. 10 Comparison between vertical strains at failure for numerical models and lab tests results

3.2 Discussion

In this section results from numerical analyses of Sankovich's panel deteriorated by DEF expansions is presented and discussed.

Figure 11 shows the evolution of the first cracking and failure loads with the expansion levels, for the fully affected panel. It can be seen that the intact panel, represented by the point of no expansion, presented a first cracking load of about 421 and 325.1 kN, for the low expansion level. This means that for a relatively low level of expansion (0.11%), the first cracking load decrease was approximately 23%.

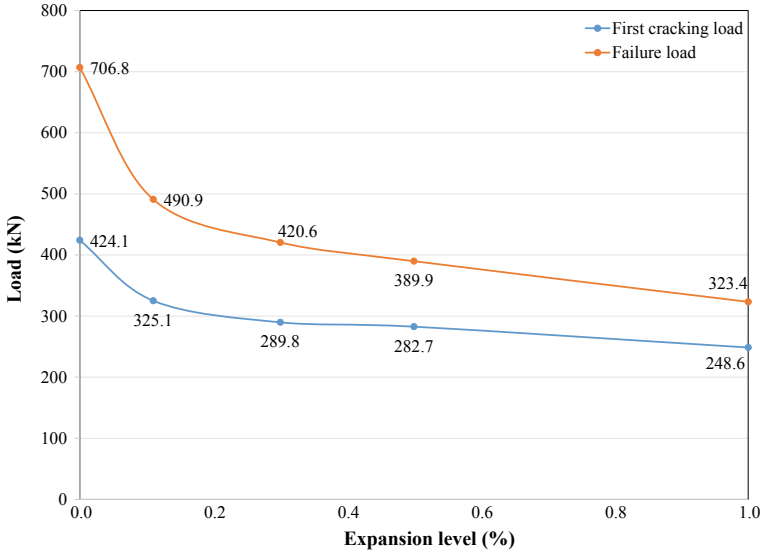

Fig. 11 First cracking and failure loads for each expansion level for the fully affected panel

For the high expansion level (1%), the first cracking load was 248.6 kN—a decrease of 41%. This fact is consistent with previous researches, which observed that an expansion of 0.1% corresponds to the first appearance of visible cracks in concrete elements affected by DEF. The decrease in the load capacity of the panel observed in a macroscopic level can, in fact, be microscopically explained by the separation between paste and aggregate, as commonly reported by several researchers [42, 43].

The failure load of the intact panel was 706.8 kN. For the fully affected panel in expansion level of 0.11% the failure load reached 490.9 kN—a decrease of 31%. The failure load for the 1% expansion level was even lower—323.4 kN, representing a decrease of approximately 54% compared with the intact panel. These results highlight the important effect of internal expansion reactions on overall panel behaviour. Similar results were found by Karthik [11], that reported the energy absorption capacity of large reinforced concrete beam-column joints subject to ASR/DEF deterioration close to 40% of that of control specimen without deterioration.

It is also possible to observe in Fig. 11 that there are important decreases in the initial levels of expansion, both at the first cracking load and at failure load. Additionally, it was observed that the effect of the discrete expansions was more pronounced at failure load. For medium expansion levels, the decrease in the first cracking and failure load were less pronounced. This fact points out to the importance of early diagnosis of the levels of expansion existing in concrete elements affected by DEF, so that one can decide regarding the need for recovery or rehabilitation interventions works.

Same analyses were performed for the partially affected panel and the results are shown in Fig. 12. It can be observed decreases of 53% and 78% in the first cracking

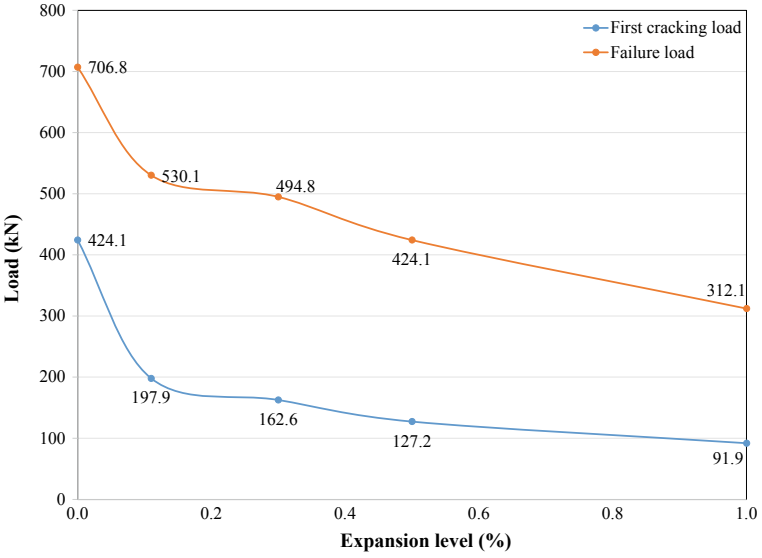

Fig. 12 First cracking and failure loads for each expansion level for the partially affected panel

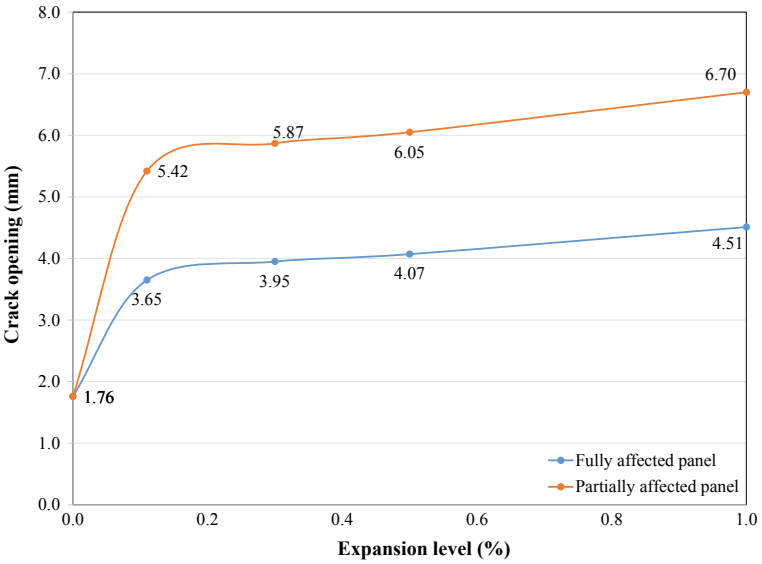

Fig. 13 Crack opening at failure for each expansion level for both fully and partially affected panel

load for low and high levels of expansions, respectively. In the same way, it was observed decreases in the failure load of 25 and 45%, for those levels of expansion.

Figure 13 shows the evolution of the maximum crack opening at failure with the expansion levels for both fully and partially affected panel. One can observe that, for low level of expansion, the maximum crack opening is approximately 3.65 mm for the fully affected panel while for the intact panels, the maximum crack opening is approximately 1.76 mm—an increase of 104%. For an expansion level of 1%, the maximum crack opening is approximately 4.51 mm for the fully affected panel—an increase of 156%.

It can also be seen in Fig. 13 the evolution of the maximum crack opening at failure with the expansion levels for the partially affected panel, from which one can realize increasing in cracks opening of 208% and 281%, for low and high level of expansions, respectively. Values of crack openings obtained might be compared by order of magnitude with those found in concrete beams deteriorated due to DEF expansion by others researches [5].

The increase in the crack opening demonstrates the potential damage of DEF expansions in concrete, since these cracks open ways to the transport of aggressive agents from outside to the inside of the element, compromising its durability. Consistently with what was observed, Karthik [5] states, additionally, that DEF induced cracks can lead to moisture ingress and rebar corrosion which can negatively impact the strength and ductility of the structure.

Compressive strain and damage evolution with the level of expansion at failure for the fully affected panel are shown in Fig. 14. It can be seen that the intact panel presented a compressive strain of about 4.7‰. For a level of expansion of 0.11%,

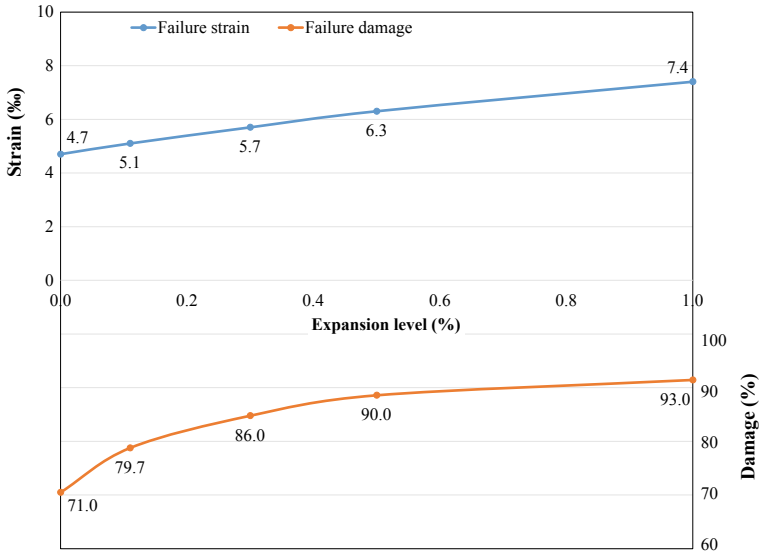

Fig. 14 Compressive strain and compressive damage for each expansion level for the fully affected panel

the compressive strain was about 5.1‰ and for the expansion level of 1%, it reached to a compressive strain of 7.4‰. This means that, for low level of expansion, the increase in compressive strain was approximately 8.5%, while that, for the high level, the increase was 57.4%. Also, when one looks at the compressive damage, the intact panel exhibited a value of approximately 71%. For the high level of expansion, the damage of approximately 98%—an increase of 38%. These results show a serious decrease in the panel stiffness caused by the DEF expansions.

Compressive strain and damage evolution with the level of expansion at failure for the partially affected panel are shown in Fig. 15. It was observed increases of about 31% in compressive strain for low level of expansion and virtually no differences for high level of expansion.

Figure 16 shows the tensile damage profile at failure for a level of expansion of 1% for the intact, fully affected and partially affected scenarios. The tensile damage profile of the panels is similar, with cracks concentrating in the centre of the panels. It can be seen that the partially affected panel, besides presenting the tensile damage distributed throughout the struts, exhibited damage about 30% on the panel's side and about 50% close to the loading area and the nodal region. The fully affected panel showed damage neither on the panel nor on the nodal region. These results show that in the scenario with the swelling expansion concentrated only in the strut region produced the worst structural performance for the panel investigated. This is an important conclusion for structural design engineers.

Figure 17 illustrates the compressive damage profile at failure at the high level of expansion for the intact, fully affected, and partially affected panels. The compressive

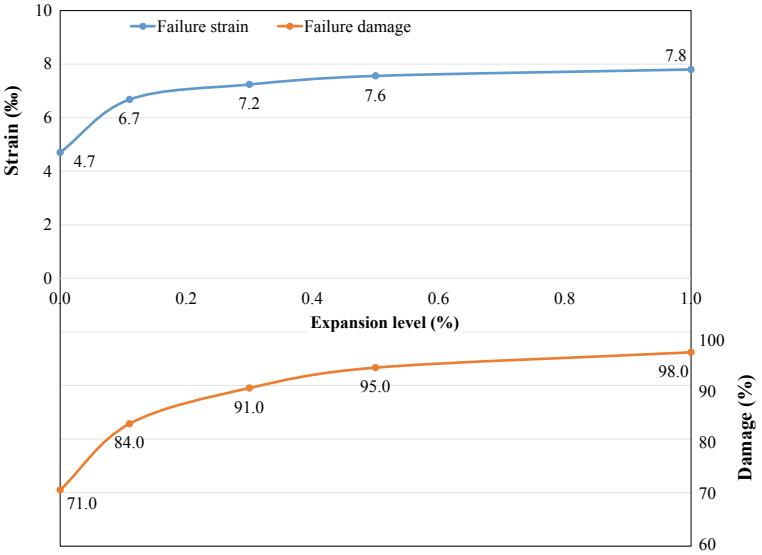

Fig. 15 Compressive strain and compressive damage for each expansion level for the partially affected panel

damage profile of the intact and fully affected panel is quite similar. The concrete crushing is concentrated at the beginning of the compression cone. In the partially affected panel, the compressive damage is distributed throughout the compression cone and the compression wedge worsens, as a result of flattening on the loading surface. This represents a loss of stiffness at the load transfer points. Compressive damage becomes more evenly distributed in the partially affected panel, which indicates more regions being crushed, even though the value of the damage in this scenario was not the biggest one. This may be happened because the failure of the partially affected panel is governed by cracking in tension.

Taking into account all the results presented this section, it can be concluded that the effects of the in decreases the mechanical properties of the concrete due to DEF expansions are relevant in the loss of load capacity, stiffness and serviceability condition of the concrete panels investigated. Table 5 summarizes results discussed in this section.

4 Conclusions

The paper discussed the structural behaviour of concrete struts deteriorated by internal swelling reaction due to delayed ettringite formation. The main conclusions found are:

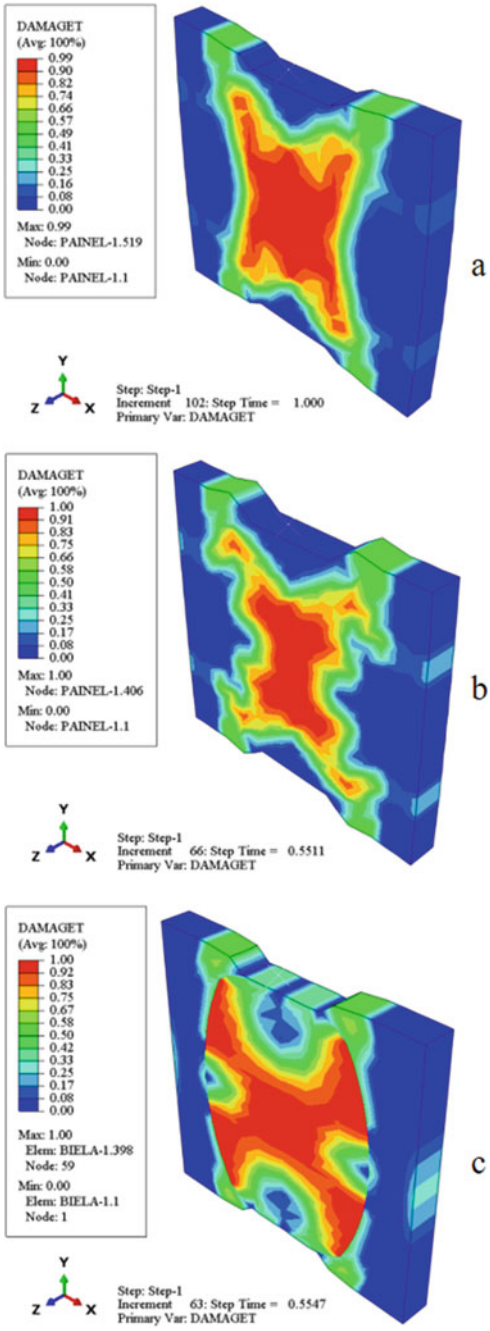

Fig. 16 Tensile damage for expansion of 1% **a** intact, **b** fully affected, **c** partially affected

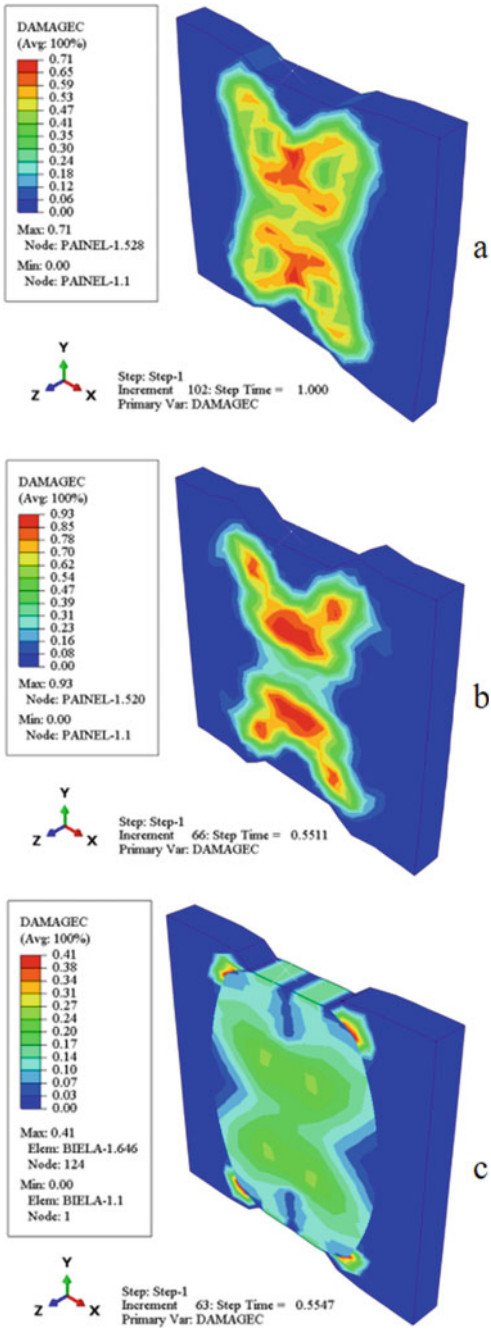

Fig. 17 Compressive damage for expansion of 1% **a** intact, **b** fully affected, **c** partially affected

Table 5 Summary of decreasing of first cracking and failure loads of panel S2-1

Scenario	Decrease in first cracking load		Decrease in failure load		Increase in crack open width	
	LLE (%)	HLE (%)	LLE (%)	HLE (%)	LLE (%)	HLE (%)
FAP	− 23	− 41	− 31	− 54	+ 104	+ 156
PAP	− 53	− 78	− 25	− 56	+ 208	+ 281

- The ABAQUS CDP proved to be an efficient numerical strategy for the representation of mechanical phenomena involved in load support mechanisms in partially loaded concrete panels with the formation of isolated bottle-shaped struts;
- Calibration of the CDPM model with Sankovich's experiments [32] enhanced the capabilities of the model;
- The effects of the internal swelling reactions, simulated numerically using a strategy of decreasing mechanical concrete properties according to Sanchez, allows to identify:
  - For both scenarios investigated, the one that most significantly affects the overall structural behaviour of the panel was the partially affect model. An explanation for this fact is that, in this situation, exactly the most important part of the load carrying mechanisms panel is being affected – its bottle-shaped strut;
  - Decreases in the first crack and failure loads of 78 and 56%;
  - Increase in cracks openings width, even for low expansion level, with values of 3.65 mm, and for high level of expansion with values of 4.51 mm;
  - Increase in compressive strain and damage failure of about 57% and 38%, respectively.

References

1. Boenig A, Funez L, Klingner RE, Fowler TJ (2001) Bridges with premature concrete deterioration: field observations and large-scale testing, N. FHWA/TX-02/1857-1. Center for Transportation Research, University of Texas at Austin, USA
2. Boenig A (2000) Bridges with premature concrete deterioration: field observations and large-scale testing. University of Texas at Austin, MSc. Thesis, USA
3. Zhang H, Li L, Wang W (2019) Effects of temperature rising inhibitor on nucleation and growth process of ettringite. J Solid State Chem 274:222–228. https://doi.org/10.1016/j.jssc.2019.03.037
4. Blanco A, Cavalaro SHP, Segura I, Segura-Castillo L, Aguado A (2018) Expansions with different origins in a concrete dam with bridge over spillway. Constr Build Mater 163:861–874. https://doi.org/10.1016/j.conbuildmat.2017.12.161
5. Karthik MM, Mander JB, Hurlebaus S (2016) Deterioration data of a large-scale reinforced concrete specimen with severe ASR/DEF deterioration. Constr Build Mater 124:20–30. https://doi.org/10.1016/j.conbuildmat.2016.07.072

6. Ayora S, Chinchón A, Aguado F (1998) Guirado, Weathering of iron sulfides and concrete alteration: thermodynamic model and observation in dams from central Pyrenees, Spain. Cem Concr Res 28(9):1223–1235. https://doi.org/10.1016/S0008-8846(98)00137-9
7. Campos A, Lopez CM, Blanco A, Aguado A (2016) Structural diagnosis of a concrete dam with cracking and high nonrecoverable displacements. J Perform Constr Fac 30(5):04016021. https://doi.org/10.1061/(ASCE)CF.1943-5509.0000869
8. Campos CM, Lopez A, Blanco A (2018) Aguado, Effects of an internal sulfate attack and an alkali-aggregate reaction in a concrete dam. Constr Build Mater 166:668–683. https://doi.org/10.1016/j.conbuildmat.2018.01.180
9. Sahu S, Thaulow N (2004) Delayed ettringite formation in Swedish concrete railroad ties. Cem Concr Res 34:1675–1681. https://doi.org/10.1016/j.cemconres.2004.01.027
10. Custódio J, Ribeiro AB (2019) Evaluation of damage in concrete from structures affected by internal swelling reactions–a case study. Proc Struct Integr 17:80–89. https://doi.org/10.1016/j.prostr.2019.08.012
11. Karthik MM, Mander JB, Hurlebaus S (2020) Simulating behaviour of large reinforced concrete beam-column joints subject to ASR/DEF deterioration and influence of corrosion. Eng Struct 222:111064. https://doi.org/10.1016/j.engstruct.2020.111064
12. Sellier A, Multon S (2018) Chemical modelling of delayed ettringite formation for assessment of affected concrete structures. Cem Concr Res 108:72–86. https://doi.org/10.1016/j.cemconres.2018.03.006
13. Sobrinho CWAP (2012) Piles caps of buildings affected by AAR—case study. In: 54th Brazilian concrete congress, Maceió, Brazil, 2012 (in Portuguese)
14. Sanchez LFM, Drimalas T, Fournier B, Mitchell D, Bastien J (2018) Comprehensive damage assessment in concrete affected by different internal swelling reaction (ISR) mechanisms. Cem Concr Res 107:284–303. https://doi.org/10.1016/j.cemconres.2018.02.017
15. Mehta PK, Monteiro PJM (2014) Concrete: microstructure, properties e materials, 4th edn. McGraw-Hill Professional Publishing, USA
16. Taylor HFW (1997) Cement chemistry, 2nd edn. Thomas Telford Publishing, UK, London
17. Taylor HF, Famy C, Scrivener K (2001) Delayed ettringite formation. Cem Concr Res 31(5):683–693. https://doi.org/10.1016/s0008-8846(01)00466-5
18. Diamond S (1996) Delayed ettringite formation-processes and problems. Cem Concr Compos 18(3):205–215. https://doi.org/10.1016/0958-9465(96)00017-0
19. Escadeillas G, Aubert JE, Segerer M, Prince W (2007) Some factors affecting delayed ettringite formation in heat-cured mortars. Cem Concr Res 37(10):1445–1452. https://doi.org/10.1016/j.cemconres.2007.07.004
20. Collepardi M (2003) A state-of-art review on delayed ettringite attack on concrete. Cem Concr Compos 25:401–407. https://doi.org/10.1016/S0958-9465(02)00080-X
21. Collepardi M, Olagot JO, Salvioni D, Sorrentino D (2004) DEF-related expansion of concrete as a function of sulfate content in the clinker phase or cement and curing temperature. Symp Paper 222:77–92
22. Yan P, Zheng F, Peng J, Qin X (2004) Relationship between delayed ettringite formation and delayed expansion in massive shrinkage-compensating concrete. Cem Concr Compos 26(6):687–693. https://doi.org/10.1016/S0958-9465(03)00060-X
23. Mielich O, Reinhardt HW, Garrecht H, Giebson C, Seyfarth K, Ludwig HM (2015) Strength and deformation properties of concrete as evaluation criteria for ASR performance tests. Beton 110(2015):554–563. https://doi.org/10.1002/best.201500018
24. Reinhardt HW, Mielich O (2012) Mechanical properties of concretes with slowly reacting alkali sensitive aggregates. In: Proceedings of the 14th ICAAR conference, Austin, TX, USA
25. Sanchez LFM, Fournier B, Jolin M, Mitchell D, Bastien J (2017) Overall assessment of Alkali-aggregate reaction (AAR) in concretes presenting different strengths and incorporating a wide range of reactive aggregate types and natures. Cem Concr Res 93:17–31. https://doi.org/10.1016/j.cemconres.2016.12.001
26. Giannini ER, Folliard KJ, Zhu J, Bayrak O, Kreitman K, Webb Z, Hanson B (2013) Non-destructive evaluation of in-service concrete structures affected by alkali-silica reaction (ASR)

or delayed ettringite formation (DEF), Final Report, Part I, No. FHWA/TX-13/0-6491-1. Center for Transportation Research, Austin, Texas, USA
27. Giannini ER, Sanchez LFM, Tuinukuafe A, Folliard KJ (2018) Characterization of concrete affected by delayed ettringite formation using the stiffness damage test. Constr Build Mater 162:253–264. https://doi.org/10.1016/j.conbuildmat.2017.12.012
28. Sanchez LFM, Fournier B, Jolin M, Bastien J (2015) Evaluation of the stiffness damage test (SDT) as a tool for assessing damage in concrete due to ASR: input parameters and variability of the test responses. Constr Build Mater 77:20–32. https://doi.org/10.1016/j.conbuildmat.2014.11.071
29. Sanchez LFM, Fournier B, Jolin M, Bastien J, Mitchell D (2016) Practical use of the stiffness damage test (SDT) for assessing damage in concrete infrastructure affected by alkali-silica reaction. Constr Build Mater 125:1178–1188. https://doi.org/10.1016/j.conbuildmat.2016.08.101
30. Seignol JF, Baghdadi N, Toutlemond F (2009) A macroscopic chemo-mechanical model aimed at re-assessment of delayed ettringite formation affected concrete structures. In: 1st international conference on computational technologies in concrete structures CTCS'09, Jeju, Korea
31. Thiebaut Y, Multon S, Sellier A et al (2018) Effects of stress on concrete expansion due to delayed ettringite formation. Constr Build Mater 183:626–641. https://doi.org/10.1016/j.conbuildmat.2018.06.172
32. Sankovich CL (2003) An explanation of the behavior of bottle-shaped struts using stress fields. University of Texas, Austin, USA, 2003. MSc. Thesis
33. Brown MD, Sankovich CL, Bayrak O, Jirsa JO, Breen JE, Wood SL (2006) Design for shear in reinforced concrete using strut-and-tie models, Report No. FHWA/TX-06/0-4371-2, University of Texas at Austin
34. ABAQUS (2018) ABAQUS user's manual. Providence, Rohde Island, USA: Dassault Systèmes. Simulia Corporation ABAQUS vs. 6.18
35. MATLAB (2012) The language of technical computing. The MathWorks, Inc., USA
36. Alfarah B, López-Almansa F, Oller S (2017) New methodology for calculating damage variables evolution in plastic damage model for RC structures. Eng Struct 132:70–86. https://doi.org/10.1016/j.engstruct.2016.11.022
37. Rossi PP (2013) Evaluation of the ultimate strength of RC rectangular columns subjected to axial force, bending moment and shear force. Eng Struct 57:339–355. https://doi.org/10.1016/j.engstruct.2013.09.006
38. Brown MD, Sankovich CL, Bayrak O, Jirsa JO (2006) Behavior and efficiency of bottle shaped struts. ACI Struct J 103(3):348–355. https://doi.org/10.14359/15312
39. Sahoo DK, Gautam RK, Singh B, Bhargava P (2008) Strength and deformation of bottle-shaped struts. Magaz Concr Res 60(2):137–144. https://doi.org/10.1680/macr.2008.60.2.137
40. Laughery L, Pujol S (2015) Compressive strength of unreinforced struts. ACI Struct J 112(5):617–624. https://doi.org/10.14359/51687711
41. Comby-Peyrot I, Bernard F, Bouchard PO, Bay F, Garcia-Diaz E (2009) Development and validation of a 3D computational tool to describe concrete behaviour at mesoscale. Application to the alkali-silica reaction. Comp Mater Sci 46(4):1163–1177. https://doi.org/10.1016/j.commatsci.2009.06.002
42. Brunetaud X, Divet L, Damidot D (2008) Impact of unrestrained delayed ettringite formation-induced expansion on concrete mechanical properties. Cem Concr Res 38(11):1343–1348. https://doi.org/10.1016/j.cemconres.2008.05.005
43. Brunetaud X, Linder R, Divet L, Duragrin D, Damidot D (2007) Effect of curing conditions and concrete mix design on the expansion generated by delayed ettringite formation. Mater Struct 40(6):567–578. https://doi.org/10.1617/s11527-006-9163-3

Concrete Samples Extracted from Pile Caps and Affected by Internal Swelling Reactions: A Diagnostic Analysis

N. Nascimento, F. A. N. Silva, A. C. Azevedo, T. Mahfoud, A. Khelidj, and João M. P. Q. Delgado

Abstract In this work, it was analyzed in detail the problem of the extensive cracking in the pile cap foundation originated by the delayed ettringite formation, possibly from a high heat of hydration coming from the concreting of the large volume of concrete. Laboratory tests were performed to evaluate the transport properties of concrete samples, as well as their physical and chemical composition using advanced analyses. The tests performed were apparent porosity, gas permeability, scanning electron microscopy, X-ray diffraction and Raman spectroscopy. The presence of crystalline products of the alkali-aggregate reaction was proven through physical–chemical analyses, such as Raman spectroscopy and EDS. As well as the ettringite crystals found in XRD standards, SEM images and the chemical composition of EDS. The porosity showed a high value (between 9 and 10%), as well as the concrete permeability (10^{-16} and 10^{-15}), determining the negative influence of ISR on the transport properties. Therefore, the methods used have proven to be effective in understanding the problem encountered and have the potential to be used in the design and execution of pile cap blocks.

N. Nascimento · F. A. N. Silva
Department of Civil Engineering, Universidade Católica de Pernambuco, Recife, Brazil
e-mail: fernando.nogueira@unicap.br

T. Mahfoud · A. Khelidj
GeM Laboratory, University of Nantes, Saint Nazaire, Nantes, France
e-mail: mahfoud.tahlaiti@icam.fr

A. Khelidj
e-mail: abdelhafid.khelidj@univ-nantes.fr

A. C. Azevedo · J. M. P. Q. Delgado (✉)
CONSTRUCT-LFC, Departamento de Engenharia Civil, Universidade do Porto, Rua Dr. Roberto Frias, s/n, 4200-465 Porto, Portugal
e-mail: jdelgado@fe.up.pt

A. C. Azevedo
e-mail: antonio.costaazevedo@fe.up.pt

J. M. P. Q. Delgado (ed.), *Masonry: Building Pathologies and Design*, Building Pathology and Rehabilitation 22, https://doi.org/10.1007/978-3-030-80496-1_6

Keywords Internal swelling reactions · Alkali-silica reaction · Delayed ettringite formation · Diagnostic of pathologies on concrete · Characterization and analysis of concrete specimens

1 Introduction

In the last decade, the occurrence of early deterioration of pile cap blocks in residential buildings and concrete bridges in the Metropolitan Region of Recife has been reported with relative frequency. This process usually starts with the occurrence of a horizontal crack of large opening in the lateral faces of the element, located approximately 30 cm from the upper face of the block, and its installation is usually attributed to the expansions of concrete resulting from the alkali-silica reaction.

The pathological manifestations associated with chemical phenomena are more common all over the world in construction works containing large volumes of concrete, such as dams and pavements [1], but in Brazil, especially in the northeast of the country, the occurrence of alkali-silica reaction (ASR) and delayed ettringite formation (DEF) in pile cap blocks and in spread footing foundations of residential buildings and bridges at early ages is very common. This fact has payed the attention of the civil construction industry and local research centers to the need to understand the mechanisms involved in this process so that mitigating or corrective measures can be adopted.

Several authors presented studies of the occurrence of alkali-silica reaction and the delayed ettringite formation occurring simultaneously. Machoviè et al. [2] analyzed the concrete microstructure through scanning electron microscopy (SEM) and found the two phenomena. Another interesting case was the one presented by Shayan and Morris [3] in which visual inspection and analysis identified the ASR, mainly because in the composition of the concrete of the bridge it was found gneiss with reactive quartz. On the other hand, the heat of hydration released during concrete casting around 80 °C caused the DEF.

In an advanced investigation of concrete cores carried out by Hasparyk [4], the two reactions were found, where in addition to visual inspection, several tests were performed, as well as analyses of the microstructure by means of SEM, EDX and XRD. A bridge deck damaged by ASR and DEF studied by Shayan et al. [5] showed significant reductions in the modulus of elasticity, as well as residual expansion. Another foundation structure that presented combined attack was studied by Hasparyk et al. [6], where the causes of the occurrence of these phenomena were the temperature around 80 °C and the presence of reactive aggregates in concrete. A comprehensive understanding of the damage generated by the combination of DEF + ASR presented by Sanchez et al. [7] showed reductions in the mechanical properties of the concrete analyzed.

Many structures in Britain and France that had in their composition high cement consumption (between 420 and 550 kg/m^3) and high equivalent alkali content (> 4.0 kg/m^3) presented several damages between 5 and 20 years after their construction,

in the presence of moisture and in a temperature close to 80 °C, besides being concreted during the summer, which potentiated the heat release [8].

DEF manifests itself when the source of sulfate ions is internal and not external, in the presence of an aggregate contaminated by gypsum or cement with high sulfate content. In addition to these factors, the process of steam-curing the concrete at temperatures above 65 °C can cause the development of delayed ettringite, since it is not stable in these conditions [9].

In concrete submitted to a high temperature during concrete casting in place, it is possible that the primary ettringite formed during the hydration reactions is decomposed [10]. When it returns to room temperature and in the presence of humidity, this ettringite can re-crystallize inside the hardened concrete, causing expansion pressures that are capable of generating cracking, which potentiates damages to the structure.

According to Bensted [9], the causes, the physical–chemical mechanisms and the kinetics of the reaction that originates the DEF are still not fully understood. However, the combination of several factors is of utmost importance for this internal expansion reaction to begin.

Water is an essential factor to produce the reaction, whether in structures that are in contact with water, susceptible to water ingress or exposed to a high humidity level, such as foundations. Other elements described in Guide Technique [11] are the maximum temperature reached by the structure and the time duration in which this temperature is maintained. Thus, if the temperature exceeds 65 °C and other key parameters are present, the probability of occurrence of DEF is high.

Ettringite is a hydrated calcium trisulfoaluminate, so the sulfate and aluminate contents are directly linked to its formation process. A necessary condition is that the cement used contains a sufficient amount of tricyclic aluminates (3CaO, Al_2O_3 or C_3A) and sulfates (SO_3). As ettringite is highly soluble in large quantities of alkalis, the use of a type of cement with a lower alkaline content would contribute to the non-occurrence of the reaction [11].

Another recommendation for the delayed ettringite formation not to occur as described in [11] is the use of mineral additions. It was observed that they contribute to a less exothermic concrete, as they reduce the amount of clinker aluminates and end up modifying the type and texture of the moisturizer. The additions indicated are those that have components with latent or pozzolanic hydraulic properties, such as blast furnace slag or fly ash, natural or artificial pozzolana). Finally, the petrographic nature and the volumetric mass of the aggregate are elements which influence heat transfers in the reactions of concrete.

Studies have shown that an isolated factor is not sufficient for the internal expansion reactions to develop, but the presence of several parameters acting simultaneously under certain conditions. Both expansion reactions (ASR and DEF) have similar symptoms and the two have moisture as a conditioning factor to develop expansion. According to Torres and Andrade researchers [8] what may be happening in the Metropolitan Region of Recife is the combination of ASR/DEF attack mechanisms.

One of the important challenges that researchers have to answer is to understand as fully as possible these phenomena of expansion that affect various concrete pile

cap foundations in the region at an early stage and how it is possible to correlate the level of damage generated with the change in strength and deformation properties of concrete and its durability. Furthermore, it is equally important to relate the results of laboratory tests to the situations found in the field so that possible design and construction strategies can be proposed to minimize the possibility of these expansion phenomena take place on concrete. That is why there is a need for a greater understanding of their features and mechanisms.

This work aims to provide a mechanical and transfer properties characterization and the physical–chemical analysis, using advanced techniques to analyze cores extracted from real buildings that have concrete elements affected by internal swelling reactions.

2 Materials and Methods

2.1 Materials

Figure 1 represents the pile cap S(P1 + P8 + P32), with the extraction sites of each core, identified by the notations (SP-01, SP-02, SP-03, SP-04, SP-05 and SP-06). The points identified by (A, B, C and D) are where were extracted the samples of smaller sizes also used for analysis and characterization. All samples were extracted in the direction parallel to the launching of the concrete and only the SP-06 was in

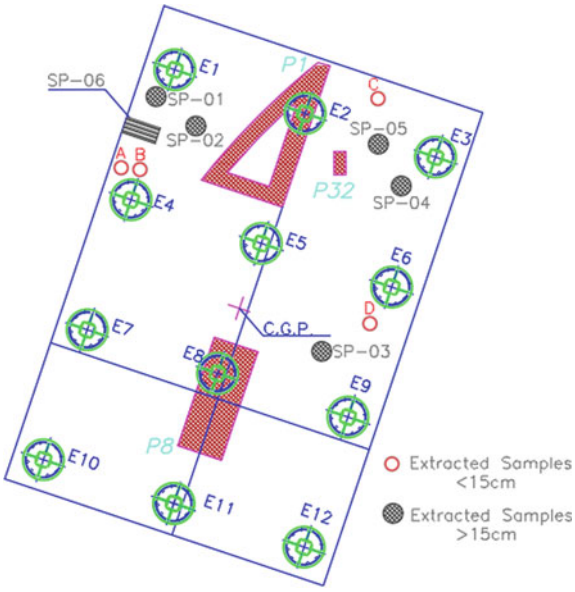

Fig. 1 Place of extraction of the samples in the Pile Cap Block S(P1 + P8 + P32)

the direction perpendicular to the launching. The face chosen was where there was longitudinal cracking along the pile cap block.

The concrete samples were extracted with two single-phase electric drills of such dimensions with 75 mm diameter—Model Husqvarna dm2 240 and Tyrolit dk32. The extraction procedure was executed in such a way that the sectioning of the block reinforcements was avoided as much as possible. The specimens were extracted from the upper part and from lateral faces of the pile cap block, totalling 6 (six) cylindrical concrete samples with dimension of $15.0 \times 7.5\ cm^2$—height and diameter, respectively. The entire sample extraction process was performed in a single day and lasted approximately 7 h (see Fig. 2).

The laboratory tests were carried out partly in the facilities of the Institut Catholique D'Arts et Métiers and other partly in the GeM—Institut de Recherche en Génie Civil et Mécanique—UMR 8183—CNRS—École Centrale de Nantes—Université de Nantes.

After choosing the parameters for characterization and diagnosis of pathological manifestations in concrete, the samples were separated, identified and prepared. In the field, it is necessary that the cores are removed from the structure to be studied. Some tests required specific treatments on the samples collected. In some cases, the sample needs to be reduced to very small sizes or even pulverized.

Fig. 2 Samples extracted from the block (SP-01 to SP-06)

A visual analysis was performed to identify possible characteristics of the internal expansion reactions and they were directed to the tests to be performed. Then, a characterization of the concrete samples affected by the reaction was performed with destructive tests and analyses.

2.2 Laboratory Tests

2.2.1 Gas Permeability and Apparent Porosity

The permeability test was performed on two concrete specimens of the pile cap block. A sample (P-02) was taken from the fragments extracted from the SP-01 sample and the sample (P-01) was separated from the point A. They were rectified and left in the dimensions 5 × 7 cm^2. The specified cell size of the permeability equipment ("debitmètre massique") was 10 cm in diameter, so the samples were wrapped in black silicone resin and placed in a rigid cylindrical mold.

This resin also had the function of waterproofing the lateral surface of the samples. Figure 3a illustrates how the concrete samples were ready for the test. The concrete gas permeability measurement test is easy and quick to perform and its results are important for assessing the durability of the material. These aspects should be considered so that its use can be more widespread in the practice of concrete structure execution.

To obtain the dry mass of the samples, it was chosen to dry them at a temperature of 60 °C in the oven until the mass was stabilized. The dry mass of the samples is obtained when the loss of relative mass of 24 h does not exceed 0.05%. Every day for twelve days the weight of the samples was measured until the stabilization.

The complete apparatus of the permeability equipment ("debitmètre massique") used in the test is shown in Fig. 3b. The intrinsic permeability is measured through a permeameter, with nitrogen being the neutral percolating gas. A manometer reads

Fig. 3 **a** Samples P-01 and P-02 prepared for the air permeability test; **b** flowmeter massique equipment; **c** system used for the apparent porosity test

the relative pressure (Pi-Patm) applied to the sample. Laboratory temperature and humidity are controlled (T = 17.8 ºC and RH = 76%).

After the concrete air permeability tests have been performed, all the water-proofing resin and the apparatus used were removed to put the samples back in the oven until the mass stabilization. To obtain the dry mass of the samples, it was chosen to dry them at a temperature of 60 °C in the oven until the mass was stabilized. The dry mass of the samples is obtained when the loss of relative mass of 24 h does not exceed 0.05%. Every day for one month the weight of the samples was measured until the stabilization.

After the stabilization of the mass has occurred by drying in the oven, the samples were wrapped in a white absorbent tissue covered with a transparent plastic, from which it was possible to remove the air present in the sample and the environment with a vacuum pump. The vacuum pump was then stopped for five minutes to check if air was coming out, as the device was well sealed, suction continued for another 48 h. After this period of time the air suction process was interrupted to introduce water into the apparatus and consequently into the samples.

Figure 3c shows the devices used for porosity tests, where you can see that at one end you have the place where the vacuum pump for air suction is installed and at the other end the water inlet is located. 48 h later, the water end was opened and it was placed the hose in a tank with water, reconnected the vacuum pump that began sucking the water until the whole system was filled. After 72 h the sample was taken and its weight was measured.

2.2.2 Scanning Electron Microscopy (SEM)

The SEM used for observations is a ZEISS ЄVO®40 equipped with a Back-scattered Electron (BSE) detector to determine the chemical composition. The microscopic examinations were carried out on fresh fractures sections on concrete specimens. The specimens were coated with a gold deposit for observations using the SEM in High-Vacuum (HV) mode.

The samples were analyzed by scanning electron microscopy and the spectrum obtained with EDX showed the chemical composition existing in each part analyzed. Some images showed only the morphology of the ettringite or other observed component.

2.2.3 X-Ray Diffraction (XRD)

Through the X-ray diffraction it is possible to obtain the detailed information of the atomic and molecular structure of materials. When a material is exposed to X-rays, a specific peak pattern of the mineral is generated. The ordinate provides the diffraction angle, which corresponds to the spacing of the crystalline arrangement. In the abscissa we see the intensity of the diffracted ray, which is proportional to its quantity in a composite sample and each peak is equivalent to a type of mineral.

XRD patterns were obtained by using an X-ray diffractometer SEIFERT MZ VI E with Co Ka radiation. Measures were done on the bulk powdered samples.

2.2.4 Raman Spectroscopy

The Raman displacement band, that is, the difference in energy between the incident and the scattered, is typically described as a wave number (wavenumber). The most used unit is 1/cm, this is equivalent to joule divided by conversion factor (hc), where h is Planck constant and c is the speed of light.

The sample selection criteria for analysis by Raman spectroscopy were: fragments of the extracted concrete samples with apparent gel edges, pores filled with ettringite and white spots inside the aggregates.

An acrylic resin PRESI Powder KM-U with a liquid catalyst PRESI KM-U suitable for this type of cold resin was used in the concrete samples. The function of resin was to allow the sample to remain flat, allowing the analysis in Raman. After placing the resin in the mold with the sample, it waited 10 min until it warmed up and hardened, and then the sample was polished on #320 silicon carbide paper and then on #120 paper in a specific machine until the surface was polished and flat. The Raman spectra were produced using the Confocal Raman Microscope SENTERRA II (Bruker) with Opus Software, 532 m wavelength laser, 20 mW power, 50× magnification, 20 s integration time with two accumulations.

3 Results and Discussion

Before starting the discussion about the results of the lab tests performed it is important to highlight that the pathological manifestations observed in the foundation block studied probably come from a variety of sources: structure design decisions, definition of materials to be used in the production of the concrete used and care in large volume concrete operations.

3.1 Visual Inspection

Visual inspections were performed on the pile cap block itself as well as on the concrete samples extracted to identify naked eye signs of expansive reactions or chemical attacks to the concrete. From these inspections, it was possible to observe to see features of these expansion reactions already in place by observing the cracking in map forms on the external surface of the pile cap block. It is worth mentioning that at the time of the extraction a report had already been made to detect the causes of degradation, as well as several tests and analyses, and the pile cap block was in the process of recovery (see Fig. 4).

Fig. 4 Map cracking on the surface of the pile cap block

The samples were first visually examined in order to find clues of chemical attacks to concrete such as AAR and DEF. Macroscopically, gel edges from the alkali-silica reaction were observed in the aggregates. Cracks on the coarse aggregates, following to the cement paste, were observed as well as cracks on transition zone reaching the larger pores.

At some locations it was possible to observe detachment between the aggregate and the paste. Some aggregates contained a kind of whitish reaction product inside, very close to its extremities and and many dark edges or spots were found around the coarse aggregate.

Several micropores were fulled with ettringite and many pores were completely filled with white material. In some fragments a large amount of white material was found covering the concrete, like as leaching. It was also observed in some larger pores little deposition of white material, a fact also observed by Hasparyk [4] in the visual inspection of concrete cores with alkali aggregate reaction.

In the preparation of some samples for some tests performed it was done polishing and after this process it was possible to find even smaller pores filled with whitish material as well as particles of aggregates with this same characteristic. The results from the visual inspection performed on the extracted specimens are summarized below:

- Alkali-silica gel edges in the aggregates;
- Pores with white material deposited at the bottom;
- White mass in several places in the concrete;
- Pores completely filled with ettringite;
- Cracking in coarse aggregates;
- Dark spots around the aggregate;
- White spots inside the aggregate;
- Leaching;
- White spot covering the concrete, mainly the mortar;
- Displacement between the aggregate and the paste;

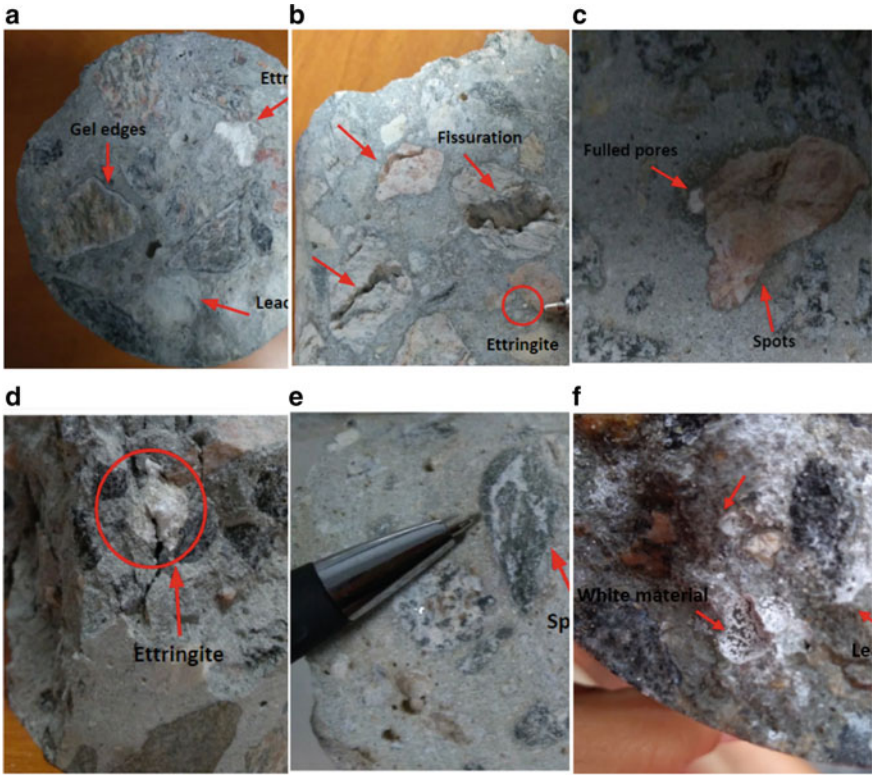

Fig. 5 Symptoms of the expansion mechanisms found: **a** gel edges; **b** ettringite in the micropores and cracking; **c** spots in the aggregate; **d** pores fulled with ettringite; **e** spots in the aggregate; **f** white material in the pores and leaching

- Cracking in the coarse aggregate following to the transition zone, with the presence of gel in these locations;

Figure 5 shows the main results of the visual inspection performed. The results of visual inspections performed on the concrete samples collected from the block are consistent with a scenario of occurence internal expansion reactions inside the element more compatible with DEF than with the ASR.

3.2 Physical–Chemical Analysis

3.2.1 Gas Permeability and Apparent Porosity

The transfer properties of both healthy and cracked concrete are very important for the study of its durability and porosity and permeability are indicators of this durability.

Table 1 Values of gas permeability and apparent porosity of concrete

Sample	K (m^2)	ε (%)
P-01	1.3×10^{-15}	11.29
P-02	3.9×10^{-16}	9.76

Table 1 summarizes the air permeability (K) values for the two samples tested. The results found mean that the concrete samples have a high permeability. In fact, the usual values of this parameter for a concrete are in the range of 10^{-18}–10^{-17} m [12, 13].

This high value of the permeability coefficient can explain the intense cracking process existing in the pile cap block investigated, which allowed the entry of moisture and development of the expansion mechanisms that deteriorated the concrete. The permeability of the samples tested was proportional to the porosity, being higher for P-01. In this sample there was a greater predominance of microcracks. In P-02 there was a large pore, which makes these transport properties smaller.

According to Collepardi [14] the microcracks resulting from the silica alkali reaction in-crease the permeability of concrete, a mechanism that may have contributed to the growth of the values of this property.

Also, from Table 1, the results obtained indicate a high porosity of concrete, a situation also confirmed by its high permeability. This explains the large amount of microcracking found in the field and consequently in the extracted samples. The pore structure of this concrete is then markedly compromised, an aspect that directly interferes with its durability and service life.

One aspect that deserves to be highlighted is that ettringite usually can cause greater expansions in small pores with low connectivity than in larger pores with wide connections [15]. This fact was observed in sample P-02 that presented a large amount of pore in its structure with porosity relatively lower than the P-01 sample that presented a larger amount of microcracks.

It can also be confirmed that ettringite deposited in free pores does not contribute to expansion [16], because in sample P-02 it was found more pores filled with ettringite.

3.2.2 Scanning Electron Microscopy (SEM)

The analysis performed through the scanning electron microstructure allowed the morphology of the samples to be evidenced by means of images. Energy Dispersive X-Ray Spectroscopy (EDX) enables microanalysis, providing chemical composition of the material, which can be used together scanning electron microscopy to get qualified information.

In the analyses performed with SEM, some specific parts that indicated the presence of delayed ettringite formation were chosen. The first point was 309, where the morphology indicated that it was an ettringite acycle. Figure 6a shows this part of the sample, with a magnitude of 1795×.

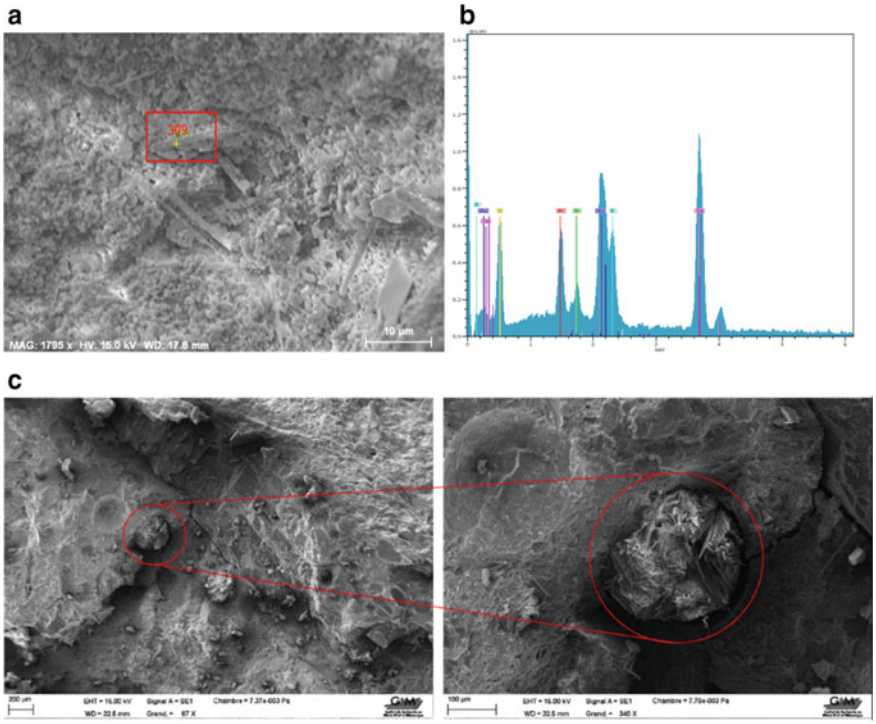

Fig. 6 **a** Acycular crystals of ettringite found in the mortar; **b** components such as: sulphur (S), aluminum (Al) and calcium (Ca) in the sample and **c** ettringite crystals completely filling a pore (23×–340×)

The chemical composition obtained by EDX is shown Fig. 6b, where the components such as Sulfur (S), Aluminum (Al) and Calcium (Ca) suggests the presence of delayed ettringite [4, 17]. Figure 6c illustrates ettringite crystals completely filling an existing pore in the concrete. The first magnitude is 23×, being increased to 340×.

At point 308 (Fig. 7a) analyzed by SEM, it is possible to observe ettringite crystals developed and deposited in a pore and the corresponding chemical composition is presented in Fig. 7b, with the presence of Sulfur (S), Aluminum (Al) and Calcium (Ca), aspect that confirms that it is delayed ettringite [4].

This particle (point 304—Fig. 8a) analyzed showed in its chemical composition Aluminum (Al), silicon (Si) and sodium (Na), indicating that there are components of delayed ettringite formation and crystalline products of alkaline reaction [4] acting together. Figure 8b illustrates the composition (Al, Si and Na) of this point analyzed.

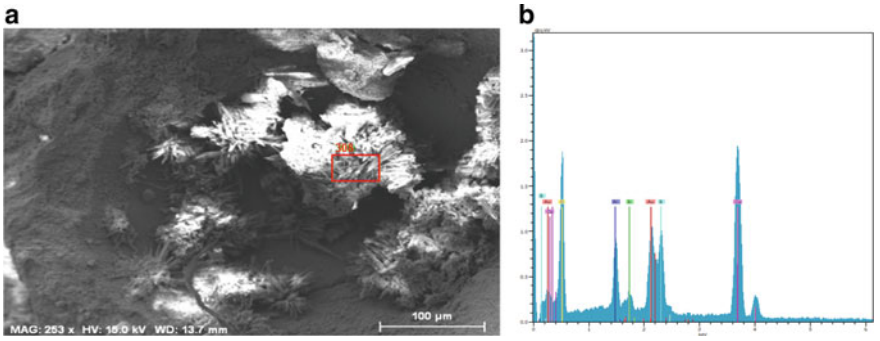

Fig. 7 **a** Ettringite crystals deposited in a pore; **b** chemical composition of the crystals

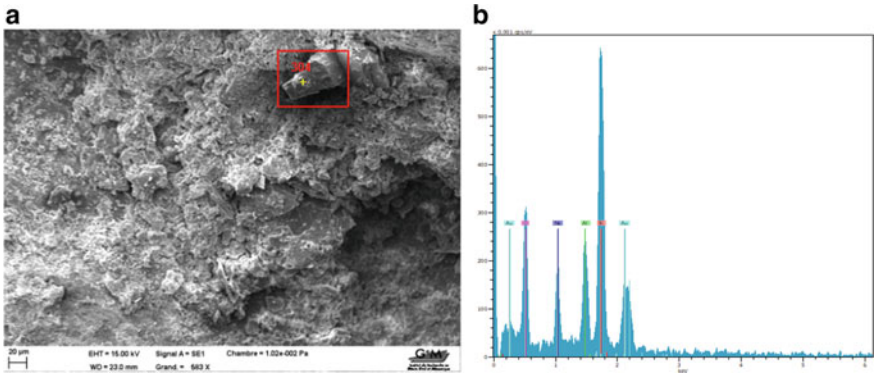

Fig. 8 **a** Aggregate particle with crystalline products of the alkali-silica reaction; **b** crystalline product of alkaline silica reaction

3.2.3 X-Ray Diffraction (XRD)

Through the X-ray diffraction it is possible to obtain the detailed information of the atomic and molecular structure of materials (mainly the crystalline ones).

In the analyses with EDX it was possible to observe a large amount of sulfur (S), aluminum (Al) and calcium (Ca), chemical elements predominantly found in crystals of ettringite [4]. The XRD analyses also proved the presence of ettringite and pyrite (sulphate) internally. These internal compounds associated with a high heat of hydration may have caused the formation of delayed ettringite. Figure 9 shows the patterns of concrete damaged by internal expansion reactions.

The highest peaks are from pyrite, followed by quartz and ettringite. They are similar to those found by [4, 9] in cases of dams affected by delayed ettringite and alkali-silica reaction, respectively. The diffraction angles that showed strong reflection were: 2 theta of 37°, 2 theta of 41° and 2 theta of 55°, with high intensities, and refer to Pirita or Sulfate. The ettringite with greater intensity is found in 2 theta

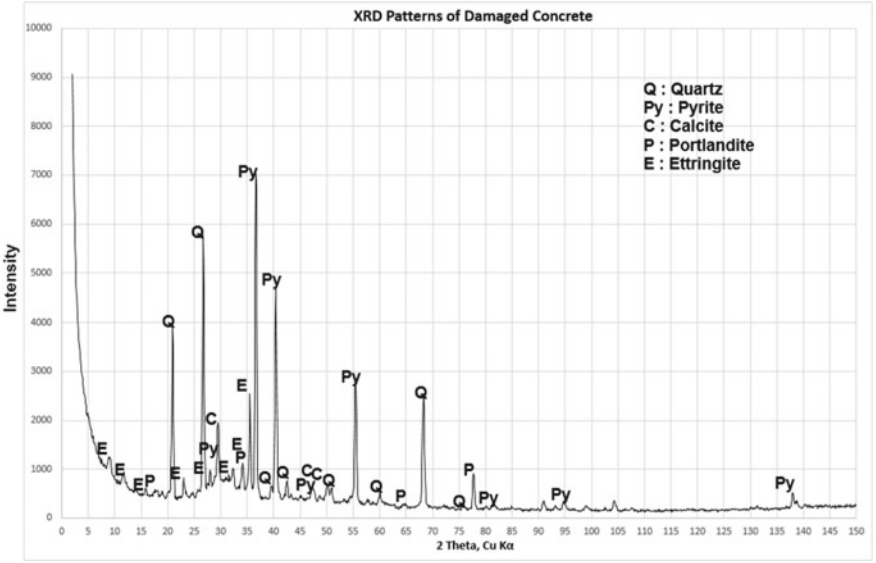

Fig. 9 Presence of pyrite (sulphate), sodium hydroxide, calcium carbonate and silicon dioxide

of 36°, corresponding to the crystals present in all the concrete, predominantly of the pores and voids.

Another high intensity peak also recognized in the diffractometer was the mineral component quartz, corresponding to the crystalline products of the alkali-silica reaction. This mineral appeared more strongly in 2 theta of 21°, 2 theta of 27° and 2 theta of 68°, indicating crystalline phases of the material. These peaks are attributed to the contamination of the paste by the reactive aggregate.

3.2.4 Raman Spectroscopy

Figure 10a represents the coarse aggregate region of the RA-02 sample in expanded resolution. Four points (a, b, c and d) were chosen to be analyzed by Raman spectroscopy.

Figure 10b illustrates the Raman spectra of the crystalline products found in different locations of the same analyzed aggregate. The Raman spectra were found between two wide bands, in the range of 100–600 cm^{-1} (low frequency region), indicating the amorphous nature of the gel. The wave numbers identified (see Fig. 10b) were similar to those found by the researchers for the aggregates that contained reactive mineral [17, 18]. When analyzing the edges of the aggregate, the bands of the crystalline product do not result in peaks, indicating only noises, a similar behavior found in [19]. The colour of the dots corresponds to the colour of the spectra, the corresponding sequence is: b, a, d and c.

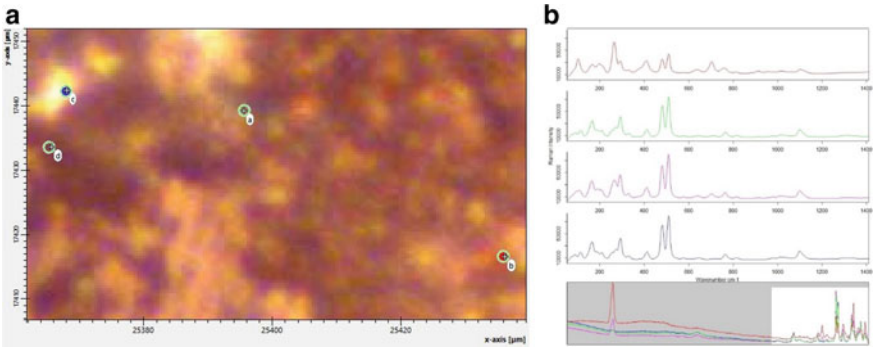

Fig. 10 **a** Points (a, b, c, d) where the Raman analysis was performed; **b** Raman spectra of the crystalline products at the four points analyzed in the RA-02 sample

In the other samples analyzed, the spectra were not generated, even performing new polishing with silicon carbide (P120), because it showed an increase in noise, causing the signal of the products no longer recognized. In a new analysis in the same sample, now in the blue and red points (see Fig. 11a), different Raman intensities were found, but still in the same wavenumber range. The colour of the dots corresponds to the colour of the spectra.

In Fig. 11b the crystalline product was found in the same range of wave numbers (from 100 to 600 cm^{-1}), being different in peak intensity.

Figure 12a shows the point from which this spectra was obtained and the Fig. 12b shows the spectrum of the crystalline product located inside a pore in the RA-05 sample. There are different peaks, the largest is in the range of 800–1000 cm^{-1}. In

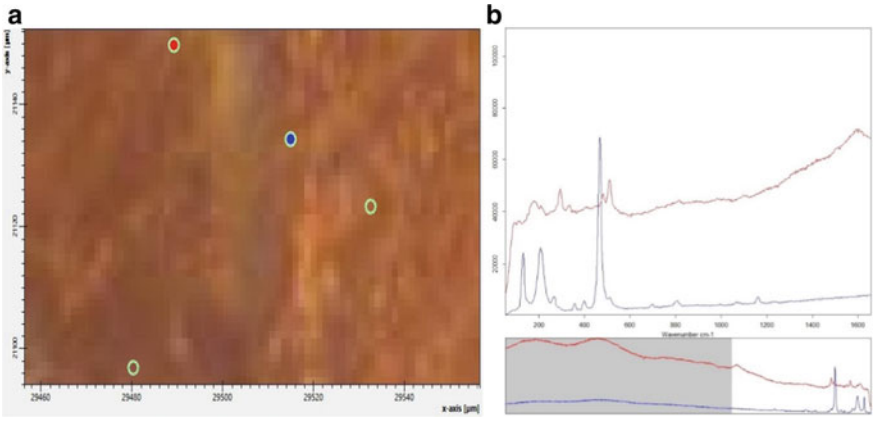

Fig. 11 **a** Points where the Raman analysis was performed (sample RA-02); **b** range of 100–600 cm^{-1} analyzed

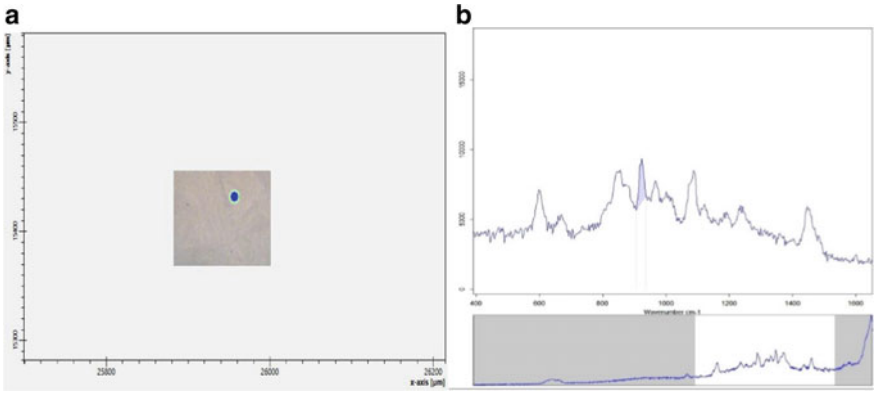

Fig. 12 **a** Crystalline product analyzed by Raman spectroscopy; **b** Raman spectra values found in the ASR products inside a pore

the wavenumber 600 cm^{-1} there is a peak, similar to what was found by [17] as a peak of the alkali-silica reaction product.

The chemical analysis performed with the Raman spectroscopy indicated possible spectra corresponding to the crystalline products of the alkali-silica reaction, which confirmed the presence of sodium in the previously obtained EDX spectra. The reactions (alkali-aggregate reaction and delayed ettringite formation) are acting concomitantly.

In resume, the main findings from the laboratory testing campaign of the extracted samples are presented below.

- High values of porosity were found, between 9 and 11%, explained by the large amount of micro-cracks in the field and in the extracted samples;
- The pore structure was much compromised in this concrete, an aspect that directly interferes with its durability and service life.

In the analysis with SEM, the morphologies identified were those of ettringite acicular crystals in the mortar and also completely filling the pores, illustrated in Fig. 13. In the dispersive energy spectroscopy the following components were obtained: sulfur, aluminum and calcium, characteristic minerals of the ettringite crystals. In the XRD standards these elements were also found, as well as the mineral pyrite (or sulfate) and the ettringite itself. Pyrite was the mineral with the highest peak intensity in the graph, confirming the high presence of DEF in the concrete.

In the microstructure of the concrete there are pores and voids, and as [16] the ettringite crystals accumulate in the available free spaces, and often the ettringite that is deposited there does not contribute to the expansion. Thus, these products resulting from the reaction were deposited in the pores of the concrete and making a tamponade of existing voids. Through the process of pore-filling the pores [4], proven in visual inspections and SEM analyses, the compressive strength of the concrete showed high values. The cracking on a map of the block in its surface did

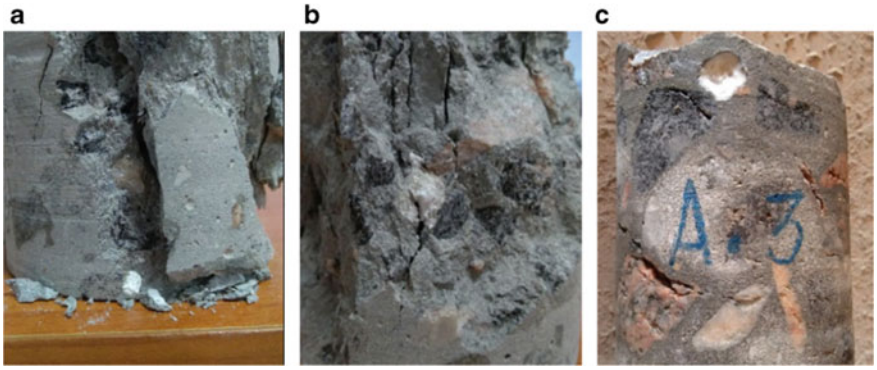

Fig. 13 Pores completely filled with ettringite crystals: **a** and **b** concrete sample after compressive rupture; **c** concrete sample after extraction

not happen in the whole block, but in half of it. The AM-02 sample presented a lower strength value compared to the other two because it was extracted from a location of the block where there was little apparent cracking, and probably the products of the reactions had not filled the existing voids.

When analyzing pores filled with internal reaction products of expansion and interface aggregate paste in Raman spectroscopy, spectra with wave numbers and peaks similar to those of crystalline products from ASR studied in [17, 19] were found.

Regardless of the origin of the microfissures in the concrete, the porosity of this material increase [14]. Water is a factor that contributes to the migration of sulfate ions [14], generating expansion reactions in different locations of a concrete structure.

The mechanisms of ASR and DEF reactions depend on the flow of liquids or gases in the microstructure, so for these internal expansion reactions to develop it is necessary to have connectivity between the pores [20]. For the progress of these reactions it was necessary to have preferential paths for the moisture to enter and then trigger the expansion in the concrete, filling free pores and later cracking the structure of the pile cap foundation. It is possible that there is still residual expansion in the concrete, and new tests are necessary to evaluate this characteristic.

4 Conclusions

Based on the cracks observed in-field and taking as reference the results of the studies and laboratory analysis in the concrete cores presented in this work, it can be stated that the concrete structure presents chemical changes that have affected its integrity. The most relevant conclusions of these studies are as follows:

- The physical–chemical characterization performed indicated that the pile cap foundation from which the specimens were extracted was affected by internal swelling reactions in the concrete, notably ASR and DEF;
- Among the two reactions referred to DEF proved to be more predominant and is, in the author's opinion, the main reason for the observed cracking;
- DEF possibly originated in the high hydration heat that may have occurred in the concreting of the important concrete volume of the pile cap block;
- The alkali-silica reaction was found in concrete through dispersive X-ray spectroscopy, with the presence of mineral components, such as silicon and quartz and by means of Raman spectroscopy, with a wave number of about 600 cm^{-1}, proving the presence of crystalline products of this reaction;
- The ettringite crystals that filled the pores were detected with the naked eye and by scanning electron microscopy and X-ray diffraction;
- The analysis with EDS obtained a predominance of sulfur, aluminum and calcium, being reaffirmed in the intensities of the XRD standards, where sulfate in the form of pyrite was found, as well as ettringite and calcite;
- Porosity values between 9 and 10% were also high, in accordance with their permeability and with the extensive pore network existing in the concrete.

References

1. Allahvedi A, Hashemi H (2015) Investigating the resistance of alkali-activated slag mortar exposed to magnesium sulfate attack. Int J Civ Eng 13(4A):379–387. https://doi.org/10.22068/IJCE.13.4.379
2. Machoviè V, Kopecký L, Němeček J, Kolář F, Svítilová J, Bittnar Z, Andertová J (2008) Raman micro-spectroscopy mapping and microstructural and micromechanical study of interfacial transition zone in concrete reinforced by poly (ethylene terephthalate) fibres. Ceramics Silikaty 52(1):54–60
3. Shayan A, Morris H (2004) Combined deterioration problems in a coastal bridge in NSW, Australia. In: Proceedings of the 12th international conference on alkali-aggregate reaction in concrete. International Academic Publishers, Beijing, China
4. Hasparyk NP (2005) Investigation of concretes affected by the alkali-aggregate reaction and advanced characterization of exudate gel. PhD Thesis, Federal University of Rio Grande do Sul, Brazil
5. Shayan A, Al-Mahaidi R, Xu A (2008) Durability and strength assessment of AAR-affected Bridge deck planks. In: Proceedings of the 13th international conference on alkali-aggregate reaction in concrete, Trondheim, Norway
6. Hasparyk NP, Kuperman SC, Torres JR (2012) Case study involving combined attack of AAR and DEF in building foundation concrete. In: Proceedings of the 54th Brazilian congress of concrete—CBC2012, Maceió, Brazil
7. Sanchez LFM, Drimalas T, Fournier B, Mitchell D, Bastien J (2018) Comprehensive damage assessment in concrete affected by different internal swelling reaction (ISR) mechanisms. Cem Concr Res 107:284–303
8. Torres IF (2016) Andrade (2016) risk analysis of the delayed ettringite formation in pile caps foundation in the metropolitan region of Recife—PE—Brasil. IBRACON J de Estruturas e Mater 9(3):357–394. https://doi.org/10.1590/S1983-41952016000300003

9. Metha PK, Monteiro PJM (2013) Concrete: microstructure, properties and materials 4 McGraw-Hill Education New York
10. Özcan A, Karakoç MB (2019) The Resistance of blast furnace slag- and ferrochrome slag-based geopolymer concrete against acid attack. Int J Civ Eng 17(10):1571–1583
11. Laboratoire Central des Ponts et Chaussées (2018) Guide technique—recommendations for preventing disorders due to delayed ettringite formation, Paris
12. Leemann A, Bernard L, Alahrache S, Winnefeld F (2015) ASR prevention—effect of aluminum and lithium ions on the reaction products. Cem Concr Res 76:192–201. https://doi.org/10.1016/j.cemconres.2015.06.002
13. Tahlaiti M (2010) Study of chloride penetration and corrosion initiation in saturated and tidal zones. PhD Thesis, La Rochelle University, France (in French)
14. Collepardi M (1999) Damage by delayed ettringite formation. Concr Int 21(1):69–74
15. Taylor HFW, Famy C, Scrivener KL (2001) Delayed ettringite formation. Cem Concr Res 31(5):683–693. https://doi.org/10.1016/S0008-8846(01)00466-5
16. Glasser FP, Damidot D, Atkins M (1995) Phase development in cement in relation to the secondary ettringite problem. Adv Cem Res 7(26):57–68. https://doi.org/10.1680/adcr.1995.7.26.57
17. Leemann A (2017) Raman microscopy of alkali-silica reaction (ASR) products formed in concrete. Cem Concr Res 102:41–47. https://doi.org/10.1016/j.cemconres.2017.08.014
18. Balachandran C, Muñoz JF, Arnold T (2017) Characterization of alkali silica reaction gels using Raman spectroscopy. Cem Concr Res 92:66–74. https://doi.org/10.1016/j.cemconres.2016.11.018
19. Merz C, Leemann A (2013) Assessment of the residual expansion potential of concrete from structures damaged by AAR. Cem Concr Res 52:182–189. https://doi.org/10.1016/j.cemconres.2013.07.001
20. Picandet V, Khelidj A, Bastian G (2001) Effect of axial compressive damage on gas permeability of ordinary and high-performance concrete. Cem Concr Res 31(11):1525–1532. https://doi.org/10.1016/S0008-8846(01)00546-4

Diagnosis and Assessment of Deep Pile Cap Foundation of a Tall Building Affected by Internal Expansion Reactions—Case Study

João M. P. Q. Delgado, F. A. N. Silva, A. C. Azevedo, T. Mahfoud, A. Khelidj, and N. Nascimento

Abstract Early deterioration of foundations of reinforced concrete building has been reported with relative frequency in last years. This this deterioration process is often characterized by an extensive mapping cracking process on concrete surfaces that occurs due to several types of internal swelling reaction. In this paper, a real case study of a tall reinforced concrete building that presented a severe process of deterioration of its deep foundations is discussed. Laboratory tests were performed in drilled concrete cores extracted from a deep pile cap block after 19 years of the begin of the construction. Test to evaluate compressive strength, static and dynamic modulus of elasticity as well gas permeability and scanning electron microscopy using advanced analyses were performed to assess information to find out the main mechanism responsible by the strong deterioration found in field inspections performed. Chemical alterations of material were observed, mainly by DEF, which significantly affected the integrity and durability of the structure. Dynamic modulus of elasticity showed to be a best indicator of damage induced by ISR in the concrete than the it's compressive strength. Rehabilitation procedures executed using strengthening procedures to provide the complete restoration of the structural integrity of the element deteriorated proved to be a good solution to retrofit pile cap deteriorated by expansions due to ISR in concrete.

J. M. P. Q. Delgado (✉) · A. C. Azevedo
Departamento de Engenharia Civil, CONSTRUCT-LFC, Universidade do Porto, Rua Dr. Roberto Frias, s/n, 4200-465 Porto, Portugal
e-mail: jdelgado@fe.up.pt

A. C. Azevedo
e-mail: antonio.costaazevedo@fe.up.pt

F. A. N. Silva · N. Nascimento
Department of Civil Engineering, Universidade Católica de Pernambuco, Recife, Brazil
e-mail: fernando.nogueira@unicap.br

T. Mahfoud · A. Khelidj
GeM Laboratory, University of Nantes, Saint Nazaire, Nantes, France
e-mail: mahfoud.tahlaiti@icam.fr

A. Khelidj
e-mail: abdelhafid.khelidj@univ-nantes.fr

J. M. P. Q. Delgado (ed.), *Masonry: Building Pathologies and Design*, Building Pathology and Rehabilitation 22, https://doi.org/10.1007/978-3-030-80496-1_7

Keywords Delayed ettringite formation · Alkali-Aggregate reaction · Diagnostic of pathologies on concrete · Internal swelling reactions

1 Introduction

Early deterioration of foundations of the reinforced concrete building has been often reported in last years. This process usually starts with a map-shaped cracking on the side and top surfaces of pile caps and, sometimes, horizontal large opening cracks in the lateral faces, located at about 30 cm from its top surface, is also reported. This cracking process is often attributed to concrete expansion due to several swelling internal reaction mechanisms and this occurrence severely affects the durability of concrete structures. In this context, the study of the mechanisms by which concrete is deteriorated by internal swelling reactions, its effects on the behavior of the material, as well as the investigation of appropriate retrofitting procedures is an open field to research. The internal swelling reaction in concrete is often related to pathological manifestations associated with chemical phenomena, most likely present in works with a large volume of concrete-like dams, bridges, roadway but, in some under developing countries, the occurrence of these reactions have been reported in deep pile caps and spread footing foundation at very early ages. Among the most common, chemical, physical, mechanical, electrochemical, or even biological attacks are usually the ones that occur frequently. Chemical reactions that include the formation of expansive products are external sulfate attack, delayed hydration of free calcium oxide (CaO), and free periclase (MgO), more commonly known as delayed ettringite formation (DEF), alkali-aggregate reaction (AAR) and corrosion of concrete reinforcement [1].

Some interesting hypotheses to understand the delayed ettringite formation was suggested by [2]. One of these hypothesis states that the origin of the sulfate ions needed to start DEF comes from the release of hydration products. The presence of water inside the concrete is also of paramount importance for the migration of such ions. No matter the origin of the internal expansion reactions, a fact corroborated by several types of research indicates that the occurrence of a strong cracking process contributes to increasing the permeability of the concrete, a fact that compromises its durability [2, 3]. Another hypothesis admits that the ettringite is deposited in the existing microcracks with two possibilities for its propagation—expansion or growth from crystals. A consistent understanding of the expansion mechanisms associated with DEF is a relevant issue for the durability of concrete structures because it severely affects the behavior of the material by DEF expansions that often demand a large amount of money to perform retrofitting or rehabilitation works. Another chemical reaction that can generate internal swelling reactions (ISR) in concrete is the alkali silica reaction (ASR) that can also affect the durability of the material because it generates a similar cracking process like those from DEF. Expansions from ASR also lead to a strong cracking process that severely affect the performance of concrete elements with impact over mechanical properties of the material, both in service and ultimate loading states [3–5].

The chemical process of the ASR starts when the silica structure is dissolved by the nucleophilic attack of hydroxide ion (OH−) that occurs due to its highly degraded structure that behaves like a hygroscopic silica gel. The reaction product is a gel known as alkali-silica gel, which is not harmful to the concrete [6, 7]. However, this gel tends to swell when it absorbs moisture present in the concrete pore solution and, if confined in the matrix, can generate internal stresses. As far as absorbs more moisture, the pressures increase inducing the development of microcracks, which in extreme situations, can lead to concrete rupture [5–8]. The pattern characteristics and extension of the cracking process provide information on the mechanism of internal expansion reactions and the magnitude of the microscopic damage to the concrete structure, explained in [1, 3]. Many concrete design codes establish tests to assess the potential reactivity of aggregates used in concrete production with a focus a mortar or concrete specimens [6, 7, 9]. On the other hand, the great challenge to be overcome in the use of these methods is the reliability of the results provided and their ability to represent the real situations found in the practices of the execution of concrete structures [5, 7]. This subject is a very important issue for the construction industry, which demands a hard-scientific work to link the field experience to lab prediction. Previous researches have already shown that the occurrences of ASR and DEF in concrete structures are important factors in decreasing the material's strength and strain properties [10, 11]. A comprehensive understanding of the damage in concrete structures due to the combination of DEF and ASR effects is presented by Sanchez et al. [1, 12] that reported low, medium and high values of decreases in the mechanical properties of concrete related with the level of expansion induced to the specimens investigated.

It is a consensus among researchers of the theme that the necessary and sufficient conditions for the occurrence of internal swelling reaction in concrete elements are the existence of a source of moisture, the use of coarse or fine reactive aggregates, and a source of alkalis hydroxides. This scenario is usually met in cities with groundwater levels very close to sea level—an aspect that provides a greater contact of moisture with the concrete foundations of buildings—where one uses concrete with high equivalent alkalis content types of cement associated with any reactive mineral contained in some aggregates.

2 Experimental Campaign

2.1 Visual Inspection

Visual inspection in one of the initial strategies used to investigate structural behavior of concrete structures. It intends to find out signal of damage processes and the occurrence of pathologies that can affect the durability and load capacity of reinforced concrete elements. The type of visual inspection to be performed is dependent on the class of information needed, i.e., inspection to gather information to identify

Fig. 1 Cracking process found in pile caps investigated

construction procedures to produce "as built" documents and drawings, investigation to identify pathologies in element and to extract drilled core samples for further physical and chemical studies. In the studied case, pile caps of a residential reinforced concrete frame building were inspected and mapped and Fig. 1 shows their situation observed during the visual inspections performed. This is a 45-storey building with a total height of approximately 120 m that began to show the first signs of deterioration of its foundations after five years of construction.

2.2 Drilled Concrete Cores Extraction

To assess damage in concrete elements, crack pattern obtained during visual inspection is not enough to obtain an accurate diagnosis and the extraction of cores close to the surface mapping cracking areas is necessary to stablish the link field observations and lab predictions.

Table 1 Drilled concrete cores information

Samples	Extraction direction	Tests
A, B, C and D	Parallel to launch	Point A—gas permeability (P-01)
SP-01	Parallel to launch	Gas permeability (P-02)
SP-02	Parallel to launch	–
SP-03	Parallel to launch	Static and dynamic modulus; compressive strength (AM-02)
SP-04	Parallel to launch	–
SP-05	Parallel to launch	Static and dynamic modulus, compressive strength (AM-1A and AM-1B)
SP-06	Orthogonal to launch	–

Table 1 presents information about the drilled concrete cores, the direction of extraction and the lab test that were performed for each sample.

2.3 Methods for Assessment and Analysis

2.3.1 Uniaxial Compression Tests

The strength of concrete is the property most valued by designers and quality control engineers [13]. In fact, in concrete design the compressive strength is considered as the main material's quality parameter used to verify its compliance with standards defined by concrete design code rules. This occurs because it is a relatively simple test to do and its cost is not very high, when compared to other tests available to assess other properties of the material [13]. Many factors affect its results, such as aggregate type and potential reactivity, water-cement ratio (w/c), age of test, molding process, curing, microcracks, porosity, and permeability, among others.

Compressive strength of concrete is affected when the material is deteriorated by ISR. Previous researches have already shown how these reactions can directly impact this material property, acting alone or in combination with other ISR [1, 3, 12–15].

According to Kubo and Nakata [16] apud by Sanchez et al. [1] compressive strength is not very affected by the effects of internal expansion reactions from ASR, even for high expansion levels, i.e., 0.30%. The author also reported that when concrete is deteriorated by DEF combined with ASR or by only DEF expansions, the loss of compressive strength in not so significant with value within the range 0.2–0.43%. By the other hand, when the ISR comes from ASR only, the loss of compressive strength is more pronounced and it could reach to values around 20 to 35%, both results for high levels of expansions [1].

Three drilled concrete cores were identified and prepared to perform compression tests (see Fig. 2). The ends of core specimens were prepared in order to have a flat and perpendicular to the longitudinal axis surface. Sawing was made prior to capping and it was performed to meet the following requirements: (a) projections, if any shall

Fig. 2 Drilled concrete cores extracted from the deep pila cap investigated

not extend more than 5 mm above the end surfaces and (b) the end surfaces shall not depart from perpendicularity to the longitudinal axis by a slope of more than 1.8 or 1:0.3 d, where d is the average core diameter. Capping of concrete cores was done to assure perpendicularity and plainness demands.

Compression strength tests performed is this research was conducted at the GeM Laboratory, University of Nantes, Saint Nazaire, France, using a servo hydraulic compression test machine RP3000 DC/LC with a maximum load capacity of 2,500 kN.

2.3.2 Static Modulus of Elasticity Tests

The static modulus of elasticity of a material under tension or compression stage can be calculated by the slope of the stress–strain curve of the concrete under axial loading. Once the behavior of concrete under axial compression is markedly non-linear, three types of static elastic modulus of concrete can be calculated: secant modulus, tangent modulus and chord modulus. The differences among these three possibilities lies in the way the slope of stress–strain curve form compression tests is calculated [13]. Tangent static modulus of elasticity was calculated because it is a property also used by designers and engineers to verify quality of concrete in order to remove concrete shoring.

The elastic characteristics of a material contribute to the definition of its stiffness which is also dependent on the degree of hydration and on the maturity of the concrete. For a concrete, the characteristics of its phases is quite different as it can been in Fig. 3) [17], from which one can see that static modulus of elasticity of the aggregates is usually greater than the elasticity modulus of the concrete that is greater than the elasticity modulus of the cement paste.

As the drilled concrete came from a deep pile cap strongly loaded, microcracks probably are present the interfacial zone transition inside the concrete mass. There

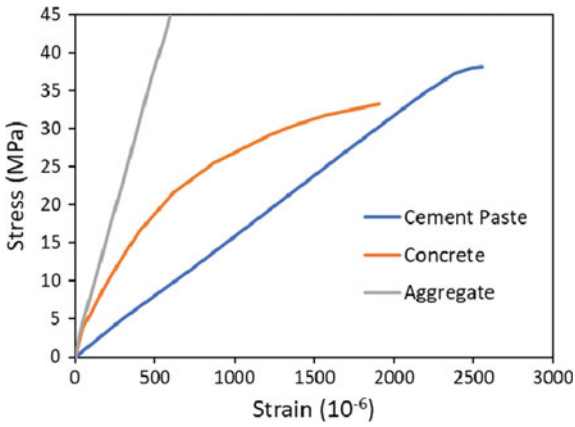

Fig. 3 Compression stress–strain curve for different phases of concrete

is a stage in which the cracks in the transition zone remain stable—when the load applied reaches to 30% of the ultimate load. In this stage, stresses and strains are proportional and the $\sigma - \varepsilon$ curve is linear. Static modulus of elasticity, also called initial tangent modulus, is equivalent to the slope of a straight-line drawn tangent to the curve $\sigma - \varepsilon$ at any point on that curve [17]. Previous researches have already reported that static modulus of elasticity of concrete is more sensitive to the effects of the internal expansion reactions than its compressive strength [1, 3, 7, 12, 14, 15].

The occurrence of DEF expansions alone or DEF combined with ASR expansions in the concrete can generate loss of stiffness of the material in a range of between 50 and 65%. When only DEF expansions are present the decrease in the values of static modulus of elasticity can reach to 67% [1]. Reactive aggregates contribute to concrete expansions process due to DEF and ASR [18].

2.3.3 Dynamic Modulus of Elasticity Tests

Dynamic modulus of elasticity of concrete is a parameter of the degradation and durability of the material. Previous researches have reported that dynamic modulus of elasticity value is often higher than the static modulus of elasticity, about 20, 30 and 40% for high, medium and low compressive strength concretes, respectively [17].

The usual way of measuring dynamic modulus of elasticity is through an electro-acoustic transducer installed on concrete surface that produces longitudinal vibrations along the length of the element studied. Little stresses are applied during the test and as a result there is no micro-cracking in the tested element and the dynamic modulus of concrete is often associated with purely elastic phenomena and is, in fact, a good parameter to assess material integrity.

Many standards describe methods to calculate the dynamic elastic moduli of concrete samples using impulse excitation technique [19–21]. This procedure has been widely used to assess concrete quality and durability parameters because, among its many advantages regarding the static tests, it provides more precise results due to the lower number of variables involved and allows to follow the evolution of damaged in the specimens tested—cracks decrease concrete rigidity and this decrease reduces the natural frequency of vibration of the material [22].

The procedure comprises of firstly exciting a test object by means of a light external mechanical impulse, and secondly of the analysis of the transient natural vibration during the subsequent frees relaxation. This excitation is given in such a way as to favor the desired vibration mode, i.e., a flexural vibration, a torsional vibration or a longitudinal vibration. In the test, the vibration probe was placed at one end of the specimen and the other received a pulse with the impactor, then the frequency was automatically generated in the apparatus, and subsequently the module was calculated, based on the standard [20]. The test procedure is illustrated in Fig. 4 and the Eq. (1) used to obtain the dynamic modulus used was the following:

Fig. 4 Dynamic modulus of elasticity test scheme

$$Ed = \frac{0.0016067\, L^3 m \,.\left(1 + \frac{5.173484\ D^2}{L^2} - \frac{0.4883\ D^2}{L^4} - \frac{5.28853\ D^4}{L^4\left(1+\frac{5.160942\ D^2}{L^2}\right)}\right) F^2}{D^4} \quad (1)$$

where Ed is the dynamic modulus of elasticity (GPa), m is the mass of the specimen being tested (g), L is the length of the specimen being tested (mm), D is the diameter of specimen being tested (mm), F is the pulse frequency (kHz). According to ASTM C215 [20], with nu = 0.2 the module was obtained.

The dynamic modulus of elasticity test was used to evaluate the degradation of the drilled concrete extracted. The tests were performed at GeM Laboratory, University of Nantes, Saint Nazaire, France and the equipment adopted was the Grindosonic, J. W. Lemmens—Mk5 Industrial.

2.3.4 Gas Permeability Tests

Permeability is a property that governs the rate of flow of a gas under pressure through the pore structure of a solid [17]. This property is useful to evaluate durability characteristics of concretes and it is often performed measuring the gas permeability of never stressed undamaged concrete specimens [23–25].

Picandet et al. [23] stated that the study of transfer properties of a cracked concrete is of paramount importance in predicting its durability, because the leaching and freezing processes depend on the flow of aggressive agents through the porous material. Mechanisms such as ASR and DEF also depend on the flow of liquids or gases in the microstructure to be generated.

Cracking process usually produce voids inside the materials, increasing its porosity and also modifying the pore structure. Microcracks are connected until they

generate macro cracks creating an interconnectivity that opens ways to the transport of aggressive agents into element, compromising its durability [25–27]. Picandet et al. [23] used the overall gas flow to control the cracking pattern in deteriorated concrete samples and the authors reported a good performance of the procedure.

As a hardened concrete element is a thin porous body, the percolation of gas through its structure can occurs through two modes of flow: viscous and slipping, the latter referred as Knudsen's flow [23]. To determine the non-viscous flow is often the use of the approach proposed by Klinkenberg, where an intrinsic permeability coefficient k_v (m^2) is associated to the viscous flow [28].

Modifications in the permeability values of a material can be related with an evolution microcracking process, orientation and opening of cracks and, this way, this parameter can indicate the level of damage imposed to a concrete element [24, 29]. Tahlaiti reported that the porosity of cement-based materials is strongly linked with their transfer properties [30].

Permeability tests were performed in two concrete drilled cores of the pile cap investigated. Samples with dimensions of 5 cm × 7 cm (height × diameter) were prepared from the core fragments extracted. As the diameter of the cell of the permeability test had a diameter of 10 cm, it was necessary to fill the empty space and this done with use of silicone resin. This resin also had the function of waterproofing the lateral surface of the samples. Figures 5 and 6 show an overview of properly worked cores, prior to testing.

The drying of the specimens in a 60 °C degree temperature oven was performed to stabilize the mass of the specimen, before the measuring its dry mass. For 12 days,

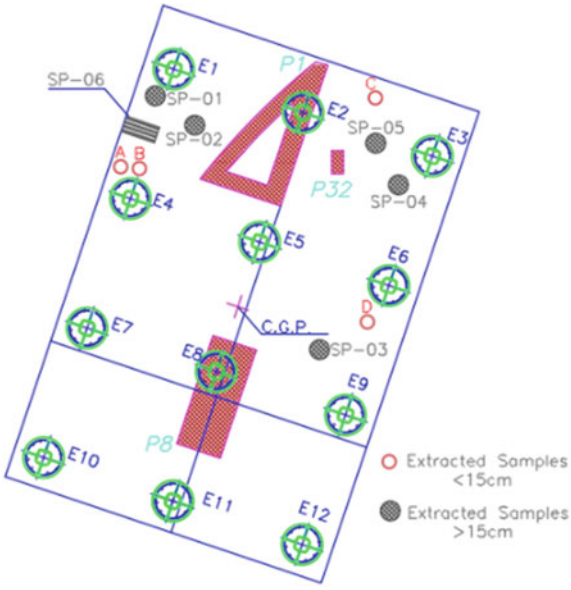

Fig. 5 Extracted samples in pile cap investigated

Fig. 6 Samples P-01 and P-02 prepared for the gas permeability test

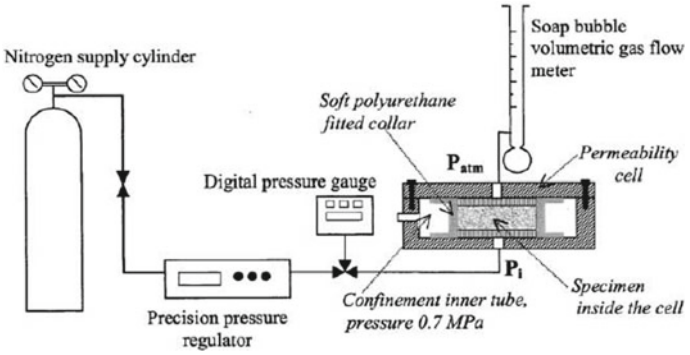

Fig. 7 Layout of permeability equipment [23]

daily measurements of the mass of the specimens were performed until the variation between one measurement and another was within the established tolerance.

The scheme of the permeability equipment was shown by [23] and demonstrates how the sample is confined in the permeability cell (see Fig. 7). The complete apparatus of the permeability equipment used in the test is shown in Fig. 8. Nitrogen was the neutral percolating gas used and laboratory temperature and relative humidity (RH) were controlled and kept constant during the tests—T = 17.8 ºC and RH = 76%).

2.3.5 Scanning Electron Microscopy (SEM) Tests

The scanning electron microscopy technique is often used for the analysis of damaged concrete because it provides qualified information on the microstructure, such as primary and secondary mineral phases in pores or cracks, morphology, chemical

Fig. 8 Flowmeter equipment

composition and other data. In another analysis performed on concrete affected by ASR, calcite, quartz and feldspar minerals were found in the veins of the aggregates that developed the reaction, illustrated in Fig. 9 [31].

Leemann [31] investigated concretes drilled cores extracted from two concrete structures—a bridge built in 1969 and a retaining wall built in 1980—and SEM analysis were used to characterize the microstructure. Cracks in the aggregates filled with ASR products as well as some fragments of calcite incorporated to the crystalline ASR products were found in concrete cores.

The SEM used for tests performed was a ZEISS EVO®40 equipped with a Back-scattered Electron (BSE) detector to determine the chemical composition. The microscopic characterizations were performed on fresh fractures sections on concrete specimens. The specimens were coated with a gold deposit for observations using the SEM in High-Vacuum (HV) model.

Fig. 9 SEM equipment used

3 Results and Discussion

3.1 Summary of ISR in Concrete Cores Compressive Strength

Compressive strength of tested concrete cores was 46 MPa. When this result is compared with that expected from the evolution of these properties with the time, according to prescriptions of several concrete design codes (44.13 MPa) one can conclude that the ISR did not affect compressive strength of the concrete. This observation is consistent with previous research [11, 22, 32] and it can be explained by the so-called stopping mechanism of the expansion cause by the aggregates [1]. This observation confirms the conclusions of several studies that states that compressive strength is not a good indicator to evaluate the effects of ISR on concrete [33]. In the opposite direction, some researchers have reported a great impact generated by ISR on the compressive strength of the concrete [34–36]. A possible explanation for this divergence may be associated with the time difference in which the two tests were performed. In fact, compressive strength tests were performed by [34, 35] after a period of 430 days of the concrete exposure to an environment favourable to DEF and the tests carried out in this paper were performed 19 years after the construction of the deep pile cap investigated.

Furthermore, it is important to highlight that authors have already reported that the effects of ISR over mechanical properties concrete is not a closed question with definitive answers and apparently contradictory results are reported. But far from being divergent, these results can be justified by the fact that the material response of concrete to ISR is very dependent on the type and nature of the reactive aggregates used [37, 38].

3.2 Summary of ISR in Concrete Cores Static Modulus of Elasticity

Force-displacements values presented in Fig. 10 were converted into stress–strain data to compute elastic modulus, using drilled concrete cores cross-section areas and lengths. Three values of the static elastic modulus were obtained for samples AM-1A, AM-1B and AM-02 and the average result obtained 16.72 GPa. This value is quite distant from expected ones, obtained using prevision calculated taking into account the evolution of static elastic modulus of concrete with the time provided in concrete design codes (37.20 MPa). The results obtained represent a decrease in the static elastic modulus of the concrete of approximately 55% that are consistent with previous researches that reported decreases in static elastic modulus of concrete within the range of 50–65%, for moderate expansion levels (0.30–0.40%) and decreases close to 85% for high expansion level, 1% [33, 35, 36].

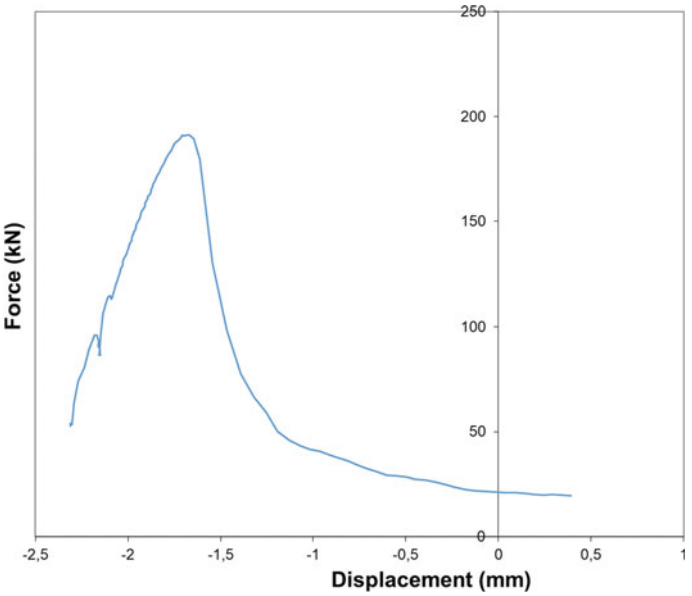

Fig. 10 Force-displacement diagram

Results obtained are compatible with the extent of the cracking mapping process found in the pile cap investigated that was formed due to the development of the ettringite crystals.

3.3 Summary of ISR in Concrete Cores Dynamic Modulus Elasticity

The average dynamic modulus of elasticity obtained for the concrete cores was about 21 GPa. This value is 26% higher than the static elastic modulus dynamic. This value is consistent with previous researches that stated that dynamic modulus of elasticity value of concrete is often higher than the static modulus of elasticity within a range of 20–40% [39]. Jalal [40] found, for undamaged concrete, values of dynamic modulus of elasticity of 38 GPa. If one compares these values, it is possible to conclude that ISR observed in concrete cores imposed a severe decrease in dynamic modulus of concrete (close to − 45%) which, in fact, translates the cracking process observed on the pile cap surface during the visual inspections and materializes the efficiency of this parameter as a good indicator of concrete damage due to ISRs [23, 41–44].

3.4 Gas Permeability

Values of permeability of concrete cores tested were 1.3×10^{-15} m^2 and 3.9×10^{-16} m^2. These results show that the concrete presented a high permeability. In fact, the usual values of this parameter for an undamaged concrete are in the range of 10^{-18}–10^{-17} m [30, 31]. Values of porosity tests indicated 11.29 and 9.76% for the two concrete cores investigates that high values compared with those available in literature [6, 45].

The high values of the permeability coefficient can explain the intense cracking process existing in the pile cap investigated that was the responsible for the early deterioration process observed in concrete elements studied, situation consistent with previous researches [2].

It is also important to highlight that the dynamic modulus of elasticity is influenced by the material porosity. As the concrete cores showed high porosity, this factor contributed significantly to the decrease of the dynamic modulus of concrete studied as it was already presented. This can be explained by the strong network of cracks in the cement paste due the DEF mechanism that increase the density of cracks in the samples.

3.5 Scanning Electron Microscopy (SEM)

In the analyses performed, some specific parts that indicated the presence of delayed ettringite formation were chosen. The first point was 305, where the morphology indicated that it was an aggregate particle with crystalline products. Figure 11 shows this part of the sample, with a magnitude of 234×.

This particle analysed (see Fig. 12) showed in its chemical composition aluminium and silica, indicating that there are components of delayed ettringite formation and crystalline products of alkaline reaction [10] acting together.

At point 307 (see Fig. 13) analysed by SEM, it is possible to observe ettringite crystals developed and filling a pore which corresponding chemical composition is presented in Fig. 14, with the presence of Sulphur (S), Aluminium (Al) and Calcium (Ca), aspect that confirms that it is delayed ettringite, as well as Silicon (Si), indicating that there are components of crystalline products of alkaline reaction [10].

3.6 Pile Caps Repair and Rehabilitation Design

The strengthening design was developed to rehabilitate all the blocks of the foundation of the analyzed building. The mapping cracks observed on the surfaces of all blocks, observed in the visual inspection, were injected with epoxy resin and the horizontal cracks of large opening were “stitched” with $\phi = 32$ mm passive vertical

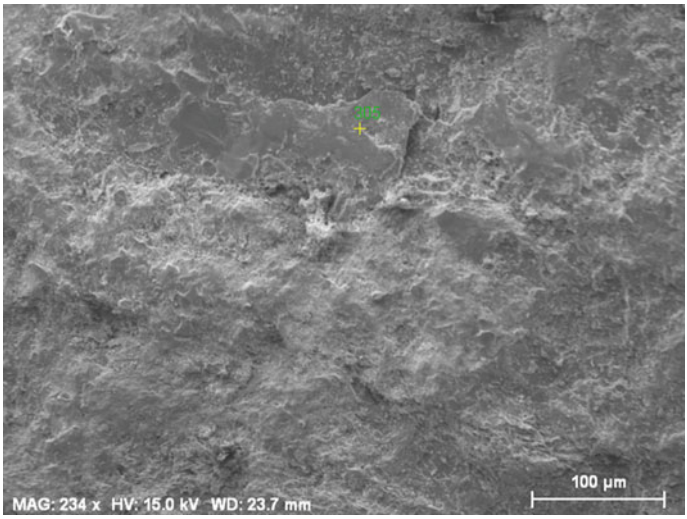

Fig. 11 Aggregate particle with crystalline products of the alkali-silica reaction

reinforcement. The rehabilitation design aimed to provide the complete restoration of the structural integrity of the element deteriorated to make it monolithic as well as to prevent addition expansion.

The main hypothesis conceived was to assure physical restraint or containment with encapsulation of the affected member by a surrounding non-reactive concrete, applied stresses and supplementary use of active and passive reinforcement. Post-tensioning with $\phi = 32$ mm Dywidag bars—ST 85/100 steel—was use in two directions. The bars were anchored in 16 mm steel plates placed on the pile cap lateral faces as it can be seen in Fig. 16.

Additional specific conditions were adopted in the rehabilitation project:

- Elimination of voids inside the pile cap block investigated with epoxy injection to restore the pre-cracking condition of the element;
- Restoration of the confinement and operation of the upper strut node in the region close to the of the column;
- Avoid moisture to get into the concrete element;
- Adoption of confinement of the lower region of the blocks to avoid pile cap interface failure;

Finite element analyses were performed to verify the level of load imposed to each pile as a result of a distribution of stresses that occurred in the element investigates duo to ASR expansions observed. Figure 15 shows the finite element model developed and the normal forces in the piles of the foundation block studied.

Details of the pile caps repair and rehabilitation design is shown in Fig. 16.

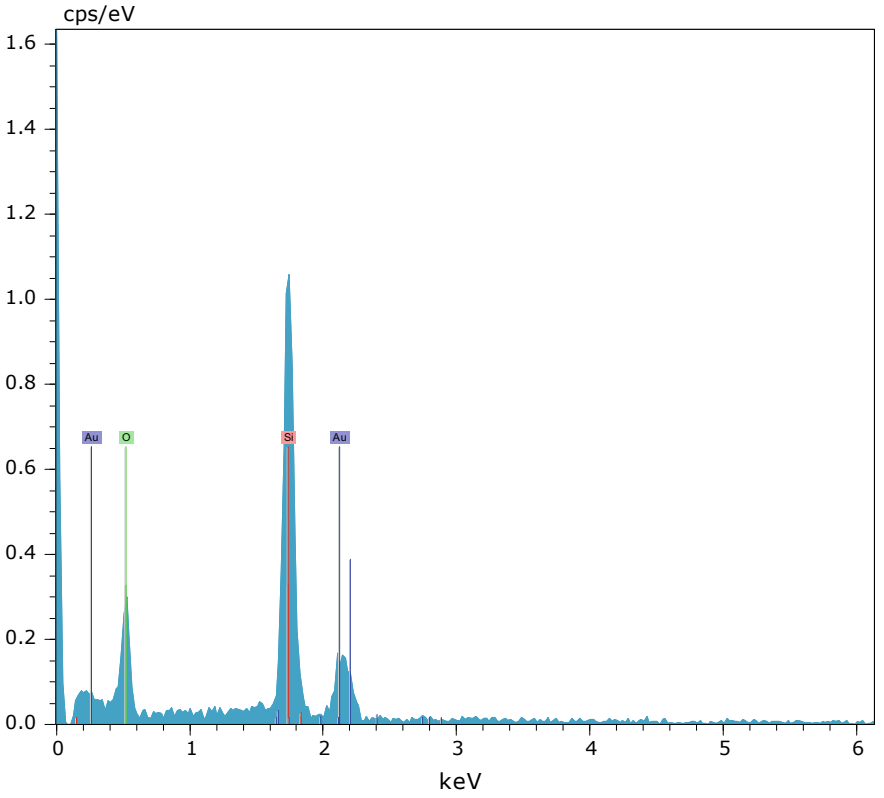

Fig. 12 Crystalline product of alkaline silica reaction

4 Conclusions

As a result of the intense cracking process observed in all the foundation pile caps of the building and based on all the physical–chemical tests performed on drilled concrete cores extracted, it can be stated that the concrete elements investigated presented chemical alterations that significantly affected the integrity and durability of the structure. Visual inspections indicated some alterations in a macroscopic level that were all confirmed during the microscopic investigations performed. Both ASR and DEF products were identified being the most frequent the latter one.

Besides the general considerations listed above, it can be concluded from the various tests carried out that:

- The compressive strength of concrete cores tested was not affected by concrete ISR, aspect that corroborate results of previous researches which states that the compressive strength is not a good indicator of the effect of ISR in concrete elements;

Fig. 13 Ettringite crystals filling a pore

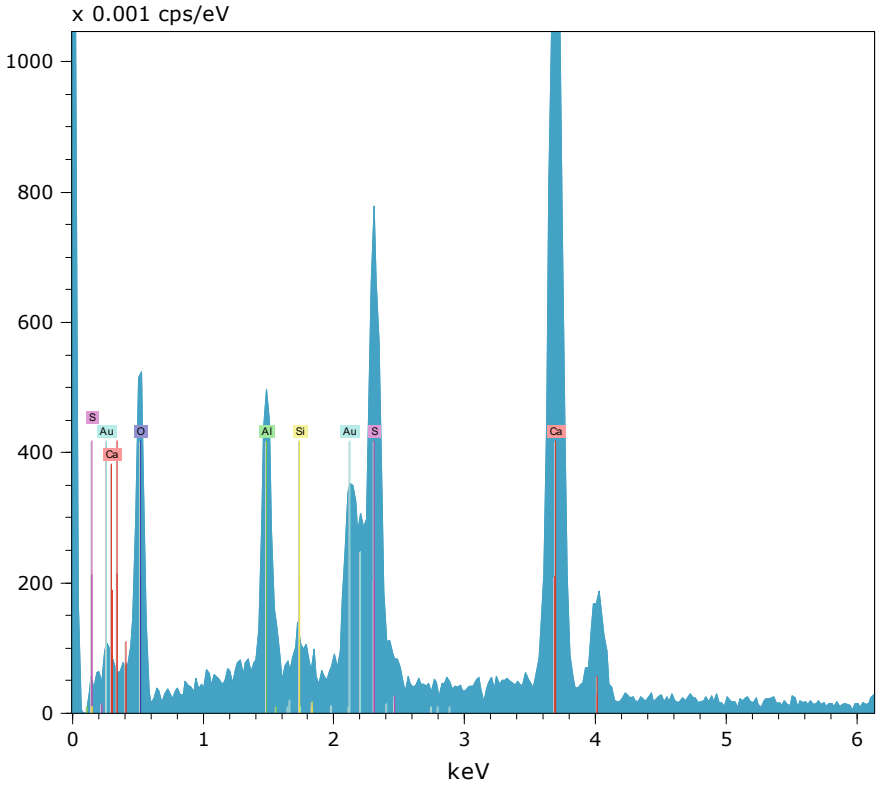

Fig. 14 Chemical composition of the crystals

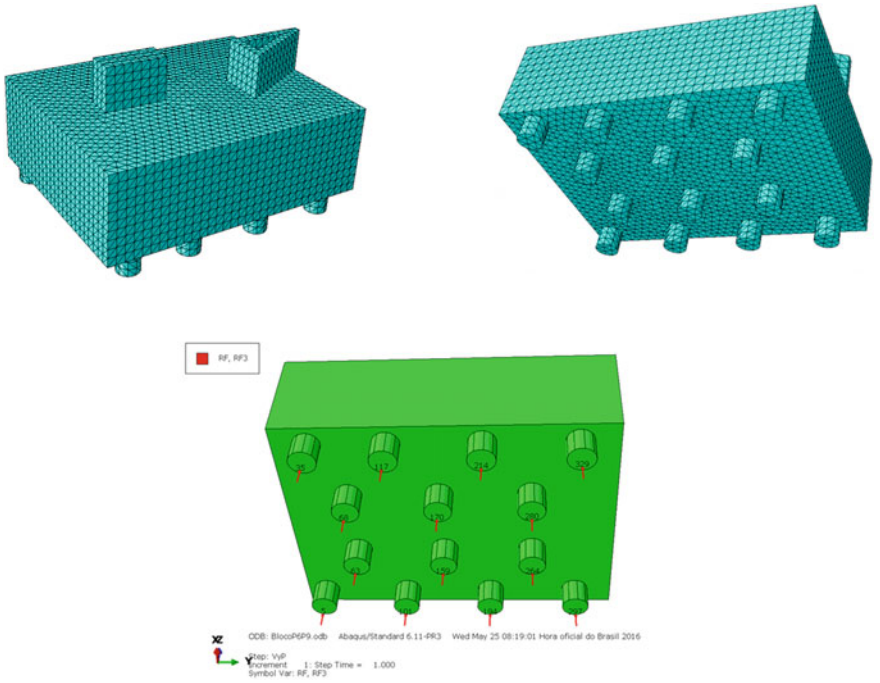

Fig. 15 Finite element model of the pile cap investigated and normal force in the piles

- Dynamic modulus of elasticity showed to be a good indicator of damage induced by ISR in the concrete element investigated;
- Rehabilitation procedures executed using using strengthening procedures to provide the complete restoration of the structural integrity of the element deteriorated proved to be a good solution to retrofit pile cap deteriorated by expansions due to ISR of concrete.

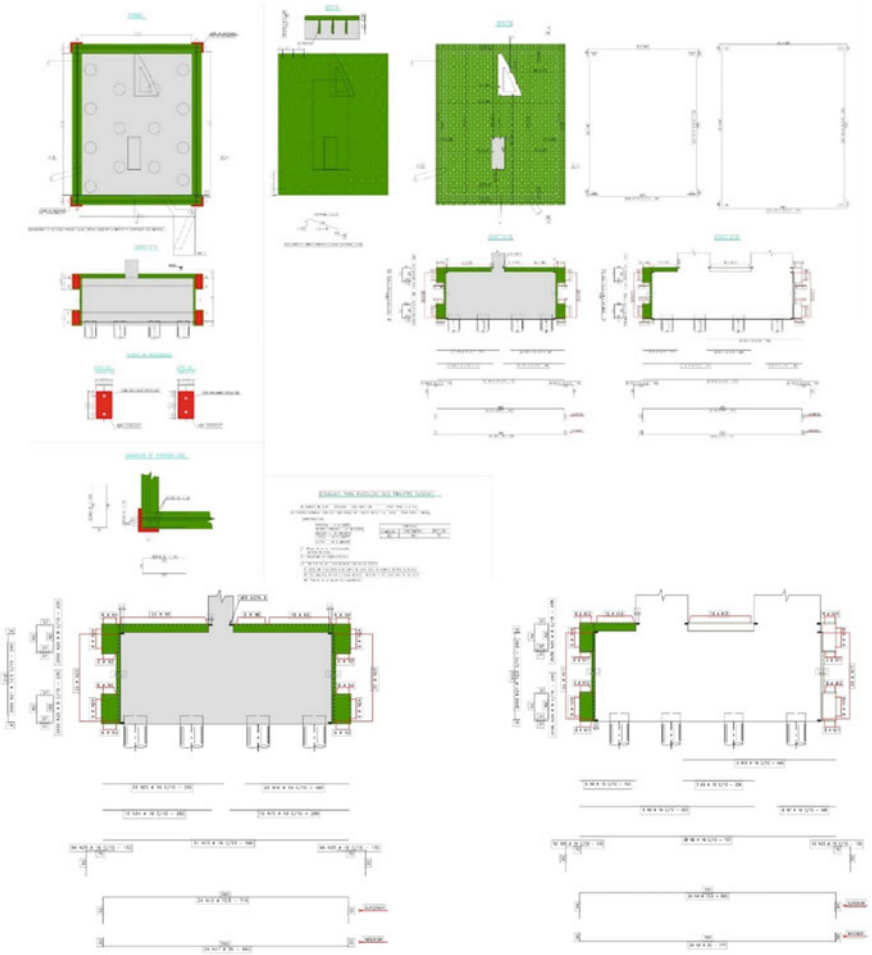

Fig. 16 Strengthening design details of the pile cap investigated

References

1. Sanchez LFM, Drimalas T, Fournier B, Mitchell D, Bastien J (2018) Comprehensive damage assessment in concrete affected by different internal swelling reaction (ISR) mechanisms. Cem Concr Res 107:284–303. https://doi.org/10.1016/j.cemconres.2018.02.017
2. Collepardi M (1999) Damage by delayed ettringite formation. Concr Int 21(1):69–74
3. Allard A, Bilodeau S, Pissot F, Fournier B, Bastien J, Bissonnette B (2018) Expansive behavior of thick concrete slabs affected by alkali-silica reaction (ASR). Constr Build Mater 171:421–436. https://doi.org/10.1016/j.conbuildmat.2018.03.159
4. Balachandran C, Muñoz JF, Arnold T (2017) Characterization of alkali silica reaction gels using Raman spectroscopy. Cem Concr Res 92:66–74. https://doi.org/10.1016/j.cemconres.2016.11.018

5. Rajabipour F, Giannini E, Dunant C, Ideker JH, Thomas MDA (2015) Alkali–silica reaction: current understanding of the reaction mechanisms and the knowledge gaps. Cem Concr Res 76:130–146. https://doi.org/10.1016/j.cemconres.2015.05.024
6. Ghanem H, Zollinger D, Lytton R (2010) Predicting ASR aggregate reactivity in terms of its activation energy. Constr Build Mater 24(7):1101–1108. https://doi.org/10.1016/j.conbuildmat.2009.12.033
7. Mohammadi A, Ghiasvand E, Nili M (2020) Relation between mechanical properties of concrete and alkali-silica reaction (ASR): a review. Constr Build Mater 258:119567. https://doi.org/10.1016/j.conbuildmat.2020.119567
8. Benmore CJ, Monteiro PJM (2010) The structure of alkali silicate gel by total scattering methods. Cem Concr Res 40(6):892–897. https://doi.org/10.1016/j.cemconres.2010.02.006
9. Carasek H, Hasparyk NP, Melo SK, Silva HHAB, Martins C (2011) Influence of hydration heat on the delayed ettringite formation (DEF) in pozzolanic Portland cement concrete. In: Proceedings of 53th Brazilian congress of concrete, Florianópolis-SC, Brazil
10. Hasparyk NP (2005) Investigation of concretes affected by the alkali-aggregate reaction and advanced characterization of exudate gel, PhD Thesis, Federal University of Rio Grande do Sul, Brazil
11. Shayan A, Al-Mahaidi R, Xu A (2008) Durability and strength assessment of AAR-affected Bridge deck planks. In: Proceedings of 13th international conference on alkali-aggregate reaction in concrete, Trondheim, Norway
12. Sanchez LFM, Fournier B, Mitchell D, Bastien J (2020) Condition assessment of an ASR-affected overpass after nearly 50 years in service. Constr Build Mater 236:117554. https://doi.org/10.1016/j.conbuildmat.2019.117554
13. Mehta PK (1993) Sulfate attack on concrete-a critical review. Materials science of concrete III. American Ceramic Society, pp 105–130
14. Li S, Deng Z, Li C, Chen D, Zhang Y (2020) Modeling of flexural strength degradation induced by alkali-silica reaction. Constr Build Mater 234:117397. https://doi.org/10.1016/j.conbuildmat.2019.117397
15. Kongshaug SS, Oseland O, Kanstad T, Hendriks MAN, Rodum E, Markeset G (2020) Experimental investigation of ASR-affected concrete—the influence of uniaxial loading on the evolution of mechanical properties, expansion and damage indices. Constr Build Mater 245:118384. https://doi.org/10.1016/j.conbuildmat.2020.118384
16. Kubo Y, Nakata M (2012) Effect of reactive aggregate on mechanical properties of concrete affected by alkali-silica reaction. In: Proceedings of 14th international conference on alkali-aggregate reaction (ICAAR), Texas, USA
17. Mehta K, Monteiro P (2014) Concrete: Microstructure, properties and materials. McGraw-Hill Education
18. Taylor HFW, Famy C, Scrivener KL (2001) Delayed ettringite formation. Cem Concr Res 31(5):683–693. https://doi.org/10.1016/S0008-8846(01)00466-5
19. ASTM E1876 (2015) Standard test method for dynamic young's modulus, shear modulus, and Poisson's ratio by impulse excitation of vibration. ASTM International, West Conshohocken, PA
20. ASTM C215 (2014) Standard test method for fundamental transverse, longitudinal, and torsional resonant frequencies of concrete specimens. ASTM International, West Conshohocken, PA
21. BS EN 12504-4 (2004) Testing concrete—part 4: determination of ultrasonic pulse velocity. British Standard
22. Christaras B, Auger F, Mosse E (1994) Determination of the moduli of elasticity of rocks. Comparison of the ultrasonic velocity and mechanical resonance frequency methods with direct static methods. Mater Struct 27:222–228. https://doi.org/10.1007/BF02473036
23. Picandet V, Khelidj A, Bastian G (2001) Effect of axial compressive damage on gas permeability of ordinary and high-performance concrete. Cem Concr Res 31(11):1525–1532. https://doi.org/10.1016/S0008-8846(01)00546-4

24. Picandet V (2001) Influence of mechanical damage on the permeability and water diffusivity of concretes. PhD Thesis, Nantes University, France
25. Malbois M, Nedjar B, Lavaud S, Rospars C, Divet L, Torrenti JM (2019) On DEF expansion modelling in concrete structures under variable hydric conditions. Constr Build Mater 207:396–402. https://doi.org/10.1016/j.conbuildmat.2019.02.142
26. Choinska M (2006) Effects of temperature, mechanical state and their interactions on the permeability of structural concrete. PhD Thesis, Nantes University, France
27. Baroghel-Bouny V (1994) Microstructural and water characterization of pasta of cement and ordinary and very high concrete performances. PhD Thesis, Paris University, France
28. Saiyouri N, Bouasker M, Khelidj A (2008) Gas permeability measurement on injected soils with cement grout. Cem Concr Res 38(1):95–103. https://doi.org/10.1016/j.cemconres.2007.08.015
29. Martin RP, Metalssi OO, Toutlemonde F (2013) Importance of considering the coupling between transfer properties, alkali leaching and expansion in the modelling of concrete beams affected by internal swelling reactions. Constr Build Mater 49:23–30. https://doi.org/10.1016/j.conbuildmat.2013.08.008
30. Tahlaiti M (2010) Study of chloride penetration and corrosion initiation in saturated and tidal zones. PhD Thesis, La Rochelle University, France
31. Leemann A (2017) Raman microscopy of alkali-silica reaction (ASR) products formed in concrete. Cem Concr Res 102:41–47. https://doi.org/10.1016/j.cemconres.2017.08.014
32. Yu XT, Chen D, Feng JR, Zhang Y (2018) Behavior of mortar exposed to different exposure conditions of sulfate attack. Ocean Eng 157:1–12. https://doi.org/10.1016/j.oceaneng.2018.03.017
33. Blight GE, Alexander MG (2011) Alkali-aggregate reaction and structural damage to concrete: engineering assessment, repair and management. CRC Press, USA
34. Martin RP (2010) Experimental analysis of the mechanical effects of delayed ettringite formation on concrete structures. PhD Thesis, Université Paris-Est., France
35. Martin RP, Renaud JC, Multon S, Toutlemonde F (2012) Structural behavior of plain and reinforced concrete beams affected by combined AAR and DEF. In: Proceedings of 14th international conference on alkali aggregate reaction ICAAR14, France
36. Noël M, Sanchez L, Tawil D (2018) Structural implications of internal swelling reactions in concrete: review and research needs. Mag Concr Res 70(20):1052–1063. https://doi.org/10.1680/jmacr.17.00383
37. Naar R (2009) Modélisation du comportement mécanique du béton par approche multi-physique (couplage chimie-mécanique): application à la réaction alcali-silice. PhD Thesis, École Nationale Supérieure des Mines de Paris, France
38. Reinhardt HW, Mielich O (2011) A fracture mechanics approach to the crack formation in alkali-sensitive grains. Cem Concr Res 41(3):255–262. https://doi.org/10.1016/j.cemconres.2010.11.008
39. Jiang L, Niu D (2016) Damage degradation law of concrete in sulfate solution and freeze-thaw environment, J Cent South Univ (Sci Tech) 47:3208–3216. https://doi.org/10.11817/j.issn.1672-7207.2016.09.040
40. Jalal M, Grasley Z, Nassir N, Jalal H (2020) Strength and dynamic elasticity modulus of rubberized concrete designed with ANFIS modeling and ultrasonic technique. Constr Build Mater 240:117920. https://doi.org/10.1016/j.conbuildmat.2019.117920
41. Zhang D, Mao M, Zhang S, Yang Q (2019) Influence of stress damage and high temperature on the freeze–thaw resistance of concrete with fly ash as fine aggregate. Constr Build Mater 229:116845. https://doi.org/10.1016/j.conbuildmat.2019.116845
42. Gao J, Yu Z, Song L, Wang T, Wei S (2013) Durability of concrete exposed to sulfate attack under flexural loading and drying–wetting cycles. Constr Build Mater 39:33–38. https://doi.org/10.1016/j.conbuildmat.2012.05.033
43. Chen F, Qiao P (2015) Probabilistic damage modeling and service-life prediction of concrete under freeze–thaw action. Mater Struct 48(8):2697–2711. https://doi.org/10.1617/s11527-014-0347-y

44. Glasser FP, Damidot D, Atkins M (1995) Phase development in cement in relation to the secondary ettringite problem. Adv Cem Res 7(26):57–68. https://doi.org/10.1680/adcr.1995.7.26.57
45. Guo JJ, Wang K, Guo T, Yang ZY, Zhang P (2019) Effect of dry–wet ratio on properties of concrete under sulfate attack. Mater 12(17):2755. https://doi.org/10.3390/ma12172755

Waterproof Roofing System Pathology Phenomenology Analysis as a Background Support for Diagnosis and Design

S. Croce and M. Fiori

Abstract Waterproofing membranes are subjected to thermal, physical, chemical, and mechanical actions, which generate interactive stresses in the cover system. These interactions, which affect life expectancy of membranes, depend on the chosen technical solution of the flat roof system, materials used, geographical locations, climate and weather conditions, construction method and usage. Therefore, waterproof membrane is subjected to stresses varying over time and space, which depend on decisions and actions taken during planning, construction, and management phases. As for other engineering fields, the definition of procedures for the analysis of stress phenomena, which occur mainly on the waterproofing element, would be desirable. Of course, this would imply the development of focused experimental test methods based on more sophisticated instruments like DMA. Modelling of aging phenomena and early decay may serve as a tool of knowledge, able to ameliorate materials and direct and optimize the design towards more reliable construction systems, avoiding a blind and exclusive reference to codes of practice.

Keywords Building pathology · Flat roof · Polymer-bitumen waterproof membranes

1 Introduction

Duration estimate of a cover system is extremely complex, both for the variety of technical solutions and for the number of functional layers (see Table 1).

This number is matched by the significant hybridization of material within construction systems, nowadays characterized by an intense evolutionary dynamism, both in the field of waterproofing membranes and thermal insulation.

S. Croce (✉) · M. Fiori
DABC, Politecnico di Milano, Milan, Italy
e-mail: sergio.croce@polimi.it

M. Fiori
e-mail: matteo.fiori@polimi.it

J. M. P. Q. Delgado (ed.), *Masonry: Building Pathologies and Design*, Building Pathology and Rehabilitation 22, https://doi.org/10.1007/978-3-030-80496-1_8

Table 1 Functional layers according to the Italian standard UNI-8178-2 [1]

Analysis of elements and functional layers of continuous roofing and design guidance for the definition of technological solutions
1. Structural element
2. Thermal insulation element
3. Waterproofing element
4. Compartmentalization and hydraulic sectoring element
5. Mechanical fixing elements
6. Vapour control layer
7. Layer of structural continuity
8. Drainage layer
9. Filtering layer
10. Primer layer
11. Slope layer
12. Protection layer from mechanical interactions;
13. Separation and protection layer against chemical interaction or physical–chemical properties
14. Layer or integrated set of single elements for protection against physical and thermo-physical interactions
15. Hydraulic protection layer
16. Sun protection layer
17. Load distribution and stiffening layer
18. Geometric regulation layer
19. Ballast layer
20. Flooring layer

In the current technological context, weather-exposed waterproof covers with BPP membranes can easily remain efficient for 20–25 years, when subjected to proper maintenance [2–5].

Of course, during this time the membrane exposed to external factors undergoes a slow stiffening which leaves it to increasing stresses of thermal origin and to greater risks due to mechanical impacts.

In the absence of a criterion for useful life evaluation, one relies indirectly on codes that can be used to evaluate the quality of a technological solution over another.

Quality of the solution can be compromised in a more or less severe way based on the activation of disorder factors during design, construction and management phases. Disorder factor identification can be carried out easily in retrospect while proves to be more difficult ex-ante.

Despite the existence of codes, it is fairly known that waterproof seal failure and consequent infiltration represents an important percentage if not majority of cases brought to the attention of jurisdiction.

Reference to codes of practice is certainly important but not sufficient. As a matter of fact, the evolutionary dynamism previously mentioned would require continuous updates, both at technical and procedural level.

Current knowledge in roofing system design can be improved by studying the phenomenological behavior of waterproof membranes at service. As a matter of exemplification, we will refer to the functional scheme of an exposed membrane, thus at the following technical solution:

1. waterproof membrane made with polymer bitumen BPP
2. thermal insulating panels
3. vapour barrier
4. structural element.

Thermal phenomena that can dynamically stress and deteriorate waterproofing elements are:

1. solar radiation and air temperature;
2. night radiation towards the sky;
3. thunderstorms and hailstorms;
4. shape memory of the membrane reinforcement.

2 Thermal Phenomena Related to Thermal Exposure

A membrane directly subjected to solar radiation assumes a higher temperature than the air one, which may reach up to 80 °C during summer. This depends on geographical position and altitude. Sudden storms may drastically lower membrane temperature.

Stress states associated with these phenomena depend on the absorption index of solar radiation of the membrane, on characteristics and thickness of the insulating layer, and on the overall technical solution. Dealing with thermal stimulation, one must consider meteorological events such as storms and hail, which may lower very quickly the temperature of the waterproof layer and cause a tensional thermal shock.

The rapid temperature decrease prevents immediate structural plastic recovery of the BPP mass. Contraction takes place in the elastic regime on a non-ductile mass. With storms, cooling speed is ruled by water temperature and surface run-off of the membrane.

In the case of hail, ice grain deposit suddenly brings the temperature of the waterproof mass close to 0 °C. Sudden temperature drops determine an enhanced tensional state due to prevented contraction, which puts under stress adherence bonds on cover support and edges. As we will see, punching action of the grains is enhanced by the thermal shock.

From the point of view of thermal strains and resulting stress state, absorption of thermal radiation coming from the upper atmosphere should be taken under consideration. Temperatures may reach -55 °C in the troposphere. During clear winter nights, large temperature drops can take place on exposed membranes characterized by a

high absorption index. This phenomenon, which may also lead to frost formation, can determine surface temperatures considerably lower than those of the air. Depending on the altitude, values far below zero might be reached.

While solar radiation generates the strongest stress cycles during summer season, when bitumen-polymer mass has greater ductility, in the case of sky radiation critical cooling conditions occur as ductility drops or ceases due to low winter temperatures. Stresses due to prevented contraction act on adherence bonds to thermal support and edges.

3 Phenomena Related to Shape Memory of the Reinforcement

The thermal factors analyzed are added to the shape memory due to production process. During production of bitumen-polymer membranes, reinforcement layer is subjected to traction due to of dragging action. This produces an elongation in the reinforcement layer which then remains locked-in due to sudden cooling of the waterproof mass and the subsequent rolling of the membrane. Stressing size is further increased during the cooling by thermal conditions in the production phase.

Currently used reinforcements are made of continuous-wire NT polyester due to their mechanical strength and high puncturing resistance. However, they are characterized by poor dimensional stability and a high thermal linear expansion coefficient [6, 7]. A membrane reinforced with NT polyester shows stability values ranging from 0.7 to 1.0%. This means that a 10 m free cloth brought to viscous state can shorten from 7 to 10 cm.

Combined pre-coupling with a second layer of fiber glass reinforcement (composit), which is far more stable both geometrically and thermally, allows to reduce instability at various degrees (see Table 2).

Inside the structure of BPP compound polymer characteristics are dominant compared to those of the distilled bitumen. On its behalf, bitumen provides waterproofing performances.

Table 2 Heat dimensional stability of BPP membranes evaluated according to the Italian standard UNI-8178-2 [1]

Type of reinforcements	Dimensional stability (%)
Non-woven NT polyester	≤ 0.5
Non-woven NT polyester pre-coupled with mono-dimensional glass fiber	≤ 0.3
Composite non-woven NT polyester pre-coupled with bi-dimensional glass fiber	≤ 0.2
Non woven NT polyester pre-coupled with reinforced glass veil	≤ 0.1

Thermal stability mainly depends on the thermoplastic behavior of the polymer that has been used. Usually, the stability of the system is characterized with respect to cold bending and heat dimensional.

Another key feature is shape stability that correspond to the limit temperature above which the waterproof mass takes on a viscous behavior. But BPP mass quality is a function of uniformity of the compounds. Typically, compound is further mixed with filler to make the membrane more consistent to during installation and service, and to make it more resistant to solar radiation.

The main purpose of mixing bitumen with polymers is to expand the thermal-stability effective range to the one that would be necessary in the specific in situ thermal conditions defined for a membrane.

Thermal stability refers to the ability of a compound to plastically adapt to daily temperature variations, relatively slow, that characterize the solar year. This ability must show while maintaining its "compactness" to be able to withstand operating loads without damage. In addition, there is the need to endure stresses that are determined by expected thermal shocks, during which the membrane cannot immediately plastically adapt to the new temperature.

In such cases, stresses related to prevented contraction develop on the BPP mass. These are also due to adherence with reinforcement and can increase considerably. For well-designed compound, such stresses are determined in a quasi-elastic regime. A lack of this can lead to microcracks within bitumen outer surfaces for a membrane excessively rigid and not appropriate to the context. Energy stored by elastic deformation is then released through plastic relaxation which eliminates stresses in a more or less rapid way.

In conclusion, thermal stability analysis of a BPP mass in a given thermal context requires insights on both elastic and plastic behavior in relation to specific dynamics of temperature changes. It is straightforward that effectiveness in terms of thermal stability of a membrane installed in the Alps, where thermal shocks at low temperatures are possible, must be evaluated differently from that of a membrane installed in Sicily.

In the first case, the need for a stability effective field shifted towards low temperatures prevails, while in the second case this must be shifted towards high temperatures.

To make another example, working in the Arabian desert the field of thermal stability must be wider due to remarkable reduction in surface temperature at night and significant overheating during the day.

4 The Prestress Condition of the Membrane

Going into details of thermally originated stress phenomena, it should be noted that foils are in a state of prestress when laid in site. Reinforcement is under tension which entity is derived from the extent pre-tensioning and thermal expansion during production. On the other hand, BPP mass is under compression.

Only after proper thermal exposure at high temperatures, larger ductility of bitumen-polymer mass would allow reinforcement to resume its original size before production process due to shape memory.

This is not the case if membrane is properly glued to the support and/or restrained at its ends on the perimeter. Dealing with roof covers, each foil is indeed connected to the other. In these conditions, reinforcement remains in tension since contraction is prevented.

During service, tensions for prevented thermal contractions, due to lowering of temperatures, further add up. As observed, stronger stress states occur in presence of thermal shocks, mechanical-thermal actions due to hail or mechanical actions during service.

Considering perfect stabilization between membrane and a bitumen polymer mass that maintains itself sufficiently ductile and shows a continuous elastic (depending on temperature) or plastic structural recovery, stresses arising from initial pre-tensioning and from thermal cycles concentrate exclusively on reinforcement.

Remaining still and stable in size, this is not capable of transmitting tension to the waterproof mass. Stresses inside bitumen polymer mass, in plastic phase, depend exclusively on the speed of its plastic structural recovery, which is function of temperature and its rate of change.

Of course, in the absence of correct stabilization by connection to support, the membrane tends to shrink as reinforcement goes back to its original size at room temperature. It should be noted that, even with stable reinforcement, shrinkage due to thermal contraction from high temperature during pre-stressing in the production phase to cooling in the water tank is still present.

Based on the above, one can state from a modelling point of view that, considering a prefect stabilization of the membrane and a BPP mass appropriate to the thermal-climatic context, reinforcement characteristics do not have relevance on the thermal stress state that generates inside the mass. Of course, this is true in the absence of disturbing factors which will be discussed later.

Reinforcement characteristics show relevance when dealing with dynamic and static mechanical actions at service. An example of perfect stabilization is the case of a membrane continuously well-glued to a concrete support, in which reinforcement remains still even in tension. BPP mass is only affected by self-thermal stresses, which result from its elastico or thermoplastic characteristics at varying temperature. Reinforcement contribution is negligible.

In general, stabilization can of course be counter-acted by an implementation that does not supply any adherence to support and perimeter and that is not able to hold the membrane in initial geometric position. Further risky conditions can be triggered by thermo-mechanical interactions with thermo-insulating panels that lay underneath. These interactions can be attributed to design and construction mistakes and can lead to additional stresses and breakdowns to those arising from membrane destabilization.

Going into details of thermally originated stress phenomena, it should be noted that foils are in a state of prestress when laid in site. Reinforcement is under tension which entity is derived from the extent pre-tensioning and thermal expansion during

production. On the other hand, BPP mass is under compression. Forces related to reinforcement elongation in the production phase depend on compound type, membrane thickness, process speed, production line, machine settings and other plant features.

Several beliefs and opposing positions on force magnitude quantification can be found on this topic. However, it can be stated that pre-tensioning magnitude is in the order of 10 kg per linear meter. According to experts, operators and builders of specialized machines for MBP production, an overall estimation ranges from about 20–30 kg/m to about 50–80 kg/m.

As previously discussed, stresses in the membrane at the time of installation arise both from pre-tensioning during production and from thermal contractions prevented by presence of the reinforcement and consolidated in cooling tanks.

High speed of the cooling process does not allow for plastic recovery of the waterproof mass. Cooling can take place with water baths in tanks around 30 m long. Another technique is based on the cooling action of a series of multiple cylinders of large diameter, ending with less consisting water baths.

The choice of which cooling technique to use depends on membrane type and surface finish, since it can favor passage between cooling rollers or not. Cooling time relates to membrane advance speed in the production cycle, which can be greatly variable, ranging on 1500–3000 m/h.

It depends on compound type, which can be more or less fluid, thickness and reinforcement. Thermo-tensional state at service depends on production process and, in particular, on cooling type, on advance speed.

Definitive stabilization of elastic and thermal elongation of the reinforcement, consolidated after the heat shock, takes place during winding phase at 30–35 °C. Reinforcement stabilization temperature can be hypothetically evaluated between that of cooling bath immersion and winding.

Reference should be made to such temperature in order to assess the magnitude of thermal stresses connected with temperature decrease at service. As a matter of fact, membrane is in pre-tensioning state during installation phase.

Pre-stressing runs out, in longer or shorter amount of time, whenever the membrane experiences maximum operating temperature. After this event, well-stabilized reinforcement, properly attached to support and edges, stays still and undergoes tension. Obviously, tension increases with decreasing temperature, anyway no tension is transmitted to the BPP mass. Dealing with thermal shock, BPP mass generates stresses in the reinforcement, since its contraction is prevented by reinforcement itself.

5 Current Quality Tests on Membrane Characteristics and Dynamic Mechanical Analysis (DMA)

Going into details of thermally originated stress phenomena, as already noted, it should be noted that foils are in a state of prestress when laid in site. Reinforcement is under tension which entity is derived from the extent pre-tensioning and thermal expansion during production. On the other hand, BPP mass is under compression. Forces related to reinforcement elongation in the production phase depend on compound type, membrane thickness, process speed, production line, machine settings and other plant features. In practice, criteria for the choice of a membrane are based on mechanical characteristics of the reinforcement and ductility range of the waterproof mass.

Regarding the thermoplastic mass, in commercial terms, reference is currently made to cold bending and heat dimensional stability. Cold bending and heat dimensional stability briefly express the concept of glass and viscose transition. These features somehow give us an idea of ductility in extreme thermal conditions and an overall indication on plastic structural recovery at the two temperatures.

Comparison between values of cold bending before and after thermal aging rather provides indirect and, as we will see, insufficient indications over progress and modes of membrane aging.

On the other hand, heat dimensional stability in the longitudinal direction shows the value of potential shrinkage of the reinforcement, which represents shape memory contribution on the potential displacement of the membrane on the edges, orthogonal to foil direction, due to improper stabilization.

A further feature for membrane evaluation is the tensile strength. However, considering well-stabilized membranes, this has negligible importance regarding stress phenomena of thermal origin.

It should be read instead when considering either external mechanical actions or reactions connected with the membrane restrain mechanism. Anyway, it should be noted that this separate procedure for quality assessment of reinforcement and bitumen-polymer mass is not of help in defining membrane quality with respect to a certain frame of conditions, but only in defining comparison analysis. It also gives no information regarding complex rheology that characterizes the whole stress history for a specific context.

In order to model the actual thermo-stress behavior, therefore the complex rheology of the membrane as a whole and of the mass itself, it would be necessary to carry on more specific analysis, focused non only on the temperature range or, better, the range of temperatures in which glass and viscose transition actually occur.

In order to model the actual thermo-stress behavior, therefore the complex rheology of the membrane as a whole and of the mass itself, it would be necessary to carry on more specific analysis, focused, not only at range of temperatures in which glass and viscose transition actually occur, but especially on fragile elastic, elastic,

plastic, viscous behavior active in the temperature range to which the membrane is subjected.

Thermal, mechanical and rheological characterization of a BPP compound behavior at service is possible through Dynamic Mechanical Analysis (DMA), which analyzes its behavior under stress at varying temperature.[1]

Test is based on tiny longitudinal torsions, during which one measures energy stored within elastic deformation and energy dissipated through heat. No dissipation arises within a perfectly elastic solid, since stresses and strains are in phase.[2] On the contrary, inside a viscose solid a phase delay of 90° is registered between stresses and strains.

More frankly, things are much more complex inside a BPP mixture. Viscoelastic polymers have intermediate characteristics for which a certain phase delay occurs during DMA test.

Analyzed parameters are the stored shear modulus G′, which is connected to the potential energy stored inside deformation, and the loss shear modulus G″, which is connected to the energy dissipated as heat through deformative plastic friction. Their values are evaluated in a wide temperature range.

Their ratio is referred to as damping factor and allows for an evaluation of glass transition temperature of the material. It can also be used to identify transitions corresponding to other molecular motions, such as those due to compound anomalies.

Test execution on thermally aged samples allows to assess the performance of the compound through time. DMA analysis shown in Figs. 1 and 2 refer to two BPP membranes with different weight percentages of polymer and with the following characteristics in Table 3. Diagrams show how the arc of temperatures, in which transition from an elastic-wise behavior to a plastic-wise one occurs, is large compared to what would happen in a glass transition of the polymer.

As for membrane 1, damping curve peak is narrower. Slope prior to glass transition is steeper, such that the membrane is subjected to larger thermomechanical variations, within the same temperature range, with respect to membrane 2.

In addition, the viscoelastic branch covers all temperatures ranging from 0 C° up to viscose stage, which starts long before the value obtained from heat dimension stability test of 143 °C. This shows a high thermal sensitivity inside the range of operating temperatures.

In the case of membrane 2, elastic branch reaches up to 50–60 °C with less steep curve. Slope of the viscoelastic branch is steeper, which is a sign of instability. Compound has a high thermal sensitivity within this branch.

DMA is also very useful to evaluate ageing process and during design phase of waterproof mixtures. This type of analysis combined with TG Thermogravimetry allows to assess in advance compound quality, techniques, thermal ageing speed, presence of anomalies related to polymer position or BPP mass incompatibility.

---

[1] Viscoelasticity and dynamic mechanical testing A. Franck, TA Instruments Germany.

[2] The storage modulus relates to the material's ability to store energy elastically. Similarly, the loss modulus (G" or E") of a material is the ratio of the viscous (out of phase) component to the stress, and is related to the material's ability to dissipate stress through heat.

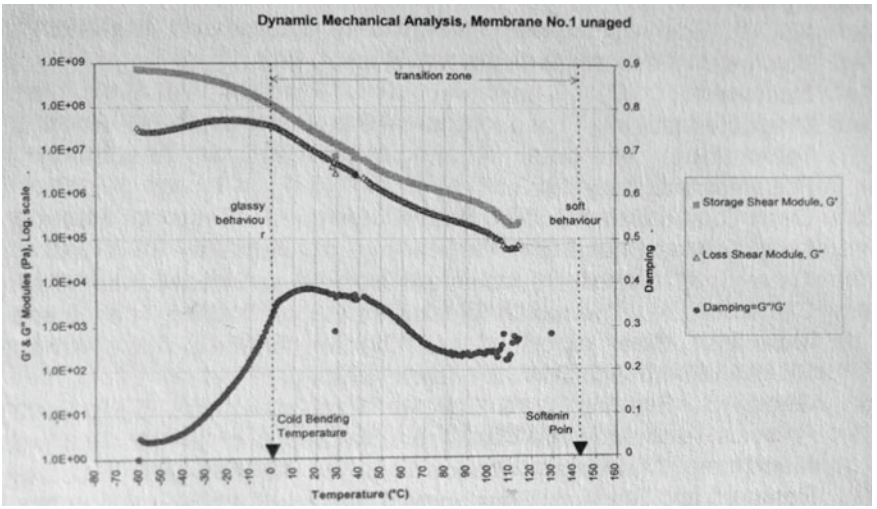

Fig. 1 DMA Unaged membrane 1. Storage and loss shear curve shows a temperature range for glass transition close to that of cold bending. For the majority of operating temperatures, the behavior of the compound is within visco-elastic phase with a high thermal sensitivity

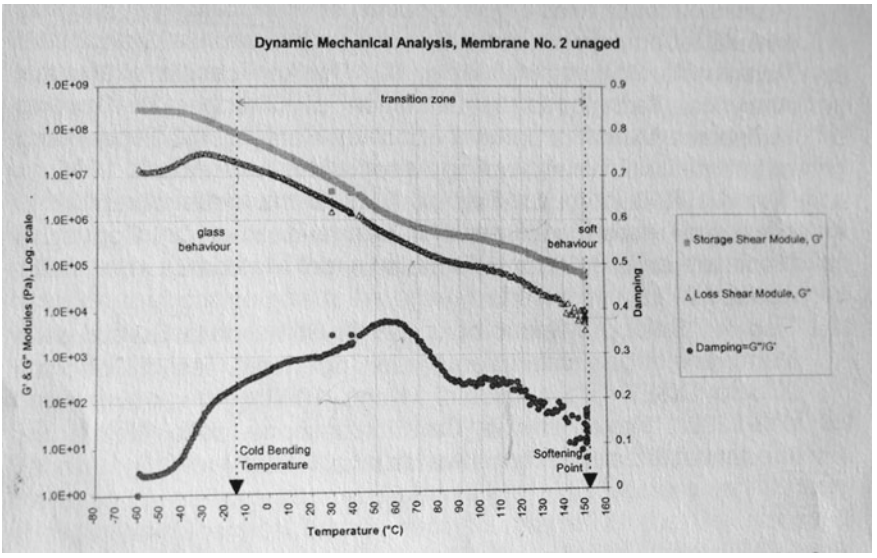

Fig. 2 DMA Unaged membrane 2. Over operating temperature range up to 50–60 °C, the compound works within the elastic field. Afterwards, the steep slope shows a high thermal sensitivity. The viscous phase intervenes at lower temperatures than heat dimensional stability test

Table 3 Test characterization of the two membranes according to italian standard

Membranes N° 1				
	Unaged	28	90	180
Cold bending (°C)	0	10	15	25
Compound softening point (°C)	143	143,5	146,0	146,0
Bitumen weight (%)	43			
Polymers (%)	6			
Filler $CaCO_3$ weight (%)	51			
Compound phase dispersion (1–10)	4 bad	4 bad	4 bad	4 bad
Membranes N° 2				
Cold bending (°C)	− 15	− 10	− 5	5
Compound softening point (°C)	143.0	143.5	146.0	146.0
Bitumen weight (%)	70			
Polymers (%)	24			
Filler $CaCO_3$ weight (%)	6			
Compound phase dispersion (1–10)	10 good	10 good	7 med	7 med

Starting from these data and by using transfer functions, it would be possible to perform congruence analysis between rheological characteristics of a membrane and a context of thermal environmental conditions.

6 Phenomenological Analysis of BBP Membrane Behavior

Thermal, mechanical and rheological characterization of a BPP compound behavior at service is possible through DMA Dynamic Mechanical Analysis, which analyzes its behavior under stress at varying temperature. Based on what explained, it is necessary to distinguish between three situations:

1. When installed membrane is a pre-stressed micro-structure: no tension is transmitted to edges or support. However, the membrane shrinks during subsequent temperature drops, thus transmitting shear stresses to horizontal constraint surfaces and "pelage" traction on vertical cuff to the support. In this case, stresses related to prevented thermal contraction depend on the temperature during membrane installation. In this situation, the membrane reacts as a single body, therefore, stresses due to prevented thermal contraction increase with BPP mass stiffness due to prestressing.
2. Following decompression and waterproof mass relaxation due to exposure at high temperature, reinforcement is stabilized under traction from support and perimetral adherence. Such stresses depend on prevented thermal contraction, which is evaluated from pre-stressing temperature and impediment to shape

memory recovery. In this situation, reinforcement under tension remains immobile and therefore does not affect the stress state in the BPP mass. On the other hand, thermal contractions of the bitumen mass are constrained by the reinforcement and can further generate stresses within the presence of thermal shocks.

3. Due to installation mistakes, the membrane detaches from the support and moves away from the perimetral edges. In this situation, the membrane decompresses and reacts thermally as a single body, being free to contract and expand.

As we shall see, this situation is the one that generates the biggest problems linked to the formation of folds. Going into the merits of stresses that arise during temperature variations, it is necessary to observe that membrane structure is commonly organized in three layers: the internal one facilitates bonding and contributes to water resistance, the middle one provides mechanical strength, the outer one maintains water resistance against deterioration driving forces of the context.

Furthermore, membrane is constructed with two materials, reinforcement and BPP mass, which are characterized by different thermal expansion coefficients and therefore may undergo stress interactions as previously observed.

Interactions differ for the three considered cases. In the first case (membrane right after installation), pre-stressing state increases bonding between the compound and the reinforcement. Membrane is characterized by a strong interaction among layers at varying temperature.

For stress analysis, reference could be made to the classical concept of linear expansion coefficient, keeping in mind that pre-stressing of the waterproof mass generates higher stresses due to the larger plasto-elastic “modulus”.

All the cover edges are interested with cyclical traction starting from the temperature at mass installation. In the second case, the bitumen polymer mass is no more pre-stressed while the reinforcement, retained still at the edges, undergoes tension: it cannot transmit any stress to the waterproof mass.

BPP mass and reinforcement stress never interact, except for the already mentioned cases involving thermal shocks. In the third case, the membrane detaches at transversal edges, and thus expands and contracts freely. Reinforcement and bitumen-polymer mass interact in a complex way.

While stress action of the waterproof mass, more rigid, prevails in contraction at low temperatures, the action in the reinforcement tends to be superior at high temperature due to a greater level of ductility.

With this regard, it should be noted that in a bitumen-polymer compound the elastic modulus increases when temperature decreases and stress due to thermal contraction increases.

Also, thermal expansion coefficient varies with temperature. As a matter of fact, in order to evaluate the stress state due to thermal contractions, proper laboratory characterization must be performed. Overall, as the membrane is no more restrained, dislocations occur during contraction. On the other hand, dislocations are prevented during expansion and folds arise.

It is evident that current evaluation features of membrane behavior are not sufficient to assess the real behavior of membrane at service. This may lead to both oversize and undersize the design.

As previously stated, reinforcement is stretched through pre-tensioning and temperature increasing during production phase. This elongation is maintained by sudden stiffening of the bitumen-polymer mass, which occurs during cooldown and consolidates membrane prestressing together with final winding.

When it gets unrolled for installation, the membrane is in a pre-stressing state: reinforcement is kept under tension by the bitumen-polymer mass which is in a state of compression. Prestressing is depleted when the membrane is kept for a certain time at maximum operating temperature. Reinforcement remains under tension with stabilized membranes. Otherwise, recoverable size scatter and dislocation might be very consistent.

Various qualitative models can be used to further study stress phenomena in the membrane after installation. Let us consider the study case of an APP bitumen-polymer sheet which is still in a state of prestress after installation. The sheet is simply supported on a non-stick surface, thus free to expand and contract.

By increasing and keeping temperature at 80 °C for a certain time, the waterproof mass acquires greater ductility and this favors structural recovery. Reaching towards temperature of heat dimensional stability, recovery is faster due to softening of the bitumen-polymer.

As compression in the bitumen-polymer mass fades, reinforcement resumes its original size unless permanent elongation has occurred. Therefore, fabric shortens longitudinally while expanding in the transversal direction. Entity of the deformation depends on the shape memory and the difference between prestressing temperature and that of the membrane.

Transversal deformation is more consistent than the longitudinal one dealing with anisotropic fabric, longitudinally reinforced with fiberglass. This is not true for perfectly isotropic reinforcement.

Having reached this condition, sheet size is further reduced due to thermal contraction if the sheet undergoes a slow cooldown towards minimum operating temperature. By acting as a single body, contractions occur starting from edges towards center, as it happens for thermal contractions at service.

Let us consider the study case of a BPP bitumen-polymer sheet, which is placed on a non-stick surface and restrained at front ends after installation. By increasing and keeping temperature at 90 °C, the waterproof mass acquires greater ductility, and this leads to depletion of prestressing.

Reinforcement could resume its size, however such event is prevented by the restrain on the foil and at the ends. Restraints are slowly loaded by a force, which increases up to the prestressing load used inside production, enhanced by the specific prevented thermal contraction of reinforcement. This depends on the difference between prestressing temperature and 90 °C.

Let us observe that the stress value to which the reinforcement is subjected during pre-tensioning does not depend on its tensile strength. Let us consider the bitumen-polymer mass to be designed and chosen in such a way that the effective range of

ductility, the so-called thermal stability, corresponds to the average hour temperature trend during the year at a specific site.

By lowering temperature from 90 °C down to the minimum operating one, with a speed that allows for a slow plastic structural recovery due to plastic memory, stress from prevented thermal contractions involve reinforcement only. When thermal shocks occur, the elastic behavior of the BPP mass may generate a consistent increase in stress and trigger membrane destabilization.

As previously examined for the restrained membrane case, and as opposed to free membranes, waterproof mass does not get involved in the reinforcement stress state.

A sound hypothesis is that overlapping connection might relax between sheets, reducing and deactivating such stresses. This would be true if all the overlaps between sheets were aligned. However, installation procedure of membranes prescribes staggered overlaps. This is done to avoid the overlap of 4 layers at junction between 4 sheets.

Dealing with such an installation scheme, overlaps prevent this translation and stabilize each sheet in their mutual position: membrane behaves as a single body. If it were not so, we would always deal with slipping, even significant, at overlaps.

In conclusion, without considering any disturbing factors activated during design, construction or management phase, or that could be related to stress interaction with the support, membrane duration does not rely only on continuous structural plastic recovery of the BPP mass and reinforcement stabilization, which corresponds to the preservation of traction. As a matter of fact, this depends on the efficiency of stabilizing constraints through time.

In good practice, stabilization of an APP bitumen-polymer layer is carried out, not only by bonding the membrane to the insulation support, but also through bond at the edges.

It should be noted that semi-adherent "flame" installation, which reaches maximum extension up to 30%, strictly relies on the operator skills. Therefore, it is not always sufficient to properly stabilize the membrane. In addition, the insulating support must be suitable for the task.

Let us remark the importance of the perimeter bonds along the side transversal to the foil, which act as an element of safety since this is the only constraint to a solid body.

In practice, this constraint should be made perfectly adherent and continuous. Dealing with less stable reinforcement, mechanical retains should be introduced.

7 Disturb Factors that Can Shorten Membrane Life

Besides issues related to stresses transmitted from the insulation support to the membrane, the appearance of widespread wrinkles and cracking is typically connected to destabilization of the membrane.

As a matter of fact, it is very difficult to find wrinkles when reinforcement is kept under tension. In such a case, reinforcement is in a state of limit extension and it has

no longer available the dimensional resources which would be required for wrinkles to form.

Detachment from the edge of the roof area orthogonal to panels causes the generation of transversal wrinkles with respect to sheet direction, longitudinal, diagonal, or fanned at corners.

Corrugation quickly leads to cracking as consequence of fatigue phenomena due to repeated thermal bending. Especially at low temperatures, a lack of ductility in the waterproof mass generates stresses in the reinforcement. These are alternatively induced by traction in the external and internal waterproof mass.

Certainly, poor support adherence or its deterioration, due to motion of the shrinking membrane, exhibits, further exposes the membrane to wind action.

Detachment from the edges of the roof could be also triggered whenever insulating panels are not installed by a perfect combination under pressure. In presence of poor support adherence, stress in the reinforcement and thermal contraction of the membrane may determine the displacement of the membrane from the edges, due to approaching panels. This leads naturally to the formation of wrinkles.

However, even with proper bonding of the insulation panels to the support in presence of high thickness, the opening and closure of a joint cavity that arises from cyclic temperature variations, produce "fatigue" cyclic stresses in the membrane which can quickly lead to wrinkles and cracking (see Figs. 3 and 4).

The outcome is dependent on the reinforcement type. Anyway, the situation is aggravated with sheets being installed in the same direction of the continuous joint among staggered insulation panels. Instead, formation of wrinkles orthogonal to the sheet direction by overlap stiffness.

Fig. 3 Corrugations due to gap presence between insulation panels

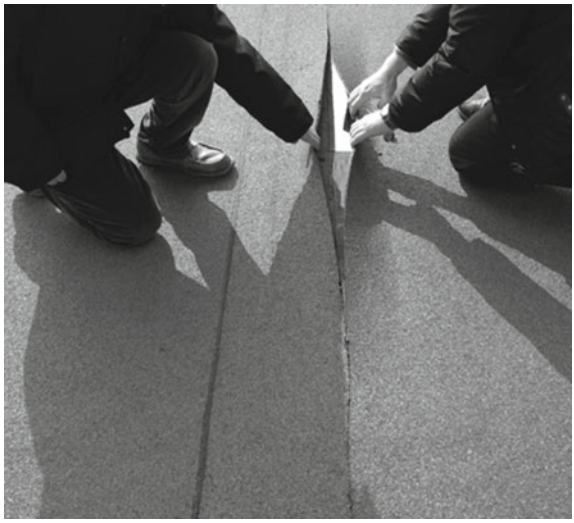

Fig. 4 Cracking due to thermal contraction before precompression destabilization phase. Cracking is favored by reinforcements anisotropy and the continuous joint between panels oriented in the longitudinal direction of the sheet

By the way, let us observe that a defective restraint of the insulation panels to the support exposes the membrane to repeated lifting due to wind gusts. This can generate stresses on cuffs which may bring the restraint to collapse.

During overheating of summer days, membrane temperature can reach values of around 80 °C. At these temperatures, ductility of the BPP mass slowly deactivates the pre-stressing state of the BPP mass. The membrane no longer works as a single body. Tension in the reinforcement, due to prestressing of the waterproof mass, are slowly stabilized as they are transferred to the adherence system to the support.

Shear stresses on support connection and pelage stresses on side cuffs begin to activate and increase.

In the case in which these tensions lead to failure of support adherence, reinforcement slowly resumes its original size due to shape memory and thermal contraction starting from the temperature of prestressing during production.

After this relaxation phase, reinforcement and bitumen mass behave as a single body at temperatures sufficiently far from heat dimensional stability. The membrane undergoes thermal expansions and contractions which generate stresses all along the perimeter.

Let us point out that considering a membrane with an adequate ductility range for the site, by adopting a reflective protection, decompression of the bitumen mass is theoretically prevented as the required temperature is not reached. Stresses along the perimeter are due only to the low thermal loading, since thermal contraction caused by production temperature is prevented by prestressing. Of course, stress on support links increase with the stiffening connected to aging. Reaching this condition, if serviceability of the protection is not to be maintained, the pre-stressing state gets deactivated, and the stabilization task is transferred to the support.

Risks concern the adoption of polymer panels which undergo softening at temperatures close to 80 °C. In this case, overheating reduces the ability of the panels to stabilize the membrane and this happens for temperatures that determine the recovery of shape memory.

Formation of wrinkles is the consequence of detachment at edges orthogonal to the development of the edges. These can be:

1. transversal;
2. longitudinal;
3. diagonal developing from fixed points or corners, mainly oriented in the direction of the sheets;
4. diagonal developing from fixed points or corners, oriented towards cover center.

These corrugations are caused exclusively from repeated shortening and lengthening of the membrane, due to thermal contraction and expansion.

7.1 Wrinkles Transversal to Sheet Direction Caused by Decompression and Subsequent Free Dislocation of the Membrane.

After a thermal contraction, the following longitudinal expansion is partially prevented by support friction. The membrane expands more easily by corrugating transversally with respect to the direction of installation (see Fig. 5).

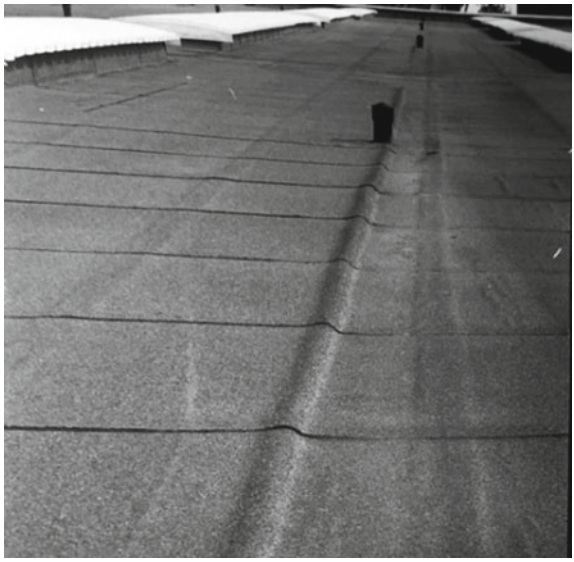

Fig. 5 Transversal wrinkling due to detachment from orthogonal edges to the direction of sheet installation

Sooner or later, repeated "fatigue" bending of the bitumen-polymer mass leads to cracking.

7.2 Longitudinal Corrugations to the Sheet Direction, Caused by Dislocation of the Membrane

Consistent "longitudinal wrinkling" might add up to transversal corrugation. As a matter of fact, let us remark that, at installation, sheets display themselves as longitudinally stretched, while laterally shortened (see Fig. 6).

Loss of the stabilization constraints allows the membrane to expand transversally to the sheets during thermal expansion phase, and the reinforcement to resume its shape. However, double-layer overlaps act against this. When entering compression, the membrane finds its freedom to expand with the formation of longitudinal wrinkles in areas of low adherence. Afterwards, these wrinkles develop into cracks due to the cyclical nature of thermal loads.

All of this happens more easily either in the case of reinforcement with no fiber glass coupling, that proves to be more unstable, or in the case where polyester is reinforced only with longitudinal fiber glass, therefore anisotropic.

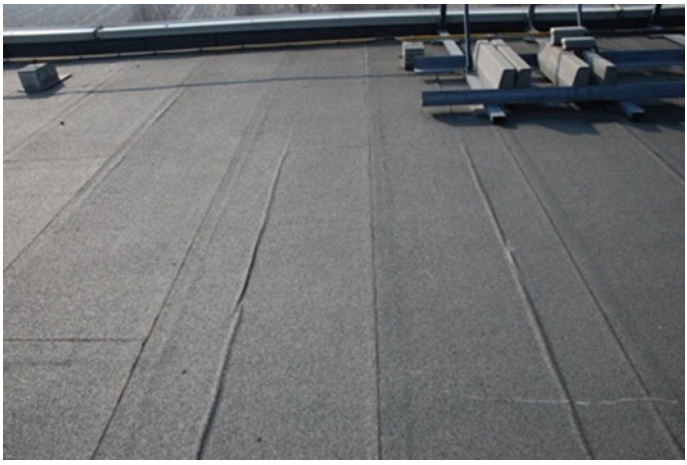

Fig. 6 Longitudinal corrugation due to relaxation of the membrane. Reinforcement was polyester, reinforced with longitudinal fiber glass, therefore anisotropic

Fig. 7 Corner corrugation, horizontal and vertical

7.3 Diagonal Corrugations Caused by Dislocation of the Membrane

Detachment from transversal edges with respect to the sheet direction occurs far away from the corner, while it is prevented or resisted at corners. As a matter of fact, dislocation of the sheet end is retained by vertical side cuffs (see Fig. 7).

This determines diagonal corrugations on the horizontal plane, mainly oriented in the direction of the sheets. Over time, the vertical side cuff of the sheet gets dragged and this determines the formation of diagonal corrugations on it, developing from corner upper end. Frequently, this leads to overlap disconnection.

7.4 Diagonal Corrugations Due to Thermal Contraction in Prestressing State

A particular aspect to highlight is the rise of edge detachment and diagonal wrinkles oriented towards cover center, even within a short time after membrane installation.

The bitumen mass is still in the prestressing phase and it is therefore relatively more rigid. As previously noted, such condition makes the membrane behave like a single body, regardless of the direction of installation of the sheets.

As temperature lowers from that of installation to the minimum operating one, stresses due to prevented thermal contraction increase consistently for stiffening of the BPP mass. For less ductile membranes, such stresses can generate gaps all along the perimeter and fan wrinkles at corners. Angle cuff resistance with respect to thermal stress towards the center of the cover is significantly higher than that of the edges further away from corners. Here, the cuff does not detach entirely with the formation of fan wrinkles oriented towards cover center.

7.5 A Particular Case of Wrinkling

A particular case of wrinkling is determined in paved roofs. The absence or insufficiency of side joint in the pavement might cause puncturing and cuff base dragging. All of this takes place during summer, when the BPP mass is most ductile and thermal expansion reaches its maximum.

During the expansion phase, pavement sides get closer to the edge and translate towards the corner.

In the absence of a suitable joint, the pavement might meet the membrane, which gets dragged towards the corners. Dragging of the membrane is prevented from above by its adherence to the vertical support.

During contraction phase, pavement that sits on the waterproofing prevents the membrane from resuming to its position,

All this together creates wrinkles on the vertical cuff that radiate diagonally from the corner. Angle is opposite to the one already examined above (see Fig. 7).

The phenomenon is cyclical so that effects grow more serious with time. Among these, overlap disconnection and, even more critical, puncturing in the waterproofing layer (see Fig. 8).

8 Stresses Under Service Loads

The stresses caused by thermal phenomena are aggravated by direct mechanical actions such as foot traffic, technical devices supported directly by waterproofing membrane, punching due to mechanical fixings of the thermal insulation.

Fig. 8 Corrugations due to floor contact with the waterproof cuff. Wrinkles have diagonal shape, pointing down. Overlaps are detached

8.1 Stresses Caused by Permanent Loads

Machinery, signs, and similar elements are often placed directly on rooftop membranes. These should be always provided with continues footings.

Certainly, placement over column-sustained plates is the most convenient solution as it allows for membrane maintenance. Evidently, this becomes even more necessary when working on existing roofs and mandatory in the case of mechanically fixed membranes.

This solution also makes repairing interventions less expensive as they would require disassembly and replacement of machinery.

While for point-wise loads deformation depends on the mechanical interface between the membrane and the support, in the case of distributed loads, sinking depends exclusively on deformative characteristics of the insulation panel under load.

Resistance to deformation under 10% load is assessed by EN 826, however, this test has a general application. Regarding roof covers, it is necessary to define some limitation. Table 4 shows a UNI standardization proposal aimed to be of reference in the design. It is based on the definition of a minimum value for compressive strength (kPa) at 10% deformation.

For example, a material with compression strength at 10% deformation equal to 50 kPa must carry a minimum load up to 5 kN/m^2 (10% of what declared).

In this regard, fibrous materials are more sensitive as they typically show a lower compressive resistance in comparison to synthetic materials.

For example, keep in mind that distributed loads associated with elements such as air treatment units (including the additional design snow load) can range around 6–8 kN/m^2. This corresponds to a pressure equal to 6–8 kPa, which leads to the

Table 4 Possible compressive resistance and ultimate load on thermo-insulating layer

Category	Type of coverage	Minimum compressive strength (kPa) at 10% deformation (mineral wool, wood fiber[a)])	Minimum compressive strength (kPa) at 10% deformation (other insulating materials)	Ultimate load on thermal insulating element kPa
1	Covers accessible for maintenance alone without heavy protection	≥ 50	≥ 100	5
2A	Covers accessible for roof and machinery maintenance	≥ 60	≥ 120	6

Prospect is valid for a thickness of the thermal insulating element ≤ 20 cm in one or more homogeneous layers, with the exception of Category

need of adopting materials with compressive strength at 10% deformation equal to 60–80 kPa.

Of course, one should evaluate whether the sinking of the thermal insulation layer and the resulting extension of the membrane is bearable by the waterproof membrane. In order to evaluate admissibility of such an extension, it would be necessary to know the actual stress/strain curve of the membrane. This would make decisions less hasty than those currently adopted.

A UNI code proposal for BPP membranes prescribes a maximum deformation of 3 mm for thermal insulation layer, which is considered acceptable by waterproofing practice but it is not experimentally tested.

This means that for a support made of a polymer thermal insulation layer with 20 cm thickness (today considered as a standard), maximum percentage of deformation of the panels should be equal to 1.5% (3 mm). This value is still very low compared to 10% as indicated by the standard EN 826.

Of course, one should know the actual stress/strain curve to perform an experimental check on the stresses activated by a 3 mm sinking. The same also applies to stress checks in the membrane.

Incidentally, let us remark that machinery loads are usually applied when the membrane is still under pre-stressing and the stress response is characterized with a strong interaction between waterproof mass and reinforcement.

Only after the relaxation of the waterproof mass, stresses shift on the reinforcement. For this reason, installation should be carried out at temperatures quite distant from cold flexibility in order to immediately stabilize the sinking.

Membrane stress state close to base edges depends on the geometric shape of the base. Sharp edges determine dangerous shear actions, while in the case of a properly curved base, starting from bottom, the membrane is only subjected to traction. In addition to those already highlighted, one critical aspect of this solution concerns strong temperature difference between loaded areas and the external one.

Pre-stressing of the membrane within protected areas lasts over time since they hardly reach the 80–90 °C of outdoor areas. Instead, the exposed area can reach plastic memory over time. Membrane stress state at edges is enhanced by rigidity of the constraint with respect to stresses connected to support sinking.

Of course, high temperature in loaded areas can also be determined by the presence of hot parts in the machinery and change accordingly the phenomenology.

Another aspect to consider concerns the possible presence of vibrating equipment which loads membrane side with fatigue phenomena.

In conclusion, let us highlight that stresses increase with time due to ageing and, therefore, stiffening of BPP mix. This process can accelerate in presence of reflective surfaces in the machinery.

A special case of distributed load is associated with “floating” square floors placed over plastic supports.

This is a solution that protects waterproofing from direct solar radiation and reduces thermal and mechanical shocks in the presence of hail.

Control of the sinking connected to the load requires of course a correct design. In the case that such pavement was reserved to public use, with a loading usually equal

to 4 kN/m^2, by considering a typical mesh of 50 cm × 50 cm with a self-weight equal to 1 kN/m^2, this would lead to a load of 1.25 kN on each support, since 4 flooring elements converge on each support.

Load distribution support, meant to avoid punching, must not have sharp edges, and have surface areas of more than 160 cm^2 and sides exceeding 10 cm. Finally, let us observe that concentrated loads depend on people passing through and positioning of loads, such as heavy flower boxes, that can be done even at low temperatures and in the presence of membranes with insufficient cold flexibility, which can generate dangerous microcracks.

8.2 Stresses Caused by Punctioning Actions

Actions able to cause a puncture of the waterproof membrane may be of man-made origin, such as trampling, or of technological origin such as the supports of ducts and plant pipes, or also weather-determined, such as hailstorms.

In general terms, it is necessary to distinguish between perfectly rigid supports and deformable supports such as insulation panels. The first case is not critical and as a matter of fact they operate as a load distribution layer. Only during summer overheating, membranes with low flowing temperature may be subjected to footprints.

However, it should be noted that membrane overheating might locally increase during summer season due to reflection of solar radiation caused by reflecting machinery and piping surfaces. In such circumstances, the abnormal softening state exposes the membrane also to premature aging.

In the case of deformable panels, membrane deformation and relative stress state depend on the punching resistance of the support and the waterproof membrane. In contrast to distributed loads, the sinking of the insulating material under punching loads is opposed by the material next to punching shear area.

Membrane resistance to local sinking interactively depends on the characteristics of the substrate and those of the membrane. Regarding the stress regime, it is necessary to distinguish between membranes adhering to the support and independent membranes. In the first case, membrane deformation is more concentrated due to support coupling. In the second case, stress interaction is less consistent and membrane deformation are larger. Of course, sinking and membrane stresses depend upon its temperature.

For the case of hail, tensions are enhanced by the punching speed and the thermal shock. The significantly cooled membrane assumes a rigid-elastic behavior, therefore it is not able to quickly recover its plastic memory.

Under the punching action of a grain, the bottom of the membrane undergoes traction. Whenever punching load determines the overcoming of the elastic phase, fractures are triggered and become the source of infiltration.

During winter, foot traffic, which also operates in a dynamic way, determines dangerous tractions on the lower surface of the membrane due to its rigidity. Therefore, fractures due to compound fragility may activate in the case of non-appropriate compounds to the climatic conditions or excessive sinking of the insulating layer.

In summer, the faster plastic recovery of the membrane makes deformation dependent only on the reinforcement and the insulating layer characteristics. It is necessary to distinguish between solutions with mechanically fixed insulating panels and membrane glued on them, and solutions in which underlying elements are glued and the membrane is mechanically fixed (see Figs. 9 and 10).

In relation to what has been previously observed, panel sinking under concentrated loads is greater since the membrane is not glued on the support. In the case of a concentrated load close to a mechanical connection, membrane downward displacements are opposed by the mechanical fastening. Membrane undergoes different stresses depending on the type of mechanical connection.

Fig. 9 Refurbishments in correspondence of mechanical fixing shafts, due to insufficient compressive resistance of the insulation panels

Fig. 10 Deformation of the mechanical fixing shaft due to direct load

In the case of plate attached underneath the shaft (pull over), device dimensions prevent puncturing for near sinking under load. However, they generate traction. Load on top of overlaps next to the plate might lead to local detachment.

Direct load on the plate can generate distortion, shaft rupture, anchorage deactivation due to current significant thicknesses of the insulating layer. In the case of plate unattached to a shaft (pull over), sinking of the insulating layer close to the device puts the membrane in contact with the mounting rod. Punching shear is generated which can lead to puncturing. Direct foot traffic not only makes perforation very likely, but also exposes the rod to deformation or rupture, creating problems of membrane stability.

In the case of plate unconstrained to the shaft and provided with a sleeve (pull through), sinking of the membrane does not determine tensioning actions in the membrane.

Regarding the membrane, two characteristics are to be evaluated: punching resistance (EN 12730) and tearing resistance (EN 12310). As far as thermal insulation panels, the feature that should be evaluated is the resistance to concentrated loads, in accordance with the EN 12430.

8.3 Mechanical Stresses Caused by Wind Action

Wind on the cover determines alternating pressures and depressions which intensify at cover edges, and, in particular, at corners.

In order to analyze phenomenology of membrane constraint against wind action, it is necessary to take into account the entire stratigraphy. Membrane and other underlying elements of the roofing system must be kept in place without dislocations (see Figs. 11 and 12).

Regarding membrane stability, this can be ensured by adherence or mechanical constraint.

Fig. 11 Lifting of waterproof membrane due to wind action in the presence of insufficient tensile strength of thermal insulation panels, restrained with mechanical fastenings

Fig. 12 Urgency ballasting of a membrane detached by the wind

8.3.1 Adherence Constraint

This constraint can be either continuous over the whole surface, or partial. In the first case, stresses present very low values per unit area. In the second case, related to torch applied solutions, the adherent surface is reduced to 20–30% of the whole cover and it depends on operators' quality.

A high value for wind traction can be estimated at 2.0 kN/m^2. On the safe side, adherence system and thermal insulation element must ensure a useful tensile resistance, calculated as orthogonal to its main plain, equal to 10 times the value of design wind action.

For torch applied systems, vertical tensile strength to be used must be correlated as directly proportional to this value. For example, tensile resistance for both glue and insulation panels over an effective adhesion surface equal to 20% shall be equal to 4 times the resistance offered by continuous adherence.

Of course, lower adherence values might determine critical situations. In this case, depression actions caused by repeated wind gusts can produce small, repeated liftings that put the membrane in tension.

In the presence of less constrained zones, these vibrating liftings generate peeling actions that gradually lead to the enlargement the detached area. These actions are mainly concentrated on edges and cuffs and can lead to the complete dislocation of the membrane (see Fig. 13).

Adherence bond between membrane and insulation panels does not only depend on adherence medium quality (primer, glue), but also from panel quality itself. These must have a perpendicular tensile strength with respect to the main faces in agreement with wind-generated tractions on the membrane. Actually, the critical aspect is the delamination of the insulation panel. For such reason, it is necessary to set mechanical quality of insulating materials with respect to the meteorological conditions of the site. Less-durable materials require special attention and, if necessary, further mechanical fasteners especially at cover edges (see Fig. 14).

The following are current values of tensile strength for the materials that are typically used as roof thermal insulation elements:

- polystyrene panels $\geq$ 100 kPa;

Fig. 13 Dislocation due to wind for insufficient adherence of the membrane to the support

Fig. 14 Delamination of surface treatment of polyurethane panels

- rock wool panels $\geq$ 15 kPa;
- polyurethane panels $\geq$ 30 kPa.

As shown, there is a high difference between listed materials with a greater sensitivity of fibrous materials, such as rock wool.

On the safe side according to the UNI 11442 [8], thermal insulation element must ensure a useful tensile strength (measured according to UNI EN 1607 [9]) perpendicular to the main plane equal to 10 times the value of design wind action.

Therefore, even for design wind pressure values not very high and equal to 2 kN/m^2, it has been discovered that, for certain types of material, one should proceed with the selection of high-performance products. That is especially the case for side areas and corners, where wind action is essentially very high.

A particular case concerns polystyrene which has a glass transition temperature that can start to 75–80 °C.

Fig. 15 Lack of restraint between membrane, insulation panel and support. Overlap of thermal insulation panels due to wind action

Above this temperature, the material enters plastic phase. Surface softening reduces mechanical properties and adherence to the membrane.

In such conditions, there is the risk that the non-perfectly attached membrane may undergo dislocations during extraordinary afternoon wind phenomena. For this material, it is necessary to take productive or systemic precautions to avoid its overheating.

One solution is to treat the membrane with reflective paintings. At the perimeter, adherence constraint might be reinforced with ballasts obtained through homogeneously distributed elements (gravel) or through light square floorings. These are solutions that prevent direct solar radiation and reduce membrane overheating.

A similar situation caused by softening of these materials at high operating temperatures may be caused by thermal shocks, such as hailstorms. Unexpected thermal contractions may cause slips and detachment of the membrane (see Fig. 15).

8.4 Membrane Bond Through Mechanical Devices

Mechanical constraint may be realized through fastening of the waterproof membrane, through fastening of the insulation layer and bonding of the membrane. Mechanical constraint device is composed of contrast element (plate or linear element), connection shaft, support constraint element (contrast element).

Regarding the mechanical device, its deactivation might be due to rupture or deformation of the connection shaft (pull-out or loosening from support), to deformation/detachment of plate/sleeve from the connection shaft, to pull-out or loosening of the connection due to pulsing wind action.

Wind actions do not cause only traction along the shaft axis, but also flexural effects due to movements of the plate caused by the wind. These are more difficult to be supported by the shaft since its mechanical inertia is low.

Regarding the importance of an efficient behavior of the device, let us note that the deactivation of even a single mechanical constraint causes a load increase in the continuous ones and the following risk of bringing them to collapse and triggering collapses more and more extended.

The procedure of mechanical constraining a membrane at junctions (overlaps) takes place according to the following steps:

1. installation of the first sheet and mechanical fastening of the membrane at selvage;
2. installation of the second sheet with proper overlapping, sheet welding at selvage with plate incorporation.

The membrane is tensioned transversely to the sheets since constraints are concentrated at overlaps. Therefore, it is necessary to use membranes with isotropic reinforcement.

Due to potential transversal expansion of reinforcement after relaxation period, the use of membranes with polyester reinforcement strengthened with longitudinal glass fiber easily leads to lengthening and wrinkling caused by vibrating lifting during summer season. Of course, these actions integrate and enhance those that are activated during and after decompression process of the BPP mass described above, which evidently include those due to thermal contractions.

With this regard, it is necessary to point out that dealing with a simply supported membrane, its tensile stabilization, as well as the one related to prevention of thermal contraction, might be theoretically entrusted to shafts of the mechanical fasteners. However, these show very low mechanical inertia with respect to the vertical axis. Therefore, membrane stabilization would be substantially entrusted to improper contact reaction between shafts and insulation panels, which tend to deform over time under cyclic actions. The result is a slow and progressive assignation of the stabilization function to the perimetral cuff. With this constraint solution, a perfect mechanical connection of the perimetral cuff to the vertical support through a metal bar becomes fundamental.

Wind-generated stresses in the membrane are due to contrast of the plate incapsulated between first and second sheet and contrast with the shaft of the perforated lower membrane.

Stresses in the membrane generated by its lifting under wind action are different depending on installation quality:

- **Method 1: correct connection**

If fastening is done in the correct way, this is placed leaving a minimum space of 10 mm between the plate and the edge of the sheet (see Fig. 16).

In this way, the plate compresses the waterproof cover against the support and the action exercised on the membrane is of the kind indicated in Fig. 17.

The two sheets are subjected to traction and shear and the ultimate limit state is connected to the tensile strength of joints between the sheets (UNI EN 12317-1 [10] Determination of tensile strength of joints).

Tensile resistance of joints are:

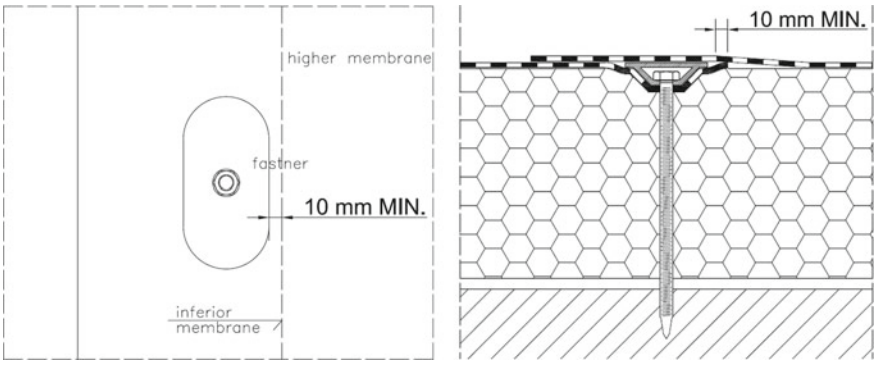

Fig. 16 Correct connection (space of 10 mm between the plate and the edge of the sheet)

Fig. 17 Action exercised on the membrane

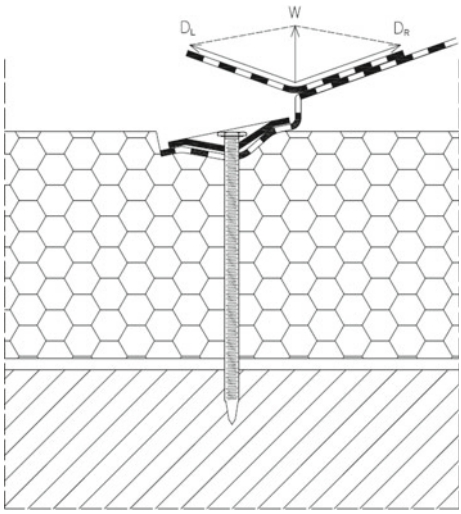

1. approximately 250 N/50 mm for non-woven fabric reinforcement of stabilized composite polyester;
2. about 400 N/50 mm for non-woven fabric reinforcement of stabilized continuous-wire composite polyester.
3. **Method 2: incorrect connection**

If fastening is done incorrectly, this is placed very close to the sheet edge (see Fig. 18). In this way, the plate does not compress the waterproof sheet over its entire crown against the support and the action exercised on the membrane is of the kind indicated in Fig. 18: a limit state connected to tearing resistance of the membrane at the nail (UNI EN 12310-1 [11]), which implies a larger set of problems.

Further variables that govern action intensity are:

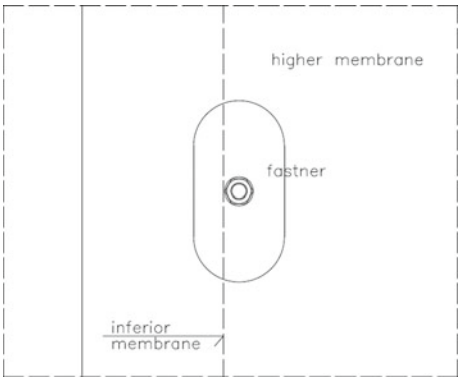

Fig. 18 Incorrect connection

1. compression capacity of the plate against the support: with more compressible support, such action appears to follow method 1. The more compressible the support is, the more the action is combined with method 2;
2. mechanical inertia of the fastener with respect to its own axis, which depends on material and cross-section. The lower the mechanical inertia, the greater the deformation of the connection with respect to its own axis.
3. Regarding tensile strength, in general values are sufficiently high taking into account wind-generated tractions

Plates used are usually rectangular with a width of 40 mm, both to reduce overlap size, as well as to offer an adequate surface. As a matter of fact, increasing plate boundary extension, therefore its length, is always advisable in order to reduce shear force.

For example, it is advisable to use rectangular plates with sides equal to 80 and 40 mm, therefore with a perimeter equal to 260 mm. As previously observed, mechanical fastener shaft is also opposing traction in the membrane. Thus, the membrane must have adequate resistance to tearing (see Fig. 19).

Tearing resistance is determined by standard EN 12310-1 [11] (nail method). Indicative values of tearing resistance are reported in detail below with reference to reinforcement type:

1. veil glass: ≈ 70/90 N;
2. stabilized non-woven polyester fabric: ≈ 140/160 N;
3. continuous-thread stabilized non-woven polyester fabric: ≈ 160/200 N;
4. glass-fiber stabilized composite non-woven polyester fabric: ≈ 200/250 N.

In particular, UNI 11442 [8] prescribes a minimum resistance for both longitudinal and transversal direction equal to 150 N, unless maximum spacing between fasteners is less than 5 cm, in which case the value can be reduced to 100 N.

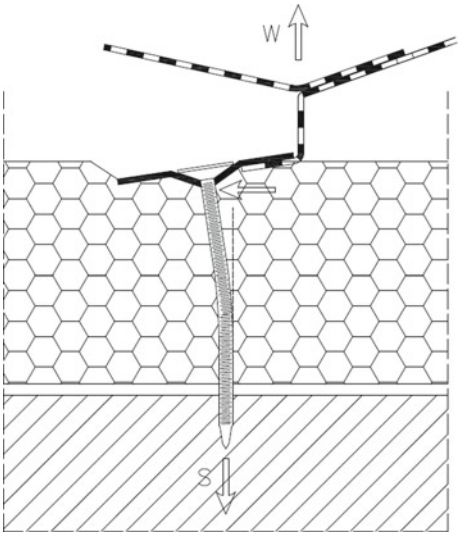

Fig. 19 Action exercised on the membrane

8.5 Thermal Insulation Bond Through Mechanical Devices

Mechanical fixing of the cover system may also be performed by mechanically constraining the insulation panels to the support and putting in adherence to them the waterproof membrane. This solution has the advantage of significantly reducing the vibrating uplift of the membrane caused by wind, provided that the insulation panel is properly restrained with respect to its thickness [12, 13].

Figure 20 shows graphical indications about their fastening processed in relation to wind action, according to Italian standard UNI 11442 [8]. As for adherence connection of the membrane to mechanically restrained panels, the same situations previously analyzed for adherence installation apply. Dealing with very thick panels (15–20 cm), these do not undergo flexural deformation under membrane-transmitted actions. Tractions due to wind action over the whole surface homogeneously infer on tensile behavior within the elastic phase of the entire thickness of insulation.

Of course, the material is under compression in correspondence of plates. However, it should be noted that for solutions involving multi-layer panels, only the first layer couples as a single body with the membrane and, with low thickness, the complex membrane panel may undergo flexural actions with maximum at the joint.

For example, in the case of large size panels of 240 × 120 cm, free span of inflection is 120 cm. Based on graphic indications of Fig. 20, let us remark that maximum uplift and maximum interaction between membrane and insulation occur at joints. Here, progressive detachment of the membrane and joint opening may generate, which may form corrugations and subsequent damage at relapse.

In this case, vibrations might lead to surface or inner delamination of the panel depending on the material. For both cases, stresses that develop at the interface

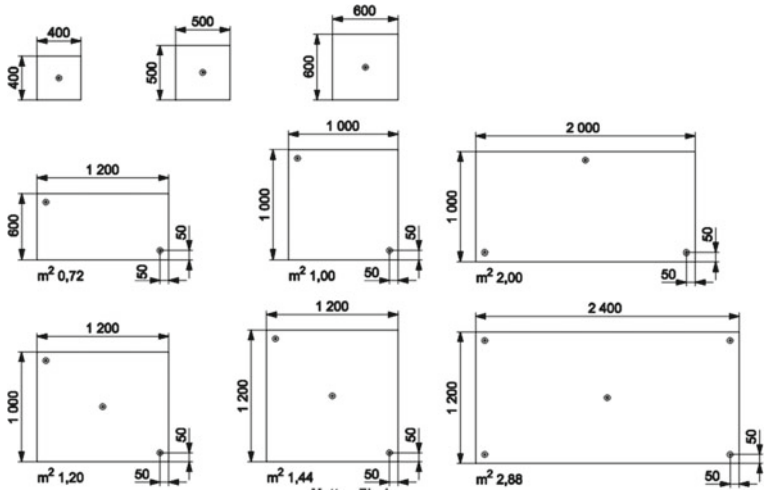

Fig. 20 Graphical indications about their fastening processed in relation to wind action, according to Italian standard UNI 11442 [8]

depend on the tensile behavior of the membrane at a specific temperature and on mechanical properties of the insulating material, which works partly in traction and compression.

For large thin panels, it might be necessary to set up additional fasteners as to reduce tension at free joints between panels. In addition to the above, flexural pulsations may lead to unbuttoning of the panel, which is certainly easier with thin and less rigid panels. Such unbuttoning can easily proceed in the surrounding restraint.

Italian standards of reference (UNI 11442 [3]) indicate a minimum surface of 30 cm^2 for the plate, which corresponds to a disk with diameter of about 60 mm; this allows to reduce the shear value over the sliding surface of the panel.

9 Conclusions

Although characterized by a significant industrial boost, disposal of knowledge, experience and codes within the flat roof sector did not consider, in opposition to other construction sectors, engineering methods for an analysis of the actual adequacy of the behavior of waterproofing solutions over time with respect to environmental loads, which are extremely variable depending on the geographic site.

The advent of EN standards, tendentially based on minimal commercial features, reduced attention and research on the behavioral characterization of membranes at service. From the code point of view, old standards from the ‘80 s, which featured detailed membrane characterization at the advent of bitumen-polymer membranes,

have been abandoned or not used. In Italy, UNI 8202 [14] series consisted of 34 parts. Research on topics discussed previously [3] also refers to those years.

Lack of research mainly interests thermo-tensional rheological aspects of membranes. Instead, the industry provided engineering tools within the wind resistance sector, as in the case of mechanical fasteners. Yet, current knowledge and scientific, instrumental and computer resources may be able to support the development of analytical models for design, which could be able to assess quality of membrane behavior under specific environmental and operating actions.

Currently even important reference to codes does not allow to assess membrane quality with respect to the context at service, if not by comparison. In the absence of this, the phenomenological analysis of waterproof membrane behavior may provide an important tool to develop a design knowledge that might prevent frequent failures in the sector of flat roofs.

This develops from the consideration that the membrane at installation is nothing more than a pre-stressed structure, where tension generated in the reinforcement during production is prevented by the bituminous mass. While exposure of the BPP mass at high operating temperatures leads to its detensioning over time, reinforcement must be maintained under tension, therefore stabilized. This should be done to prevent that tension from thermal contraction and shape memory may generate stresses on support and edge connection, such as to discard its functionality.

As a matter of fact, most of the issues that take place on waterproof membranes are caused by its destabilization. It is therefore necessary to deepen the subject by bringing the attention back on installation quality and control methods on bonding efficiency between the layers that make up the element package, which constitutes the technical solutions of covering systems.

References

1. UNI 8178 (2019) Edilizia - Coperture - Parte 2: Analisi degli elementi e strati funzionali delle coperture continue e indicazioni progettuali per la definizione di soluzioni tecnologiche, Italy
2. UNI 11345 (2010) Attività di controllo per le fasi di progetto, esecuzione e gestione di coperture continue, Italy
3. Croce S, Tiso A, De Angelis E, Pasetto G, Favaro M, Satta G (1998) Evaluation of polymer modified membranes durability by dynamic mechanical analysis. In: Proceedings of the international waterproofing association XTH congress, Copenhagen, Denmark
4. Annales de l'Institut Technique du Bâtiment et des Travaux Publics, Progres qualitative recents des revetements d'étanchéité. Enseignements du Symposium de Washington, n°365, 1978
5. Croce S (1981) Processual analysis of flat roof pathologies. SKI ISRR Brighton—roof and roofing, new materials, industrial application, use and performance, Brighton, UK
6. Croyere G, Chaize A (1981) Mesure de coefficient de dilatation thermique des revetements d'etaincheité. SKI ISRR Brighton - Roof and roofing, new materials, industrial application, use and performance, Brighton, UK
7. Schieroni M, Gagnor R (1981) Membranes 'essais de resistance aux mouvments cycliques. SKIING ISRR Brighton—roof and roofing, new materials, industrial application, use and performance, Brighton, UK

8. UNI 11442 (2015) Criteri per il progetto e l'esecuzione dei sistemi di coperture continue - Resistenza al vento, Italy
9. UNI EN 1607 (2013) Isolanti termici per edilizia - Determinazione della resistenza a trazione perpendicolare alle face, Italy
10. UNI EN 12317-1 (2001) Flexible sheets for waterproofing—Bitumen sheets for roof waterproofing—determination of shear resistance of joints, Italy
11. UNI EN 12310-1 (2001) Flexible sheets for waterproofing—Bitumen sheets for roof waterproofing—determination of resistance to tearing (nail shank), Italy
12. Croyère G (2005) Théorie de l'étanchéité par revêtements déformables à base de bitume. Edition MEPLE, France
13. Cahiers du CSTB (1986) Comportement méchanique des revetements d'étanchéité associés à un support isolante, CSTB 2105
14. UNI 8202 (1984) BUILDING—water proof sheets—determination of high temperature flowing, Italy